



This is a post-peer-review, pre-copyedit version of an article published in PNAS. The final authenticated version is available online at: <https://doi.org/10.1073/pnas.1809037116>

Classification: BIOLOGICAL SCIENCES: Plant Biology

Title: Selective auxin agonists induce specific AUX/IAA protein degradation to modulate plant development

Short title: Intruding selectively within plant auxin perception

Thomas Vain^{a,1*}, Sara Raggi^{a*}, Noel Ferro^b, Deepak Kumar Barange^{a,f}, Martin Kieffer^c, Qian Ma^a, Siamsa M. Doyle^a, Mattias Thelander^d, Barbora Pařízková^e, Ondřej Novák^{a,e}, Alexandre Ismail^g, Per Anders Enquist^h, Adeline Rigal^a, Małgorzata Langowska^a, Sigurd Ramans Harborough^c, Yi Zhangⁱ, Karin Ljung^a, Judy Callis^j, Fredrik Almqvist^f, Stefan Kepinski^c, Mark Estelleⁱ, Laurens Pauwels^{k,1} and Stéphanie Robert^{a,2}

Author ORCIDs

Thomas Vain: 0000-0002-8153-907X; Sara Raggi: 0000-0002-7925-5772; Siamsa M. Doyle: 0000-0003-4889-3496; Barbora Pařízková: 0000-0002-8125-2271; Ondřej Novák: 0000-0003-3452-0154; Judy Callis: 0000-0002-0622-078X; Fredrik Almqvist: 0000-0003-4646-0216; Laurens Pauwels: 0000-0002-0221-9052; Stéphanie Robert: 0000-0002-0013-3239

Author Affiliations

^aUmeå Plant Science Centre, Department of Forest Genetics and Plant Physiology, Swedish University of Agricultural Sciences, SE-901 83 Umeå, Sweden

^bInstitute of Physical and Theoretical Chemistry, University of Bonn, Germany

^cCentre for Plant Sciences, University of Leeds, Leeds, LS2 9JT, UK

^dDepartment of Plant Biology, Swedish University of Agricultural Sciences, the Linnean Centre for Plant Biology in Uppsala, Box 7080, SE-75007 Uppsala, Sweden

^eLaboratory of Growth Regulators, Centre of the Region Haná for Biotechnological and Agricultural Research, Faculty of Science of Palacký University & Institute of Experimental Botany CAS, Šlechtitelů 27, CZ-783 71 Olomouc, Czech Republic

^fDepartment of Chemistry, Umeå University, SE-901 87 Umeå, Sweden

^gSup'Biotech, IONIS Education Group, 94800 Villejuif, France

^hLaboratories for Chemical Biology Umeå, Chemical Biology Consortium Sweden, Department of Chemistry, Umeå University, SE-901 87 Umeå, Sweden

ⁱUniversity of California San Diego and Howard Hughes Medical Institute 9500 Gilman Dr. #0116 La Jolla, CA 92093-0116, United States of America

^jUniversity of California, Davis, Department of Molecular and Cellular Biology, One Shields Avenue, Davis, CA 95616, United States of America

^kGhent University, Department of Plant Biotechnology and Bioinformatics, 9052 24 Ghent, Belgium

¹VIB Center for Plant Systems Biology, 9052 Ghent, Belgium

¹Present address: Epigenetic Regulations and Seed Development, UMR232/DIADE, Institut de Recherche pour le Développement (IRD), Université de Montpellier, 34394 Montpellier, France

²To whom correspondence may be addressed: Email: Stephanie.Robert(at)slu.se;
Phone: +46 (0)90-786 8609; Fax: +46 90 786 81656

*These authors contributed equally to this work.

Keywords: Auxin, chemical biology, selective agonist, prohormone, hormone perception, skotomorphogenesis

Abstract

Auxin phytohormones control most aspects of plant development through a complex and interconnected signaling network. In the presence of auxin, AUXIN/INDOLE-3-ACETIC ACID (AUX/IAA) transcriptional repressors are targeted for degradation by the SKP1-CULLIN1-F-BOX (SCF) ubiquitin-protein ligases containing TRANSPORT INHIBITOR RESISTANT 1/AUXIN SIGNALING F-BOX (TIR1/AFB). CULLIN1-neddylation is required for SCF^{TIR1/AFB} functionality as exemplified by mutants deficient in the NEDD8-activating enzyme subunit AUXIN-RESISTANT 1 (AXR1). Here, we report a chemical biology screen that identifies small molecules requiring AXR1 to modulate plant development. We selected four molecules of interest, RubNeddin1 to 4 (RN1 to 4), among which RN3 and RN4 trigger selective auxin responses at transcriptional, biochemical and morphological levels. This selective activity is explained by their ability to consistently promote the interaction between TIR1 and a specific subset of AUX/IAA proteins, stimulating the degradation of particular AUX/IAA combinations. Finally, we performed a genetic screen using RN4, the RN with the greatest potential for dissecting auxin perception, which revealed that the chromatin remodeling ATPase BRAHMA is implicated in auxin-mediated apical hook development. These results demonstrate the power of selective auxin agonists to dissect auxin perception for plant developmental functions as well as offering opportunities to discover new molecular players involved in auxin responses.

Significance statement

The plant hormone auxin coordinates almost all aspects of plant development. Throughout plant life, the expression of hundreds of genes involved in auxin regulation is orchestrated via several combinatorial and cell-specific auxin perception systems. An effective approach to dissect these complex pathways is the use of synthetic molecules that target specific processes of auxin activity. Here, we describe new synthetic auxins, RubNeddins (RNs), which act as selective auxin agonists. The RN with the greatest potential for dissecting auxin perception was RN4, which we used to reveal a new role for the chromatin remodeling ATPase BRAHMA in apical hook development. Therefore, the understanding of RN mode of action paves the way to dissecting specific molecular components involved in auxin-regulated developmental processes.

/body

Introduction

The survival and reproductive success of all living organisms depend on their ability to perceive and integrate environmental and internal signals. As sessile organisms, plants have developed strategies to adapt to their surroundings, including an extensive developmental plasticity (1). Plant morphological changes are executed through regulation of hormone levels and signaling (2). The phytohormone auxin is involved in almost all aspects of plant development and adaptation. Auxin perception within the nucleus is mediated by the TRANSPORT INHIBITOR RESISTANT 1/AUXIN SIGNALING F-BOX [TIR1/AFB]-AUXIN/INDOLE-3-ACETIC ACID [AUX/IAA] (TIR1/AFB-AUX/IAA) co-receptor complex (3). The TIR1/AFB1-5 F-box proteins are subunits of the S-PHASE KINASE ASSOCIATED PROTEIN 1-CULLIN 1-F-BOX (SCF)-type E3 ligase and act as auxin receptors (4). Formation of the SCF^{TIR1/AFB}-AUX/IAA-auxin complex leads to the ubiquitination of the AUX/IAA transcriptional repressors, targeting them for rapid degradation by the 26S proteasome (4). Removal of AUX/IAAs liberates the auxin response-activating AUXIN RESPONSE FACTOR (ARF) transcription factors from repression (4) and leads to the occurrence of auxin-transcriptional response. There is significant variation in auxin-induced degradation rates among different AUX/IAA proteins, and at least some of this variation is attributable to the specificity in the interactions between the 29 AUX/IAAs and 6 TIR1/AFB F-box proteins in *Arabidopsis* (4-6). Amino acids within and outside the degron domain II (DII) of the AUX/IAA proteins determine the interaction strength of the co-receptor and specify AUX/IAA stability (5-7). The multiplicity of the potential co-receptor assembly is the first element mediating the complexity of the auxin response.

The ubiquitin-proteasome pathway plays an essential role in plant hormone signaling (8-10). Modification of the relevant components by the ubiquitin-like protein, RELATED TO UBIQUITIN/NEURAL PRECURSOR CELL EXPRESSED DEVELOPMENTALLY DOWNREGULATED PROTEIN 8 (RUB/NEDD8), which is catalyzed by a cascade of enzymatic reactions analogous to ubiquitination, is critical for the full activity of the proteasome complex (11). In plants, the CULLINs (CUL1, CUL3, and CUL4) are NEDD8-modified proteins that form multimeric E3 ubiquitin ligase complexes (12). CUL1 acts as a scaffold within the SCF-type E3 ligases and neddylation states of CUL1 are essential for the ubiquitin ligase activity of the SCF complex (13). Loss of components of the neddylation pathway, such as the

NEDD8-activating enzyme subunit AUXIN RESISTANT 1 (AXR1), reduces the response to several phytohormones including auxin (14-17).

To understand how auxin perception mediates multiple aspects of plant development, we established an AXR1-dependent developmental defect-based chemical biology screen. Using this approach, we identified new small synthetic molecules, RubNeddins (RNs), which selectively promote SCF^{TIR1/AFB}-AUX/IAA co-receptor assembly, allowing local and precise modulation of auxin signaling pathways. Furthermore, these synthetic selective agonists possess the ability to identify and distinguish the molecular players involved in different aspects of auxin-regulated development, thereby dissecting the diversity of auxin action. We demonstrated this by employing these agonists to reveal different roles for specific AUX/IAA proteins during lateral root and apical hook development. In particular, the use of the selective auxin agonist RN4 revealed a new role for the chromatin remodeling ATPase BRAHMA in apical hook development.

Results

The rubylation/neddylation pathway is required for RubNeddins (RNs) to alter seedling development

In order to address the complexity of auxin response, we established a chemical biology screen to isolate synthetic molecules targeting the NEDD8-mediated signaling pathway in *Arabidopsis* (Fig. S1A and B). We reasoned that some of these molecules might also target the auxin signaling pathway (Fig. S1A). This strategy is complementary to previous ones aiming at isolating auxin-related small molecules (18-19). Compounds affecting auxin-related developmental processes such as primary root growth, hypocotyl elongation and gravi- or photo-tropism responses in wild type but not in *axr1-30* seedlings were selected (Fig. S1B). This screening strategy, based on differential effects upon the two genetic backgrounds (Col-0 wild type versus *axr1-30*), was essential to filter out chemical activities with general impacts on seedling growth. We hypothesized that a small molecule for which activity was dependent on the AXR1 signaling machinery could be recognized by one or several TIR1/AFB-AUX/IAA co-receptor complexes. Out of 8,000 diverse compounds (ChemBridge), we identified 34 small molecules (4.25 ‰) that selectively affected the growth of wild type compared to *axr1-30* seedlings. Four molecules, named RubNeddin (RN) 1 to 4, were ultimately selected as they showed a dose-dependent activity and a high potency on wild type seedling development in the micromolar range (Fig. S1C-E). In detail, RN1 activity decreased lateral root number and primary root length, but increased hypocotyl length and adventitious root formation (Fig. 1A and B, Fig. S2A). RN2 application resulted in the inhibition of primary root growth and lateral root formation, without affecting hypocotyl length (Fig. 1A and C). RN3 promoted the number of lateral roots (Fig. 1A and D). RN4 activity increased hypocotyl elongation and inhibited lateral root formation (Fig. 1A and E). Overall, these structurally similar compounds triggered specific morphological changes in wild type, while *axr1-30* was resistant to these effects, demonstrating that they require a functional RUB/NEDD8 signaling pathway.

The RNs act as developmental regulators in several land plants

We then analyzed RN effects on *Populus* (poplar) and *Physcomitrella patens* (moss). RN1, which induced hypocotyl elongation and promoted adventitious root formation,

and RN3, which increased lateral root number in *Arabidopsis*, were applied to three different lines of poplar explants (Fig. S2B-D). The poplar lines were selected for their different rooting abilities; T89 is an easy rooting hybrid while SwAsp 19 and 35 have a low rooting capacity even when treated with indole-3-butyric acid (IBA), an auxin commonly used as a rooting agent. Interestingly, both RN1 and RN3 promoted adventitious root formation preferentially in the SwAsp lines. Next, the effects of the RNs were investigated in moss and compared to those of IAA (Fig. S3). Similar to IAA, most of the RNs inhibited caulonemal colony outgrowth (Fig. S3A). The RN-induced effects on shoots were more diverse. At the tested concentrations, while no effect of RN1 was observed, application of RN2 caused a clear increase in shoot length, RN3 treatment resulted in thinner leaves and RN4 slightly reduced shoot size (Fig. S3B). At low concentration, IAA increased the number of buds/shoots per colony after one week (Fig. S3C), while it reduced bud/shoot formation after two weeks regardless of the concentrations tested (Fig. S3D). This dual effect of IAA was mimicked by RN4. RN1 and RN3 treatment resulted mainly in an increase of the bud/shoot number per colony after one week and RN2 only reduced bud/shoot formation after two weeks. These results demonstrate that the activities of the RNs are mediated by pathways present in several species.

The RNs partly function as prohormones

RN1, RN3 and RN4 share structural similarities with previously described prohormones (19-20). Since prohormones are hydrolyzed *in vivo* to release the active hormone moieties (21), we examined the potential metabolism of the RN compounds in liquid treatment media and *in planta* (Fig. S4). In RN-supplemented MS media without plants, negligible concentrations of free acids were detected at the 0 h time point, except for 2,4-dichlorophenoxyacetic acid (2,4-D) originating from RN2 and 2,4,5-trichloroacetic acid (2,4,5-T) from RN3 (Fig. S4D). Importantly, in these plant-free media, no obvious degradation of RN compounds was observed 24 h after treatment. However, in the presence of seedlings, higher levels of the corresponding free acids, 2,4-D, 2,4,5-T and RN4-1, were found after 24 h in the media treated with RN1, RN3 and RN4, respectively, although the level of 2,4-D in RN2-treated media was not changed (Fig. S4D). As expected, in *Arabidopsis* seedlings treated by the RNs for 24 h, all free acids were detected in the range from 0.4 to 2% relative to the levels of the corresponding RNs (Fig. S4E). These results imply that even though the RN compounds are fairly stable in liquid media, their biological activities might result from their metabolism *in planta* to the free acids 2,4-D (RN1 and RN2) and 2,4,5-T (RN3), which are known to possess auxinic activity and RN4-1 (RN4), which contains a bromo group, an electron-withdrawing substituent that can give rise to a high auxinic activity (22). To address this possibility, we first determined the appropriate treatment concentrations of 2,4-D, 2,4,5-T and RN4-1 that lead to their accumulation within roots to similar levels as found after treatments with RN1, RN3 and RN4, respectively (Fig. S5A, C and E). Then, using these determined treatment concentrations, we investigated the effects of 2,4-D on primary root length in 5-d-old seedlings (Fig. S5B) and of 2,4,5-T and RN4-1 on lateral root density in 8-d-old seedlings (Fig. S5D and F). The results revealed that 2,4-D, at an *in planta* concentration intermediate to that resulting from treatments with 0.5 and 2 μ M RN1, had an effect on primary root length that was correspondingly intermediate between these two concentrations of RN1 (Fig. S5B). This suggests that the effect of RN1 on primary root length is likely to be due to the release of 2,4-D. However, in the case of lateral root density, a much weaker effect for 2,4,5-T, or no effect at all for RN4-1,

compared to the relevant RN compound was found (Fig. S5D and S5F). These results show that the effects of RN3 and RN4 on lateral root density are only partially, or not at all, due to their degradation to the free acids 2,4,5-T or RN4-1, respectively.

We next performed a structure activity relationship (SAR) analysis by comparing the effects of various RN analogues, 2,4-D, 2,4,5-T and RN4-1 on plant development and on the expression pattern of the auxin responsive promoter *DR5* in seedlings of *pDR5::GUS* (23) (Fig. S6). The SAR analysis indicated that the absence of chlorine at position C2 in the 2,4-D substructure of RN1 (analog RN1-1) or the complete loss of the 2,4-D moiety (analog RN1-2) significantly reduced the effects of RN1 on plant development (Fig. S6A and E), implying that the 2,4-D substructure is important for RN1 activity. Modification of the 2,4-D core structure in RN2 (analog RN2-2) abolished its potency, whereas analogs displaying a side chain modification (RN2-1 or RN2-3) were as potent as RN2 (Fig. S6B and F), indicating that the activity of RN2 is most probably attributable to the release of 2,4-D in the growing media. Like RN2, none of the RN2 analogues visibly altered the *pDR5::GUS* expression pattern compared to the DMSO control. RN3 mainly promoted lateral root number, while its effect on primary root elongation was mild (Fig. 1D). Analog RN3-2 and RN3-3, with modifications on the phenylpiperazine side chain, behaved similarly to RN3 (Fig. S6C, G and H). However, removal of the whole side chain from RN3, generating 2,4,5-T, abolished its positive effect on lateral root number and introduced a strong inhibitory effect on primary root length (Fig. S6H), suggesting a difference in potency between the two compounds. Moreover, the activity of RN3 was significantly compromised by disruption of the substructure of 2,4,5-T (analog RN3-1) via loss of the three chlorines (Fig. S6C, G and H). These results suggest that the 2,4,5-T substructure is critical for RN3's potency. Further comparisons using analogs only differing in the number of chlorines on the 2,4,5-T substructure, such as between RN3-2, RN3-4 and RN3-6, or between RN3-3, RN3-5 and RN3-7, indicated that C5 chlorination of the 2,4,5-T moiety is crucial for RN3's selective activity. Intriguingly, while RN3 did not alter the *pDR5::GUS* expression pattern compared to the DMSO control, fluorination of the phenyl in RN3 induced *pDR5::GUS* expression in some cases (analog RN3-3 compared to RN3-2), while reducing it in other cases (analog RN3-5 and RN3-7 compared to RN3-4 and RN3-6, respectively) (Fig. S6C). These results reinforce the importance of C5 chlorination of the 2,4,5-T moiety for the selective activity of RN3.

We showed that RN4 releases the free acid RN4-1 *in planta* (Fig. S4D and E and Fig. S5E), possibly by hydrolysis. As expected, considering the presence of a bromo group, this compound strongly induced *pDR5::GUS* expression, in contrast to RN4 itself (Fig. S6D). While RN4-1 significantly enhanced hypocotyl elongation, it was not as potent in this regard as RN4 (Fig. S6D and I). Comparison of the effects of modifications of the RN4-1 substructure (analog RN4-2) and of the hydroxymethylphenylamine substructure (analog RN4-10) of RN4 indicate that while the intact auxinic RN4-1 moiety is indispensable for RN4's effect on the hypocotyl, the non-auxinic side chain is also required to induce maximal hypocotyl elongation (Fig. S6D and I). Further comparison between RN4-2 and RN4 as well as their free acids (RN4-3 and RN4-1, respectively) highlight the key contribution of the bromophenoxy methylation to the selective activity of RN4 on hypocotyl rather than primary root (Fig. S6DI and J). Consistent with the SAR results, even though RN4-2 shows a bipartite structure, it was still able to induce *pDR5::GUS* expression (Fig. S6D). RN4-10, in which the non-auxinic moiety of RN4 is modified, induced

pDR5::GUS expression slightly more than RN4 (Fig. S6D). We also designed RN4 analogs with predicted low hydrolysis capacity (RN4-4, RN4-8, RN4-9, and RN4-11). As expected, none of these analogs could induce hypocotyl growth (Fig. S6D and I), indicating that the typical bipartite prohormone structure of RN4 is important for its effect on hypocotyl elongation and that hydrolysis is required to liberate this activity. Moreover, except for RN4-9, these compounds could not induce pDR5::GUS. Interestingly, the analog RN4-11, generated by methylation of RN4 on the amide bond, inhibited primary root elongation without affecting hypocotyl length (Fig. S6J). As the predicted corresponding free acid RN4-1 did not reduce primary root length, this result indicates that the full, non-hydrolyzed RN4 structure possesses additional auxin-like activity.

Overall, we showed that RN1, RN3 and RN4 function as prohormones, being metabolized *in planta* to release more potent auxin agonists, while the effects of RN2 are most likely due to its degradation to 2,4-D. However, our SAR results also suggest that the non-hydrolyzed forms of RN1, RN3 and RN4 display additional auxin-like effects and therefore might themselves act as selective auxin agonists.

The RNs act as selective auxin agonists

AXR1 is a component of the neddylation pathway targeting, among others, the CUL proteins (11). To determine which CUL proteins might be involved in mediating the effects of each RN, we tested their potency on the loss of function *cul1-6*, *cul3a/b*, and *cul4-1* mutants. We limited these tests to RN1, RN3, and RN4 as we showed that RN2 activity is most probably due to its *in vitro* cleavage into 2,4-D, an already well described synthetic auxin. All three tested RNs had a lesser effect on the *cul1-6* mutant than on other CUL mutant lines (Fig. 2A), indicating that they function at the level of or upstream of CUL1. Given that signaling pathways mediated by AXR1 and CUL1 converge at the SCF complex and that the chemical structures and activities of the three RNs are related to auxin, we hypothesized that auxin receptor F-box proteins might also be required for RN activities. To test this, we examined *tir1* single and *tir1/afb* multiple mutants and found that the RN-induced phenotypes were strongly reduced when the compounds were applied on *tir1-1* and *tir1-1afb1-3afb3-4* (24-25) (Fig. 2B). Thus, a functional SCF^{TIR/AFB} complex is essential for the effects of the RNs. To further confirm this result, we tested the effect of co-treatment of the compound auxinole (26), an auxin antagonist specific for SCF^{TIR1/AFB}, together with each of the three RNs or the endogenous auxin IAA in the wild type. The RN-induced phenotypes were inhibited by auxinole (Fig. 2C), demonstrating that auxin co-receptor complex formation is essential for RN activities.

Next, we employed a molecular modeling strategy to explore the possible interactions of the RNs with the DII degron of AUX/IAA7 in the auxin-binding pocket of TIR1. Docking experiments validated that the physical property of the auxin-binding pocket was promiscuous enough to accommodate the potential steric hindrance of RN1, RN3, or RN4 (Fig. 3A-C; Movie S1). The calculated free energies (ΔG) of binding also revealed thermodynamic stability for the three RNs inside the auxin pocket of TIR1 (Fig. 3A-C and Fig. S7A). The positive control IAA was able to bind TIR1 with a $\Delta G_{(IAA-TIR1)}$ of -11.68 , whereas the negative control Tryptophan (Trp) was not, with a $\Delta G_{(Trp-TIR1)}$ of 63.34 (Fig. S7A). Among the RN analogs, RN4-1 and RN4-2 showed stronger thermodynamic stability compared to IAA. RN2 and the inactive analog RN4-8 could not dock inside the auxin-binding site to stabilize TIR1

(Fig. S7A). This last result confirmed once again that RN2 activity is most likely due to its cleavage into 2,4-D.

To experimentally confirm the binding of the RNs within the auxin co-receptor complex, we tested their ability to promote the interactions between TIR1 and AUX/IAA proteins using *in vitro* pull-down assays. First, TIR1-myc protein purified from wheat germ extract and four different GST-AUX/IAA proteins were used (27-29). IAA stimulated the interaction of TIR1-myc with all AUX/IAAs tested (Fig. 3D and Fig. S7B). All three RNs stimulated the recovery of TIR1-myc in complex with GST-SHY2/IAA3 or GST-AXR2/IAA7 to a similar extent (Fig. 3D and Fig. S7B). In the case of GST-AXR5/IAA1, RN1 stimulated the interaction with TIR1-myc while RN3 had little effect and surprisingly, RN4 decreased the basal interaction (Fig. 3D and Fig. S7B). When GST-AXR3/IAA17 was used as bait, RN1 strongly promoted the interaction with TIR1-myc, while RN3 had little effect and again, RN4 reduced the basal interaction (Fig. 3D and Fig. S7B). These data imply that RN3 and RN4 are able to selectively promote the interactions between specific TIR1 and AUX/IAA protein combinations in this system, while RN1 and IAA promoted each interaction, as shown previously for IAA (27-29). To test that these effects on TIR-AUX/IAA complex formation were not dependent on metabolism of the RN compounds in the wheat germ extract, we next performed a complementary pull-down experiment using insect cell-expressed TIR1 (as a His-MBP-FLAG-TIR1 fusion protein) with bacterially-expressed GST-AXR2/IAA7 or GST-AXR3/IAA17 in the presence of the RNs or the RN4 degradation product RN4-1 (Fig. S7C and D). In this system, the RNs again promoted selective interactions between TIR1 and AXR2/IAA7 or AXR3/IAA17, this time in the absence of potential plant hydrolases (in insect cells). Importantly, the promotion and inhibition of TIR1 interaction with AXR2/IAA7 and AXR3/IAA17 respectively by RN3 and RN4 were identical in the two *in vitro* systems. Moreover, the degradation product RN4-1 behaved differently from RN4, by not promoting the interaction between TIR1 and AXR2/IAA7 and slightly promoting the interaction between TIR1 and AXR3/IAA17, which might explain these compounds' different activities *in vivo*. In fact, we were able to confirm that the observed TIR1-AXR/IAA interactions in this system were induced or repressed specifically by the RNs and not by their free acid degradation products, as no 2,4-D, 2,4,5-T or RN4-1 could be detected at relevant time points in the pull-down reactions treated with RN1, RN3 or RN4, respectively (Fig. S7E). These data demonstrate that RN3 and RN4 are able to selectively promote the interactions between TIR1 and certain AUX/IAA proteins. Hence, our results suggest that RN3 and RN4 are not just prohormones, but also act consistently as selective auxin agonists in two different *in vitro* experimental conditions and their effects on plant development may therefore be attributable to selective auxin agonistic activity.

To test whether the RNs might also act as selective auxin agonists *in planta*, we assayed their potency in promoting the *in vivo* degradation of the AUX/IAA proteins. In a 1-h time course, IAA significantly increased the degradation rate of the four tested AUX/IAA-LUCIFERASE (LUC) proteins, while the RNs had different potency depending on the AUX/IAA proteins used (Fig. 3E-H and Fig. S7D-G). Therefore, the RN molecules act as selective auxin agonists both *in vitro* and *in vivo*, but the specificity of the interactions seems to be dependent on the experimental conditions, as the predicted behavior of AUX/IAA proteins based on their sensitivity to RN3 and RN4 in our *in planta* LUC assays did not always match that in our *in vitro* pull-down assays. While the conditions tested *in vivo* reflect RN capacity to enhance

the interactions of the different SCF^{TIR1/AFB}-AUX/IAA co-receptors within a complex molecular surrounding, those tested *in vitro* reflect the interactions in much simpler conditions. Nonetheless, our results imply that altering interaction affinity within each co-receptor complex with selective auxin agonists might modulate a multitude of specific plant development aspects.

RN3 and RN4 induce selective early transcriptional responses

The *in vitro* assays indicated that RN3 and RN4 are the most selective auxin agonists, showing different effects on different AUX/IAA proteins. Moreover, RN3 and RN4 induced distinct developmental processes, particularly on lateral root development. While RN3 enhanced the density of lateral roots without affecting primary root length in the wild type, RN4 inhibited lateral root development (Fig. 1). As these RNs promoted fast degradation of AUX/IAA proteins fused to LUC, we investigated how their activities fine-tuned events downstream of co-receptor complex formation. To this end, we performed transcriptome-wide expression profiling of *Arabidopsis* cell suspension cultures treated with IAA, RN3 and RN4, to characterize the early transcriptional responses induced by these compounds (Dataset 1). Analysis of the differentially expressed genes (DEGs) revealed subsets that were up- or down-regulated specifically by one, two or all three chemical treatments (Fig. S8A and Table S1). Among the early auxin-responsive genes identified, *AXR5/IAA1*, *IAA2*, *SHORT HYPOCOTYL 2 (SHY2)/IAA3* and *IAA30* were significantly up-regulated by IAA, RN3 and RN4 (Fig. 4A and Table S1). *IAA5* and *IAA16* expressions were induced specifically by IAA and RN3, while *IAA10* and *IAA29* expressions were upregulated selectively by IAA and RN4, revealing some differences between RN3 and RN4 in their capacity to induce early-responsive AUX/IAA genes. In total, 121 genes were differentially up-regulated by IAA, RN3 and RN4, such as *LATERAL ORGAN BOUNDARIES-DOMAIN 16 (LBD16)*, *BASIC HELIX-LOOP-HELIX 32 (BHLH32)*, *PINOID-BINDING PROTEIN 1 (PBP1)* and *PIN-FORMED 3 (PIN3)* (30-33) (Fig. 4A), confirming the potential of the RNs to modulate auxin-related developmental processes. The genes *CINNAMATE 4 HYDROXYGENASE (C4H)*, *TRANSPARENT TESTA 4 (TT4)*, *TT5*, *DEHYDRATION RESPONSE ELEMENT-BINDING PROTEIN 26 (DREB26)* and *EARLY-RESPONSIVE TO DEHYDRATION 9 (ERD9)* were commonly up-regulated by IAA and RN3 but not by RN4. These five genes are known to be tightly regulated in a tissue-specific and auxin-dependent manner to modulate lateral root density and architecture (34-38). Among the genes commonly regulated by IAA and RN4 but not RN3, we identified *MYELOBLASTOSIS 77 (MYB77)* and *BREVIX RADIX (BRX)* transcription factors, which have been shown to control lateral root formation in an auxin-dependent manner (39-40). These results correlate with the differential effects of RN3 and RN4 on lateral root development. Taken together, these data demonstrate the potential of RN3 and RN4 to specifically identify auxin-responsive genes involved in defined developmental processes such as lateral root formation. Overall, we showed that RN molecules are able to selectively trigger specific auxin perception machinery, inducing expression of specific sets of gene, and resulting in distinct developmental traits.

RN3 and RN4 induce specific subsets of auxin responsive promoters

We further investigated the abilities of RN3 and RN4 to selectively induce later auxin responses using various auxin-responsive reporter lines after 45 min, 5 h or 16 h of RN treatment. We found that neither the auxin-responsive reporter *pDR5::GUS* nor

the indicator of nuclear auxin perception *p35S::DII-Venus* (41) showed any response to RN treatment in the primary root (Fig. 4B and Fig. S8B and D). However, in the root-hypocotyl junction, the expression of *pDR5::GUS* was promoted by either longer treatment (24 h) or higher concentration (50 μ M) of RN3 or RN4 (Fig. 4C and Fig. S8C). To determine whether these effects were specific to the RNs or rather due to their free acid degradation products, we first determined the appropriate treatment concentrations of 2,4,5-T and RN4-1 that lead to their accumulation within the roots to similar levels as found after 16-h treatments with RN3 and RN4, respectively (Fig. S9A and B). While treatment with 2,4,5-T, similar to RN3, had no effect on *pDR5::GUS* expression in the root (Fig. S9C) treatment with RN4-1, in contrast to RN4, induced *pDR5::GUS* expression in the root (Fig. S9D). For other auxin-responsive reporter lines tested, RN3 and RN4 induced expression patterns that partially overlapped with those induced by IAA (Fig. 4B and C). In the primary root, the RN compounds induced *pSHY2/IAA3::GUS* and *pBODENLOS(BDL)/IAA12::GUS* expression with different patterns compared to that induced by IAA, but did not stimulate *pMASSUGU2(MSG2)/IAA19::GUS* expression (Fig 4B). Both compounds also promoted the expression of *pGATA23::GUS*, a marker of lateral root founder cell identity (42). RN4 additionally induced *pSHY2/IAA3::GUS* expression in the hypocotyl and the shoot apical meristem (SAM) (Fig. 4C). In contrast to the primary root, RN3 and RN4 induced *pMSG2/IAA19::GUS* expression in the hypocotyl (Fig. 4C), although only RN4 induced hypocotyl elongation (Fig. 1B). Treatment of these auxin-responsive reporter lines with 2,4,5-T induced similar expression patterns in the primary root as treatment with RN3 (Fig. S9C), suggesting that the observed effects of RN3 may in fact be due to 2,4,5-T activity. However, as found for the *DR5* promoter, RN4-1 induced the expression of most of the other promoters tested more strongly than RN4 in the primary root (Fig. S9D), suggesting that these two compounds affect auxin-responsive promoter expression rather differently. Despite the release of RN4-1 during RN4 treatment, the effects of RN4 appear to be prominent as this compound did not induce *pDR5::GUS* in spite of the presence of RN4-1. Our data indicates that RN3 and RN4 may be able to induce specific auxin-regulated promoters, which might be responsible for their selective activities on plant development. Indeed, these RNs activate some but not all modules of the auxin signaling pathway within the same tissue, confirming their selective auxin agonist activities.

A summary of the results obtained for the four RNs is presented in Table S2. In particular, RN3 and RN4 behave as auxin agonists, which selectively promote or inhibit AUX/IAA degradation in a reproducible manner leading to specific transcriptional regulation and developmental outputs.

AUX/IAA sensitivity to RN3 and RN4 in planta

We hypothesized that as the RN molecules show selectivity towards the auxin co-receptor complex, they might help to dissect specific functions of individual AUX/IAAs in distinct developmental processes. One approach to achieve this could be to investigate the responses of AUX/IAA gain-of-function mutants to auxin treatment; however, such a genetic approach could prove problematic due to high redundancy among the AUX/IAAs. As a potentially more effective alternative, we challenged such mutants with the specific auxin analogs RN3 and RN4.

We first focused on lateral root development as RN3 and RN4 had opposite effects on this process (Fig. 1D and E). Furthermore, based on our transcriptomic

analysis, RN3 and RN4 induce different sets of IAA-responsive genes that are known to be involved in the regulation of lateral root development (Fig. 4A). We therefore investigated the sensitivities of 8-d-old seedlings of AUX/IAA gain-of-function mutants *axr5-1/iaa1* (28), *axr2-1/iaa7* (46), *shy2-2/iaa3* (44-45) and *solitary root (slr-1)/iaa14* (43) to treatments of RN3 and RN4 with regards to lateral root development. We tested the sensitivities of these gain-of-function mutants to RN3, which increases lateral root density in Col-0 and Ler, with the Col-0 accession interestingly showing much higher sensitivity to this effect (Fig. 5A). We found that most of the mutants were also sensitive to this effect, with the exception of *slr-1/iaa14* (Fig. 5A). The mutant *shy2-2/iaa3* was more sensitive to this effect of RN3 than the wild type (Fig. 5A); however, it is important to note that in this mutant, this compound mainly induced the slight emergence of lateral root primordia rather than the emergence of well-developed lateral roots. These data suggest that apart from SLR/IAA14, the AUX/IAAs we tested are not required for the stimulatory activity of RN3 on lateral root density. We next aimed to characterize RN4 activity on lateral root development in these mutants. RN4 reduced lateral root density in Col-0 and Ler (Fig. 5B). Compared to Col-0, *axr5-1/iaa1* was resistant to this effect of RN4 at 5 μ M, while *axr2-1/iaa7* was sensitive at both tested RN4 concentrations (Fig. 5B). Interestingly, *shy2-2/iaa3* was sensitive to RN4 at 5 μ M, but resistant at 2 μ M, compared to Ler (Fig. 5B). Our results suggest that AXR5/IAA1 and SHY2/IAA3 might be degraded by RN4 to reduce lateral root density.

By using the RN molecules, we revealed potential contributions of specific AUX/IAAs to the complicated process of lateral root development. However, the sensitivities of the *aux/iaa* gain-of-function mutants to the RNs in terms of lateral root development did not exactly match the RN-induced AUX/IAA degradation/stabilization results found with our binding affinity assays. Lateral root development is a complicated process that requires the formation of a new meristem and emergence through several root layers, suggesting that the specific tissue context may affect RN activity and selectivity. We therefore decided to switch our focus to apical hook development in etiolated seedlings, a rather simpler process than lateral rooting, but one also regulated by auxin (47). Apical hook development is characterized by differential growth between the two sides of the apical hypocotyl and comprises the formation, maintenance and opening phases (48-49). We first tested the effects of RN3 and RN4 on apical hook development in the wild type (Fig. S10A). While 2 μ M RN3 did not affect apical hook development, RN4 completely abolished hook formation in a dose dependent manner (Fig. S10A and B).

We decided to exploit RN4 to understand whether selected AUX/IAAs play specific roles during apical hook development. We tested the effects of 0.5 μ M RN4 on hook development in the gain-of-function mutants *axr5-1/iaa1*, *axr2-1/iaa7* and *axr3-1/iaa17* for six days in the dark. All three mutants showed altered apical hook development compared to the wild type in control conditions (Fig. 5C, E and G). A detailed analysis of these results indicates that AXR5/IAA1 and AXR3/IAA17 need to be degraded for a proper apical hook to develop, while AXR2/IAA7 is likely stabilized during the formation phase and degraded during the maintenance phase. Similar to the wild type, *axr5-1/iaa1* showed sensitivity to RN4 during the formation phase, with no hook being present at 24 h; however, by 36 h the mutant had attained a slight hook curvature of 50 degrees, which then started opening directly (Fig. 5D). The mutant *axr2-1/iaa7* was resistant to RN4 in the formation phase (Fig. 5F) and *axr3-1/iaa17* was sensitive to RN4 (Fig. 5H). Taken together, these results indicate

that all three AUX/IAAs tested here play a role during apical hook development. In particular, our results suggest that AXR2/IAA7 is stabilized during apical hook formation while AXR5/IAA1 stabilization occurs during the maintenance phase.

The effects of 0.5 μM RN4 on AUX/IAA mutants during the first 24 h of apical hook development (Fig. 5D, F and H) correlate strikingly with our *in vitro* pull-down assay results (Fig. 3D). AXR2/IAA7 proteins strongly interacted with TIR1 in the presence of RN4 (Fig. 3D and G and Fig. S7B), suggesting that a stabilized version of this AUX/IAA should confer resistance to the RN4 auxin agonist, which is indeed what we found with the *axr2-1/iaa7* gain-of-function mutant (Fig. 5F). In contrast, AXR5/IAA1 and AXR3/IAA17 did not interact with TIR1 when RN4 was present in the pull-down assay (Fig. 3D, E and H and Fig. S7B) and the corresponding gain-of-function mutants were sensitive to the effects of RN4 on hook development (Fig. 5D and H).

Overall, our study of the effects of RN4 in particular on the AUX/IAA gain-of-function mutants, distinguishes the involvement of specific AUX/IAAs in lateral root and apical hook development. Thus, we demonstrated the potential of such selective auxin agonists in dissecting auxin perception controlling specific developmental processes *in vivo*.

Mutation in the ATPase domain of *AtBRM* confers resistance to RN4

RN4 represents a useful tool to investigate the role of auxin during early stages of skotomorphogenesis. In order to identify new molecular players involved in apical hook development, we performed a forward genetic screen of sensitivity to RN4, using an EMS-mutagenized Col-0 population and selected those mutants that were able to form an apical hook in the presence of 0.5 μM RN4 in the dark, which we named *hookback* (*hkb*) mutants. We then further selected only those of the mutants that were sensitive to the effects of 75 nM 2,4-D on seedling phenotype in the light (Fig. S10E). Using this strategy, we could exclude known auxin resistant mutants that might appear in the screen. Several independent *hkb* lines, each carrying a single recessive mutation, were isolated from the screen and we focused on characterizing one of these, *hkb1*. In contrast to Col-0, *hkb1* had formed well-curved apical hooks in the presence of RN4 24 h after germination, while under mock-treated conditions there were no major differences between the two genotypes (Fig. 6A). Whole genome sequencing of *hkb1* revealed the presence of one non-synonymous EMS-like mutation (C to T nucleotide substitution) in the coding region of the *AT2G46020* gene that encodes for the SWItch/Sucrose Non-Fermentable (SWI/SNF) chromatin remodeling ATPase *BRAHMA* (*BRM*). To confirm that the mutation in *BRM* is responsible for the resistance of *hkb1* against the negative effect of RN4 on apical hook formation, we carried out several analyses. First, we checked the phenotypes of available T-DNA mutants for *BRM*, including *brm-1*, *brm-2*, *brm-4* and *brm-5* (*ectopic expression of seed storage proteins3, essp3*) (50-51). However, we focused our investigations on *brm-5* because both *hkb1* and *brm-5* contain a mutation in the ATPase domain (52) and 4-w-old plants of the two mutants showed similar phenotypes, including twisted leaves and less siliques than wild type (Fig. 6B). Importantly, *brm-5* showed similar resistance to the effect of 0.5 μM RN4 on apical hook formation to that shown by *hkb1* (Fig. 6C and D). These results strongly suggest that the mutation in the ATPase domain of *BRM* in *hkb1* is responsible for the resistance of this mutant to RN4. Next, we crossed *hkb-1* with *brm-5* and the F2 generation was analyzed. The *hkb1xbrm-5* mutant showed the same apical hook phenotype and similar RN4 resistance as the

single *hkb1* and *brm-5* mutants (Fig. 6C and D), confirming that the mutation that confers resistance against RN4 in *hkb1* is in the *BRM* gene.

Our results suggest that BRM may function as a negative regulator of apical hook formation. Considering the resistance of both the *axr2/iaa7* gain-of-function mutant and *hkb1/brm-5* to the effect of RN4 on apical hook formation, we hypothesize that AXR2/IAA7 might negatively regulate BRM-induced gene transcription. We suggest that RN4 induces degradation of AXR2/IAA7, which may lead to BRM-mediated promotion of transcription of genes negatively regulating apical hook formation, potentially through chromatin remodeling.

Overall, our results show that selective auxin agonists can enable us to dissect the roles of specific AUX/IAAs in developmental processes, leading to the dissection of the molecular mechanisms of these processes.

Discussion

Complicated auxin perception modules translate auxin signals into a multitude of developmental responses (53-54). Several studies have demonstrated that IAA displays different affinities for different SCF^{TIR1/AFB}-AUX/IAA co-receptor complex combinations (6, 55) and specific auxin perception modules have even been shown to act sequentially during development (56). In this work, we isolated the RNs as selective auxin agonists and revealed their potential to dissect the complex and redundant mechanisms of auxin perception machinery that control specific aspects of plant development. We employed RN4 in particular as a tool to characterize specific auxin perception modules and their potential targets. Remarkably, we even found variability of RN sensitivity between different accessions in both *Arabidopsis* and poplar, pointing to future challenges towards developing the most suitable auxin agonists for specific species and/or accessions. However, it is important to emphasize that we identified degradation products released from all four RNs *in planta*, which in some cases also induced plant responses. This finding highlights that is essential to investigate the stability of any such identified auxin agonists and take into account any degradation products released.

Auxin behaves like molecular glue within the SCF^{TIR1/AFB}-AUX/IAA complex (53) by fitting into a space between the TIR1/AFB receptor and AUX/IAA co-receptor and extending the hydrophobic protein interaction surface. It has long been known that the auxin-binding pocket of SCF^{TIR1/AFB} is promiscuous, a feature which was heavily investigated during the early years of auxin research in the 1940s (57-58). During this time, several auxinic compounds were discovered including NAA, 2,4-D and picolinate auxins such as picloram (59), which are widely used today for basic research and agricultural applications. The 2,4-D and NAA modes of action are similar to that of IAA, as they also enhance the binding affinity between TIR1 and the AUX/IAAs. Their affinity to the co-receptor complex is lower than that of IAA, but they are more stable metabolically, which explains their robust activity. Although the full details of the mode of action of these synthetic auxins are not yet known, they have been instrumental in the discoveries of crucial auxin signaling components such as AXR1, AXR3/IAA17, AXR5/IAA1, AFB4 and AFB5 (60-64). Thus, synthetic compounds with auxin-like activities hold the potential to dissect the convoluted mechanisms of auxin signaling. Moreover, our isolation and characterization of RN4 revealed different activity and selectivity compared to most of the currently available synthetic auxins and thus open up new possibilities to identify novel actors in auxin biological responses.

Here, we have shown the selective capacity of RN3 and RN4 to promote the interaction of TIR1 with specific AUX/IAA co-receptors, highlighting a strong potential for such auxin agonists in defining AUX/IAA involvement in specific transcriptional responses and developmental traits. This potential was strongly supported by our genetic approach, showing that different AUX/IAA gain-of-function mutants display defined sensitivities to RN3 and RN4 in terms of lateral root development. Importantly, we uncoupled the effects of RN3 and RN4 on TIR1-AUX/IAA interactions and lateral root development from their free acid degradation products, thus confirming the usefulness of these RN compounds as selective auxin agonists. Multiple AUX/IAA-ARF modules act sequentially over time and space to orchestrate lateral root development (56, 65). Our data indicates that RN3 may promote development of lateral roots through SLR/IAA14 degradation and the stabilization of SHY2/IAA3, but we cannot yet conclude whether degradation of additional AUX/IAAs is also required for this effect. On the other hand, the resistance of the *axr5-1/iaa1* mutant to high concentrations of RN4 revealed a novel role for AXR5/IAA1 as a positive regulator of lateral root development.

Moreover, we used the RN with the greatest potential, RN4, as a tool to identify which of several AUX/IAA proteins are directly involved in apical hook development and revealed the implication of novel auxin-signaling components such as the SWI/SNF chromatin remodeling ATPase BRM. Remarkably, BRM has already been shown to be involved in auxin-dependent floral fate acquisition (66). In the inflorescence, when MONOPTEROS (MP)/ARF5 is free from AUX/IAA repression, it recruits BRM or its homolog SPLAYED (SYD) to remodel chromatin and thus promote gene transcription. Interestingly, in a yeast-three-hybrid assay, AXR3/IAA17 and BDL/IAA12 have been shown to prevent the association of MP to BRM (66). According to these results and our data showing the resistance of *axr2-1/iaa7* and *hkb1/brm-5* to RN4-mediated suppression of apical hook formation, we hypothesize that BRM, by associating with an unknown ARF transcription factor, might promote transcription of genes negatively regulating hook formation. We also hypothesize that AXR2/IAA7 might prevent the association of the ARF to BRM. Application of RN4 prompts the degradation of AXR2/IAA7, which may facilitate the association of the ARF to BRM, promoting transcription of downstream genes negatively regulating apical hook formation, potentially through chromatin remodeling. However, the hypothesis that stabilization of AXR2/IAA7 during apical hook formation blocks BRM activity raises the question of whether MP plays a role during hook development or whether BRM is recruited by other ARFs.

The different affinities of AUX/IAA proteins for IAA, RN3 and RN4 might lie in differences in residues within the DII domain. Our study thus brings us a step closer to a better quantitative understanding of the TIR1-AUX/IAA interaction system of auxin perception in a tissue-specific manner. Besides IAA, several other phytohormones including jasmonate-isoleucine, gibberellin, brassinosteroids and abscisic acid (ABA), also function by modulating the protein-protein interactions of their co-receptors (67). Isolation of novel molecules modulating such interactions could therefore also be useful in uncovering the signaling components of these phytohormones.

Auxins have many uses in agriculture, horticulture, forestry and plant tissue culture (57). The selective auxin agonists described here may also find niche applications in these fields. RN activities in the low micromolar range and

conservation of their specific developmental effects in land plants enforces this possibility. Moreover, the availability of models for ligand-bound co-receptors may allow rational design of a wider array of auxin agonists using RN structures, in particular RN4, as a starting point. Indeed, a rational design approach has already paved the way for developing agrochemicals interacting specifically with a subset of ABA receptors (69). Such an approach might also have the potential to overcome the limitations of some of the RNs, for example by enhancing stability to eliminate the release of degradation products.

Overall, the isolation and characterization of chemical modulators of plant hormone signaling is an effective way to better understand the specificity of hormonal receptors. Because of the availability of genetic and genomic methods, most chemical biology approaches are performed in model species such as *Arabidopsis*. However, chemicals which induce well-characterized effects in *Arabidopsis* can be applied to non-model species to improve crop and tree value in agriculture and forestry, respectively. The complexity of the genomes of such non-model species may also be unraveled by the use of chemicals for which target proteins or pathways are known, giving a better understanding of evolutionary mechanisms.

Materials and Methods

See *SI Appendix* for detailed experimental procedures.

Arabidopsis thaliana seedlings were grown on ½ MS medium supplemented with 0.05% MES, 1% sucrose and 0.7% agar at pH 5.6. Stock solutions of all compounds were dissolved in DMSO, which was also used in equal volume as a solvent control. Docking experiments were performed using SwissDock (69-70) with the ZINC ID of the RNs and 2P1Q crystal structure of TIR1 with the DII domain of AXR2/IAA7 (58). The best conformation was chosen according to the FullFitness (Kcal/mol). The corresponding binding energies for every conformation of each ligand were calculated using Hybrid-DFT-D3. *In vitro* pull-down assays, with epitope-tagged TIR1 expressed with TnT-T7 coupled wheat germ extract (Promega), were performed as described previously (29, 71). For the luciferase assay, 7-day-old seedlings were incubated in Bright-Glo luciferase assay system (Promega) luciferine solution (LS) for 30 min before treatment with 50 µM compounds dissolved in LS. Light emission was recorded for 5 min using a LAS-3000 (Fujifilm) and the natural log of the normalized relative light unit (RLU) was calculated as described previously (72). The degradation rate k (min^{-1}) was used to compare treatments. The transcriptomic responses induced by the RNs were investigated by RNA-Seq, using *Arabidopsis thaliana* ecotype Col-0 cell suspension culture (73) treated with 50 µM RN3, RN4, or IAA for 30 min. Total RNA was extracted from filtered cells using the RNeasy Plant Mini Kit (QIAGEN) and sent to the SNP&SEQ Technology Platform in Uppsala University for sequencing. Genes were considered significantly differentially expressed if the adjusted p-values after FDR (False Discovery Rate) correction for multiple testing were lower than 0.05. For GUS assays, seedlings were fixed in 80% acetone, washed with 0.1 M phosphate buffer and transferred to 2 mM X-GlcA (Duchefa Biochemie) in GUS buffer (0.1 % triton X100; 10 mM EDTA; 0.5 mM potassium ferrocyanide; 0.5 mM potassium ferricyanide) in the dark at 37 °C before stopping the reaction with 70 % ethanol.

Acknowledgments

For extended acknowledgments, see *SI Appendix*. This work was supported by Vetenskapsrådet VR 2013-4632 and VINNOVA (TV, MŁ, SMD, PAE, StR), Vetenskapsrådet VR 2016-00768 (QM), The Knut and Alice Wallenberg Foundation (AR), The Knut and Alice Wallenberg Foundation ShapeSystems grant 2012-0050 (SMD, StR, QM and KL), the Olle Engkvist Byggmästare Foundation (SaR), Kempestiftelserna (QM, DKB, PAE), the Carl Tryggers Foundation (QM, MT), SweTree Technologies (SMD), EMBO short term fellowship (TV), Seth M Kempe short term fellowship (TV), a travel grant from the Bröderna Edlunds Foundation (TV), National Science Foundation MCB-0929100 (JC), National Institutes of Health NIH GM43644 (ME), the Biotechnology and Biological Sciences Research Council BB/L010623/1 (SK) and the Ministry of Education, Youth and Sports of the Czech Republic (the National Program for Sustainability I Nr. LO1204 to BP and ON). LP was funded by a postdoctoral scholarship and research grant 1507013N of the Research Foundation Flanders (FWO). Chemical Biology Consortium Sweden (CBCS) is primarily funded by the Swedish Research Council (PAE).

Footnotes

Author contributions: TV, LP, StR designed research; TV, SaR, NF, MK, QM, SMD, MT, BP, AR, MŁ performed research; NF, DKB, MK, BP, ON, AI, PAE, SRH, YZ, KL, JC, FA, SK, ME contributed new reagents or analytic tools; TV, SaR, NF, SMD, MT, ON analyzed data; TV, SaR, SMD, StR wrote the paper.

The authors declare no conflict of interests.

References

1. Teichmann T, Muhr M (2015) Shaping plant architecture. *Front Plant Sci* 6:233.
2. Wolters H, Jürgens G (2009) Survival of the flexible: hormonal growth control and adaptation in plant development. *Nat Rev Genet* 10(5):305–17.
3. Calderon-Villalobos LI, Tan X, Zheng N, Estelle M (2010) Auxin perception--structural insights. *Cold Spring Harb Perspect Biol* 2(7):a005546.
4. Weijers D, Wagner D (2016) Transcriptional Responses to the Auxin Hormone. *Annu Rev Plant Biol*. doi:10.1146/annurev-arplant-043015-112122.
5. Dreher KA, Brown J, Saw RE, Callis J (2006) The *Arabidopsis* Aux/IAA protein family has diversified in degradation and auxin responsiveness. *Plant Cell* 18(3):699–714.
6. Calderón Villalobos LIA, et al. (2012) A combinatorial TIR1/AFB-Aux/IAA co-receptor system for differential sensing of auxin. *Nat Chem Biol* 8(5):477–85.
7. Moss BL, et al. (2015) Rate motifs tune Aux/IAA degradation dynamics. *Plant Physiol*. doi:10.1104/pp.15.00587.
8. Downes B, Vierstra RD (2005) Post-translational regulation in plants employing a diverse set of polypeptide tags. *Biochem Soc Trans* 33(Pt 2):393–9.

9. Hochstrasser M (2009) Origin and function of ubiquitin-like proteins. *Nature* 458(7237):422–9.
10. Kelley DR, Estelle M (2012) Ubiquitin-mediated control of plant hormone signaling. *Plant Physiol* 160(1):47–55.
11. Mergner J, Schwechheimer C (2014) The NEDD8 modification pathway in plants. *Front Plant Sci* 5:103.
12. Hua Z, Vierstra RD (2011) The cullin-RING ubiquitin-protein ligases. *Annu Rev Plant Biol* 62:299–334.
13. Petroski MD, Deshaies RJ (2005) Function and regulation of cullin-RING ubiquitin ligases. *Nat Rev Mol Cell Biol* 6(1):9–20.
14. Leyser HM, et al. (1993) *Arabidopsis* auxin-resistance gene AXR1 encodes a protein related to ubiquitin-activating enzyme E1. *Nature* 364(6433):161–4.
15. Timpte C, Lincoln C, Pickett FB, Turner J, Estelle M (1995) The AXR1 and AUX1 genes of *Arabidopsis* function in separate auxin-response pathways. *Plant J* 8(4):561–569.
16. Schwechheimer C, et al. (2001) Interactions of the COP9 signalosome with the E3 ubiquitin ligase SCFTIR1 in mediating auxin response. *Science* 292(5520):1379–82.
17. Tiryaki I, Staswick PE (2002) An *Arabidopsis* mutant defective in jasmonate response is allelic to the auxin-signaling mutant *axr1*. *Plant Physiol* 130(2):887–94.
18. Zhao, Y, et al. (2003) *SIR1*, an upstream component in auxin signaling identified by chemical genetics. *Science* 301(5636):1107–1110.
19. Christian M, Hannah WB, Lüthen H, Jones AM (2008) Identification of auxins by a chemical genomics approach. *J Exp Bot* 59(10):2757–67.
20. Savaldi-Goldstein S, et al. (2008) New auxin analogs with growth-promoting effects in intact plants reveal a chemical strategy to improve hormone delivery. *Proc Natl Acad Sci U S A* 105(39):15190–5.
21. Ettmayer P, Amidon GL, Clement B, Testa B (2004) Lessons learned from marketed and investigational prodrugs. *Journal of Medicinal Chemistry* 47(10):2393–2404.
22. Aibibuli Z, Wang Y, Tu H, Huang X, Zhang A (2012) Facile synthesis and herbicidal evaluation of 4H-3,1-benzoxazin-4-ones and 3H-quinazolin-4-ones with 2-phenoxyethyl substituents. *Molecules* 17(3): 3181–3201
23. Ulmasov T, Murfett J, Hagen G, Guilfoyle TJ (1997) Aux/IAA proteins repress expression of reporter genes containing natural and highly active synthetic auxin response elements. *Plant Cell* 9(11):1963–71.
24. Kepinski S, Leyser O (2005) The *Arabidopsis* F-box protein TIR1 is an auxin receptor. *Nature* 435(7041):446–51.

25. Dharmasiri N, Dharmasiri S, Estelle M (2005) The F-box protein TIR1 is an auxin receptor. *Nature* 435(7041):441–5.
26. Hayashi K, et al. (2012) Rational design of an auxin antagonist of the SCF(TIR1) auxin receptor complex. *ACS Chem Biol* 7(3):590–8.
27. Gray WM, Kepinski S, Rouse D, Leyser O, Estelle M (2001) Auxin regulates SCF(TIR1)-dependent degradation of AUX/IAA proteins. *Nature* 414(6861):271–6.
28. Yang X, et al. (2004) The IAA1 protein is encoded by AXR5 and is a substrate of SCF(TIR1). *Plant J* 40(5):772–82.
29. Parry G, et al. (2009) Complex regulation of the TIR1/AFB family of auxin receptors. *Proc Natl Acad Sci U S A* 106(52):22540–5.
30. Goh T, Joi S, Mimura T, Fukaki H (2012) The establishment of asymmetry in *Arabidopsis* lateral root founder cells is regulated by LBD16/ASL18 and related LBD/ASL proteins. *Development* 139(5):883–893.
31. De Rybel B, et al. (2014) Integration of growth and patterning during vascular tissue formation in *Arabidopsis*. *Science* 345(6197):1255215–1255215.
32. Vilches-Barro A, Maizel A (2015) Talking through walls: mechanisms of lateral root emergence in *Arabidopsis thaliana*. *Curr Opin Plant Biol* 23:31–8.
33. Benjamins R (2003) PINOID-mediated signaling involves calcium-binding proteins. *Plant Physiol* 132(3):1623–1630.
34. Buer CS, Djordjevic MA (2009) Architectural phenotypes in the transparent testa mutants of *Arabidopsis thaliana*. *J Exp Bot* 60(3):751–63.
35. Lewis DR, et al. (2011) Auxin and ethylene induce flavonol accumulation through distinct transcriptional networks. *Plant Physiol* 156(1):144–64.
36. Krishnaswamy S, Verma S, Rahman MH, Kav NN V (2011) Functional characterization of four APETALA2-family genes (RAP2.6, RAP2.6L, DREB19 and DREB26) in *Arabidopsis*. *Plant Mol Biol* 75(1–2):107–27.
37. Chen J-H, et al. (2012) Drought and salt stress tolerance of an *Arabidopsis* glutathione S-transferase U17 knockout mutant are attributed to the combined effect of glutathione and abscisic acid. *Plant Physiol* 158(1): 340-351.
38. Jiang H-W, et al. (2010) A glutathione S-transferase regulated by light and hormones participates in the modulation of *Arabidopsis* seedling development. *Plant Physiol* 154(4):1646–58.
39. Shin R, et al. (2007) The *Arabidopsis* transcription factor MYB77 modulates auxin signal transduction. *Plant Cell* 19(8):2440–53.
40. Li J, et al. (2009) BREVIS RADIX is involved in cytokinin-mediated inhibition of lateral root initiation in *Arabidopsis*. *Planta* 229(3):593–603.
41. Brunoud G, et al. (2012) A novel sensor to map auxin response and distribution

- at high spatio-temporal resolution. *Nature* 482(7383):103–6.
42. De Rybel B, et al. (2010) A novel aux/IAA28 signaling cascade activates GATA23-dependent specification of lateral root founder cell identity. *Curr Biol* 20(19):1697–706.
 43. Fukaki H, Tameda S, Masuda H, Tasaka, M (2002) Lateral root formation is blocked by a gain-of-function mutation in the *SOLITARY-ROOT/IAA14* gene of *Arabidopsis*. *The Plant Journal* 29(2): 153-168.
 44. Tian Q, Reed J W (1999) Control of auxin-regulated root development by the *Arabidopsis thaliana* *SHY2/IAA3* gene. *Development* 126(4): 711-721.
 45. Goh T, Kasahara H, Mimura T, Kamiya Y, Fukaki H (2012) Multiple AUX/IAA–ARF modules regulate lateral root formation: the role of *Arabidopsis* *SHY2/IAA3*-mediated auxin signalling. *Phil. Trans. R. Soc. B* 367(1595): 1461-1468.
 46. Nagpal P, Walker L M, Young J C, Sonawala A, Timpte C, Estelle M, Reed J W (2000) *AXR2* encodes a member of the Aux/IAA protein family. *Plant Physiol* 123(2): 563-574.
 47. Abbas M, Alabadí D, Blázquez M A (2013) Differential growth at the apical hook: all roads lead to auxin. *Frontiers in Plant Science* 4: 441
 48. Raz V, Ecker J R (1999) Regulation of differential growth in the apical hook of *Arabidopsis*. *Development* 126(16): 3661-3668.
 49. Žádníková P, Petrášek J, Marhavý P, Raz V, Vandebussche F, Ding Z, Schwarzerová K, Morita M T, Tasaka M, Hejátko J, Van Der Straeten D (2010) Role of PIN-mediated auxin efflux in apical hook development of *Arabidopsis thaliana*. *Development* 137(4): 607-617.
 50. Hurtado L, Farrona S, Reyes J C (2006) The putative SWI/SNF complex subunit BRAHMA activates flower homeotic genes in *Arabidopsis thaliana*. *Plant Molecular Biology* 62(1): 291-304.
 51. Tang X, Hou A, Babu M, Nguyen V, Hurtado L, Lu Q, Reyes J C, Wang A, Keller W A, Harada J J, Tsang E W (2008). The *Arabidopsis* BRAHMA chromatin-remodeling ATPase is involved in repression of seed maturation genes in leaves. *Plant Physiol* 147(3): 1143-1157.
 52. Farrona S, Hurtado L, Bowman J L, Reyes J C (2004) The *Arabidopsis thaliana* SNF2 homolog AtBRM controls shoot development and flowering. *Development* 131(20): 4965-4975.
 53. Wang R, Estelle M (2014) Diversity and specificity: auxin perception and signaling through the TIR1/AFB pathway. *Curr Opin Plant Biol* 21:51–8.
 54. Salehin M, Bagchi R, Estelle M (2015) SCFTIR1/AFB-based auxin perception: mechanism and role in plant growth and development. *Plant Cell* 27(1):9–19.
 55. Havens KA, et al. (2012) A synthetic approach reveals extensive tunability of auxin signaling. *Plant Physiol* 160(1):135–42.

56. Lavenus J, et al. (2013) Lateral root development in *Arabidopsis*: fifty shades of auxin. *Trends Plant Sci* 18(8):450–8.
57. Jönsson Å (1961) Chemical structure and growth activity of auxins and antiauxins. *Encyclopedia of Plant Physiology* (Springer Berlin Heidelberg), pp 959–1006.
58. Tan X, et al. (2007) Mechanism of auxin perception by the TIR1 ubiquitin ligase. *Nature* 446(7136):640–5.
59. Ma Q, Grones P, Robert S (2017) Auxin signaling: a big question to be addressed by small molecules. *Journal of Experimental Botany* 69(2):313–328.
60. Maher E P, Martindale S J B (1980) Mutants of *Arabidopsis thaliana* with altered responses to auxins and gravity. *Biochemical Genetics* 18(11): 1041–1053.
61. Estelle MA, Somerville C (1987) Auxin-resistant mutants of *Arabidopsis thaliana* with an altered morphology. *MGG Mol Gen Genet* 206(2):200–206.
62. Woodward AW, Bartel B (2005) Auxin: regulation, action, and interaction. *Annals of Botany* 95(5): 707–735.
63. Walsh TA, et al. (2006) Mutations in an auxin receptor homolog AFB5 and in SGT1b confer resistance to synthetic picolinate auxins and not to 2,4-dichlorophenoxyacetic acid or indole-3-acetic acid in *Arabidopsis*. *Plant Physiol* 142(2):542–52.
64. Prigge MJ, et al. (2016) The *Arabidopsis* auxin receptor F-Box proteins AFB4 and AFB5 are required for response to the synthetic auxin picloram. *G3 Genes/Genomes/Genetics* 6(5):1383.
65. De Smet I, et al. (2010) Bimodular auxin response controls organogenesis in *Arabidopsis*. *Proc Natl Acad Sci U S A* 107(6): 2705–2710.
66. Wu M F, Yamaguchi N, Xiao J, Bargmann B, Estelle M, Sang Y, Wagner D (2015) Auxin-regulated chromatin switch directs acquisition of flower primordium founder fate. *Elife* 4: 09269.
67. Rigal A, Ma Q, Robert S (2014) Unraveling hormone signaling by the use of small molecules. *Frontiers in Plant Science* 5.
68. Park S-Y, et al. (2015) Agrochemical control of plant water use using engineered abscisic acid receptors. *Nature* 520(7548):545–548.
69. Grosdidier A, Zoete V, Michielin O (2011) SwissDock, a protein-small molecule docking web service based on EADock DSS. *Nucleic Acids Res* 39(Web Server issue):W270–7.
70. Grosdidier A, Zoete V, Michielin O (2011) Fast docking using the CHARMM force field with EADock DSS. *J Comput Chem* 32(10):2149–59.
71. Yu H, et al. (2013) Mutations in the TIR1 auxin receptor that increase affinity for auxin/indole-3-acetic acid proteins result in auxin hypersensitivity. *Plant Physiol* 162(1):295–303.

72. Gilkerson J, et al. (2009) Isolation and characterization of *cull1-7*, a recessive allele of CULLIN1 that disrupts SCF function at the C terminus of CUL1 in *Arabidopsis thaliana*. *Genetics* 181(3):945–63.
73. Fülöp K, et al. (2005) The Medicago CDKC;1-CYCLINT;1 kinase complex phosphorylates the carboxy-terminal domain of RNA polymerase II and promotes transcription. *Plant J* 42(6):810–20.

Figure Legends

Figure 1. Four RN chemicals trigger different morphological changes. (A) Col-0 seedlings were grown on RN-supplemented media for eight days. DMSO was used as control. Images display the effects of the RN at a representative concentration: RN1: 2 μ M; RN2: 0.5 μ M; RN3: 2 μ M; RN4: 5 μ M. (B-E) RN1 (B), RN2 (C), RN3 (D) and RN4 (E) selectively affected primary root length (RL), hypocotyl length (HL) and the number of lateral roots (LR). (B-E) For each graph, the RN structure is reported. Statistics were performed using ANOVA and Tukey's test. Means \pm SEM are shown, $n = 10$ seedlings for each concentration of the dose response, different letters are displayed for p -value < 0.05 . Scale bars indicate 1 cm (A). Concentrations in μ M are indicated in brackets (B-E).

Figure 2. RN-induced phenotypes require the formation of a functional auxin-SCF^{TIR1/AFB} complex. (A-C) Relative (treated/DMSO) (A-B) or absolute (C) hypocotyl length (upper charts) and lateral root density (lower charts) were measured for wild type (Col-0) and mutant seedlings grown on media supplemented with RN compounds for seven days. DMSO was used as control. (A) *axr1-30*, *cull1-6*, *cul3a/b* and *cul4-1*. (B) *tir1-1* and *tir1-1afb1-3afb3-4*. (C) Auxinole competition assay on Col-0. Statistics were performed using ANOVA and Tukey's test. Means \pm SEM are shown, $n = 30$ seedlings across 3 independent replicates, p -value: $**P < 0.01$, $***P < 0.001$ (A-B) or different letters are displayed for p -value < 0.05 (C). Concentrations in μ M are indicated in brackets.

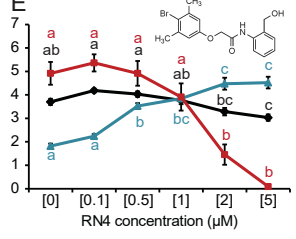
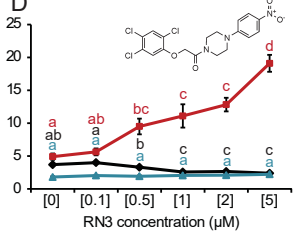
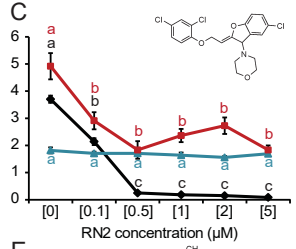
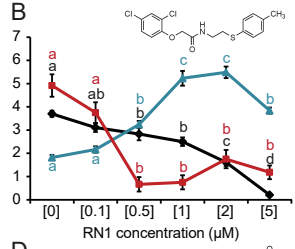
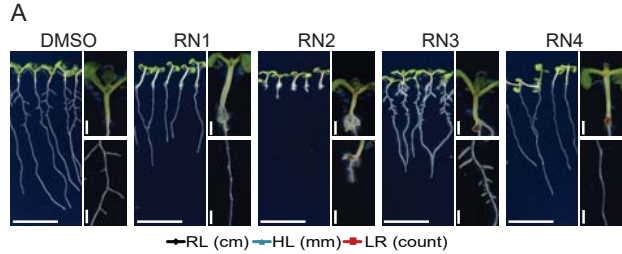
Figure 3. RN3 and RN4 act as selective agonists of auxin. (A-C) The RNs showed different thermodynamic stabilities from the calculated free energies (ΔG). RN1 (A), RN3 (B) and RN4 (C) were sterically favorable for the binding of the AUX/IAA7 DII degron. TIR1 is presented in gray and the AUX/IAA7 DII degron, which was included afterwards to observe any conflict with the RNs, is in purple. Thermodynamic stability was computed within the TIR1 auxin binding pocket and the most stable conformation(s) is represented. (D) The potential of the RNs (at 50 μ M) to promote the formation of the co-receptor complex was performed using *in vitro* translated TIR1-myc and recombinant GST-AUX/IAAs. Depending on the GST-AUX/IAA translational fusion used for the *in vitro* GST pull-down, the RNs selectively increased the recovery of TIR1-myc. (E-H) AUX/IAA degradation was assayed *in planta* using *Arabidopsis* lines constitutively expressing different AUX/IAA-LUCs in the presence of RNs at 50 μ M. Effects of the RNs on the *in vivo* degradation rate k of AXR5/IAA1-LUC (E), SHY2/IAA3-LUC (F), AXR2/IAA7-LUC (G) or AXR3/IAA17-LUC (H) translational fusions. Statistical analyses were performed using the Student's t-test. Means \pm SEM are shown, $n = 30$ seedlings across 5 independent replicates, p -value: $\cdot P < 0.1$, $*P < 0.05$, $**P < 0.01$, $***P < 0.001$.

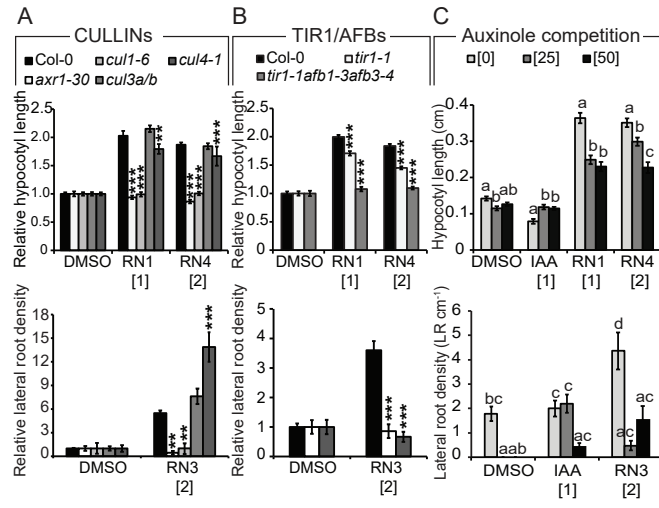
Figure 4. RN3 and RN4 activate independent auxin responses. (A) Selected sets of upregulated genes in cell culture representing: IAA-specific-induced genes (dark

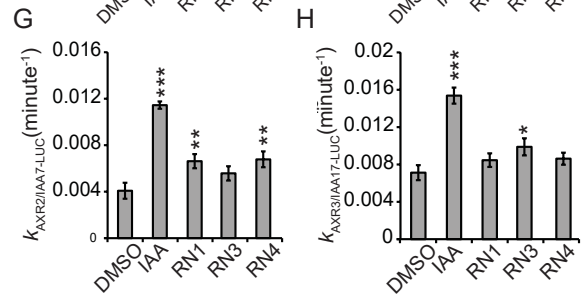
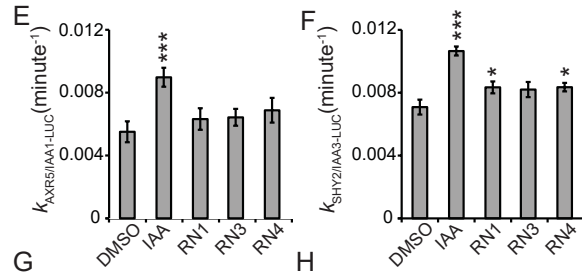
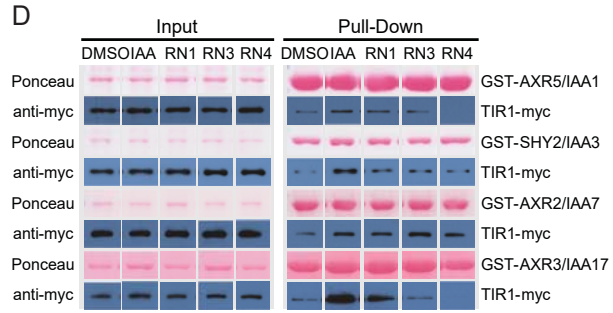
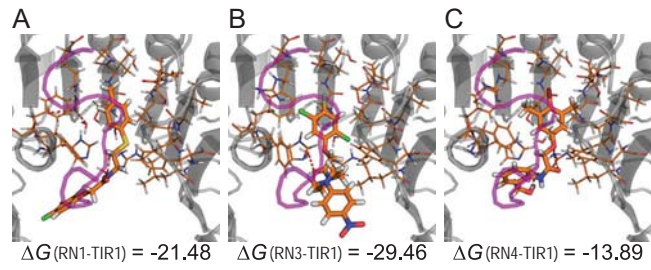
blue); IAA-, RN3- and RN4-induced genes (light blue); IAA- and RN3-specific-induced genes (lilac) and IAA- and RN4-specific-induced genes (green) (see Dataset 1 for the complete list of genes and Table S1 for fold induction values of the selected genes). (B-C) Five-d-old seedlings expressing p*DR5*::GUS, p*SHY2/IAA3*::GUS, p*BDL/IAA12*::GUS, p*MSG2/IAA19*::GUS or p*GATA23*::GUS transcriptional fusions treated with IAA, RN3 and RN4 at 10 μ M for 16 h. DMSO was used as control. (B) Representative primary roots after GUS staining. (C) Representative hypocotyl-root junctions after GUS staining. Scale bars indicate 100 μ m (B) and 1 mm (C).

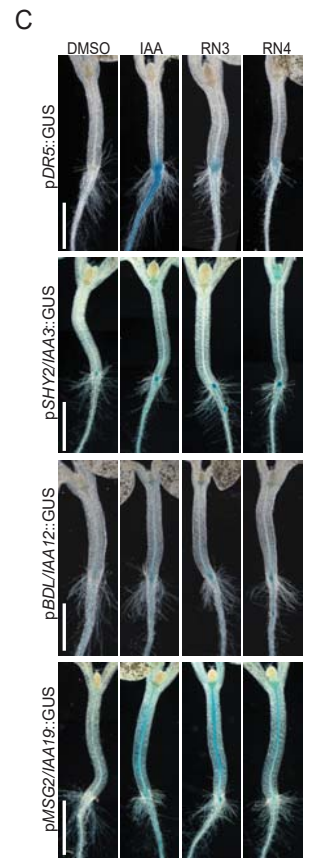
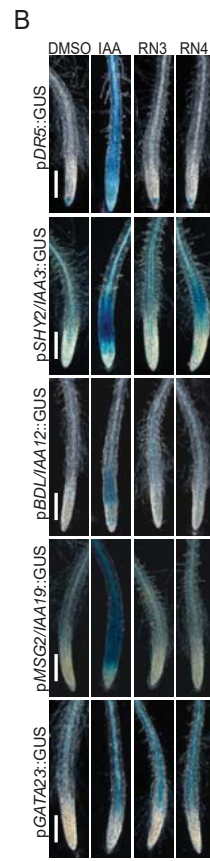
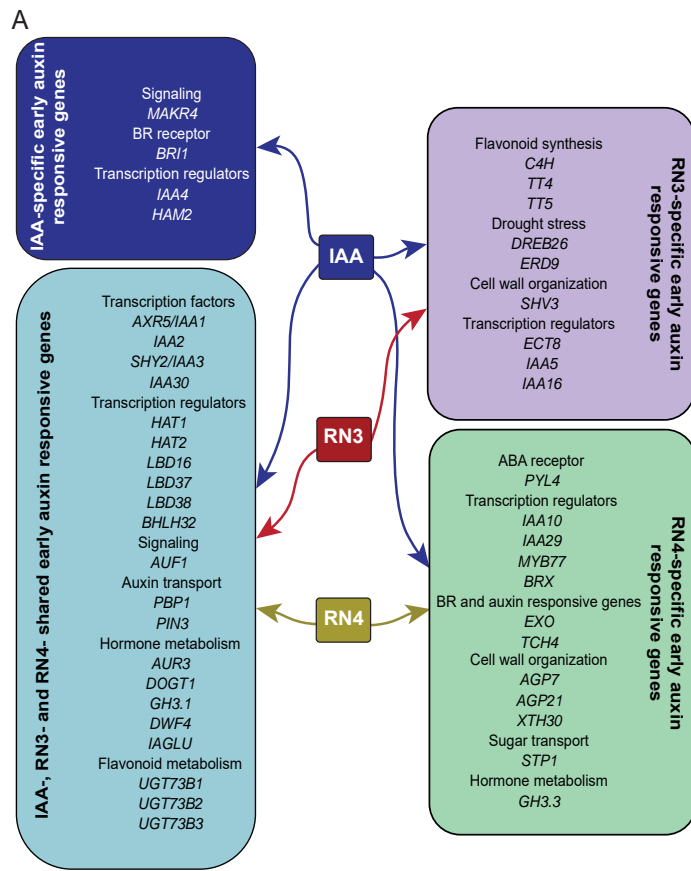
Figure 5. RN-induced phenotypes require the degradation of specific AUX/IAAs. (A-B) Relative lateral root density (treated/DMSO) was measured for gain-of-function mutants *axr5-1/iaa1*, *axr2-1/iaa7*, *slr-1/iaa14* and *shy2-2/iaa3* and their respective wild type grown on media supplemented with RN3 (A) and RN4 (B) for eight days. DMSO was used as control. Statistical analyses were performed using Student's t-test (A), or ANOVA and Tukey's test (B) to compare the effect of RN3 (A) or RN4 (B) relative to the DMSO control for each genotype, as indicated with triple asterisks and square brackets (A) or different letters (B). The Student's t-test was used to compare the relative effect of RN3 (A) or RN4 (B) on the mutants to that on the relevant wild type, as indicated with single asterisks. (C-H) Gain-of-function mutants *axr5-1/iaa1* (C, D), *axr2-1/iaa7* (E, F) and *axr3-1/iaa17* (G, H) were grown in the dark on DMSO (C, E, G) and RN4 (D, F, H) supplemented media for 6 days. Measurement of apical hook angle was performed every three hours. Means \pm SEM are shown, $n > 20$ seedlings across 3 independent replicates, p-value: * $P < 0.05$, ** $P < 0.01$, *** $P < 0.001$, different letters indicate significant differences at $P < 0.05$. Concentrations in μ M are indicated in brackets.

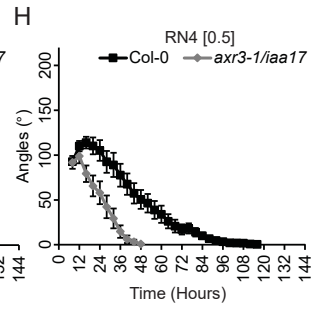
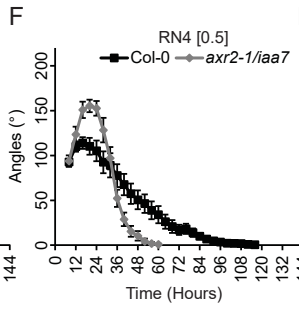
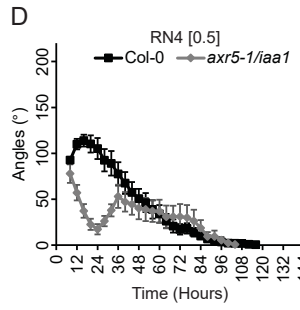
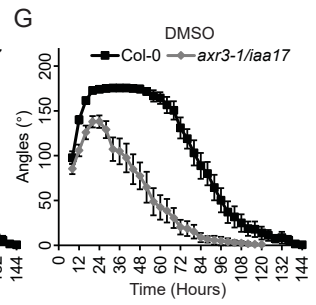
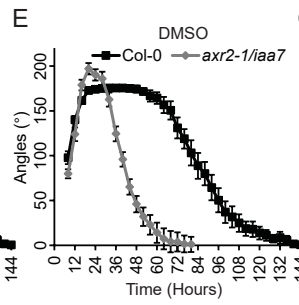
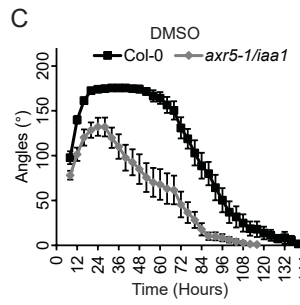
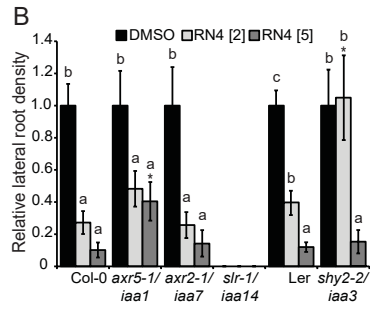
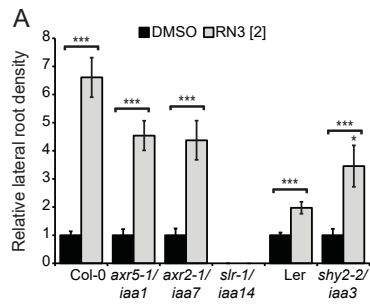
Figure 6. The *hkb1* mutant is resistant to the RN4 effect on apical hook development and carries a mutation on *BRAHMA* (*BRM*). (A) Comparison of apical hook phenotype in Col-0 and *hkb1* seedlings 24 h after germination in the dark. The seedlings were grown on media supplemented with DMSO (upper panel) or RN4 (lower panel). (B) Four-w-old Col-0, *hkb1* and *brm-5* grown in long-day greenhouse conditions. (C-D) Apical hook angle in Col-0, *hkb1*, *brm-5* and *hkb1xbrm-5* grown on DMSO (C) and 0.5 μ M RN4 (D) supplemented media for 6 days in the dark. Measurement of apical hook angle was performed every three hours. Means \pm SEM are shown, $n > 18$ seedlings across 2 independent replicates. Scale bars indicate 2 mm (A) and 1 cm (B). Concentrations in μ M are indicated in brackets.

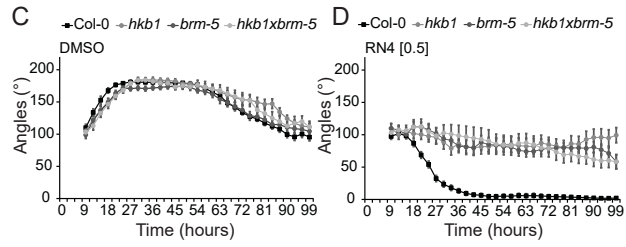
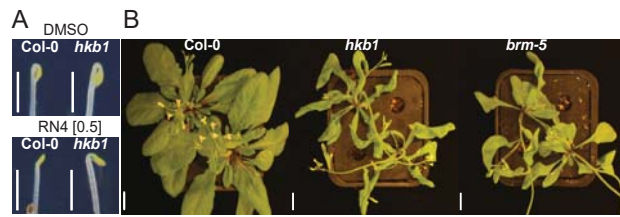














Supplementary Information for

Selective auxin agonists induce specific AUX/IAA protein degradation to modulate plant development

Thomas Vain, Sara Raggi, Noel Ferro, Deepak Kumar Barange, Martin Kieffer, Qian Ma, Siansa M. Doyle, Mattias Thelander, Barbora Pařízková, Ondřej Novák, Alexandre Ismail, Per Anders Enquist, Adeline Rigal, Małgorzata Łangowska, Sigurd Ramans Harborough, Yi Zhang, Karin Ljung, Judy Callis, Fredrik Almqvist, Stefan Kepinski, Mark Estelle, Laurens Pauwels and Stéphanie Robert.

Corresponding author: Stéphanie Robert

Email: stephanie.robert@slu.se

This PDF file includes:

- Supplementary Materials and Methods
- Figs. S1 to S10
- Tables S1 to S2
- Caption for Movie S1
- Caption for Dataset 1
- One Supplementary Document “Chemical Synthesis and Characterization”
- Extended Acknowledgments
- References for SI Appendix

Other supplementary materials for this manuscript include the following:

- Movie S1
- Dataset S1

Supplementary Materials and Methods

Plant materials and growth conditions

Seedlings of *Arabidopsis thaliana* were grown at 22°C with 16 h light per day (or in darkness for apical hook analysis) on vertical plates containing growth medium (GM): 1/2 MS (Duchefa Biochemie, Haarlem, The Netherlands); 0.05 % morpholinoethanesulfonic acid (Sigma-Aldrich); 1 % sucrose; 0.7 % agar (Duchefa Biochemie); pH 5.6. Short-term chemical treatments were performed in liquid GM, from which the agar was omitted. Two-day cold stratification of seeds was performed prior to seedling growth. The generation of the *Arabidopsis* lines *axr1-30* (SAIL_904_E06) (1), pDR5::GUS (2), *cul1-6* (3), *cul3a-3cul3b-1* (4), *cul4-1* (5), *tir1-1* (6), *tir1-1afb1-3afb3-4* (7), AXR5/IAA1-LUC (8), AXR3/IAA17-LUC (9), pMSG2/IAA19::GUS (10), pSHY2/IAA3::GUS (11), pBDL/IAA12::GUS (11), GATA23::GUS (12), p35S::DII-Venus (13), *axr5-1* (14), *axr2-1* (15), *slr-1* (16), *shy2-2* (17), *axr3-1* (18), *brm-1* (19), *brm-2* (19), *brm-4* (20) and *brm-5* (20) have been previously described. The SHY2/IAA3-LUC and AXR2/IAA7-LUC transgenic lines and the *hkb1* and *hkb1xbrm-5* mutants were created/identified in this work.

Chemical treatments

For the chemical biology screen, phenotypic screening was performed on a diverse set of 8,000 compounds (ChemBridge) in 24-well plates containing solid growth media supplemented with chemicals dissolved in dimethyl sulfoxide (DMSO) at 17 µM. *Arabidopsis* seedlings of Col-0 and *axr1-30* were grown side by side (in the same well) for 5 days in the wells. DMSO controls were present in each plate. Compounds were selected for their capacity to alter development of Col-0 without affecting *axr1-30*. The 34 hits were repeated three times using DMSO and 1-Naphthaleneacetic acid (NAA) as negative and positive controls. Dose responses were performed in 24-well plates from newly ordered compounds using the ChemBridge identification number (CBID, www.hit2lead.com). Stock solutions of the RNs and all other compounds used were dissolved at 10 mM in DMSO for all further experiments. For the ChemBridge IDs of RN1-4, see Table S2. DMSO treatments were used in equal volume as solvent control. For germination and growth of seedlings on chemicals, seeds were sown directly on chemical-supplemented media. Short-term chemical treatments were performed in liquid GM, from which the agar was omitted.

Chemical synthesis of RN1, RN3 and RN4 and purity assessments of the four RNs

We synthesized the four RN compounds with confirmed chemical identities and their purities in stock solutions were estimated to be higher than 97.99% (Supplementary document 1).

Adventitious root induction in poplar

The poplar lines used in this study were the *Populus tremuloides* x *tremula* hybrid aspen clone T89 (21) and lines number 19 and 35 from the Swedish Aspen (SwAsp) collection of natural populations of *P. tremula* (22). *In vitro* clonal propagation of the lines was performed by transferring shoot cuttings from 4-w-old *in vitro* plants to fresh ½ MS medium (Duchefa Biochemie) at pH 5.6 with 0.27% Phytigel (Sigma) and maintaining the cuttings on a day/night cycle of 16 h at 22 °C / 8 h at 18 °C. Cuttings were kept in shade by covering with white paper until 2 weeks old, after which the paper was removed. Stock solutions of 10 mM indole-3-

butyric acid (IBA), RN1 and RN3 were made in DMSO. For poplar chemical treatments, 7 cuttings per line and treatment were propagated as usual, but to medium supplemented with solvent (control) or 1 μ M or 5 μ M IBA, RN1 or RN3 and 4 biological replicates were performed, on different weeks. Nine days after treatment, all cuttings were transferred to fresh treatment-free medium and growth was continued for 3 more weeks. The number of adventitious roots per cutting was counted 4 weeks after treatment.

Moss growth tests

Physcomitrella patens, subspecies *patens*, strain Gransden 2004, was used. Protonemal tissue was cultivated as described previously (23). Small pieces of protonemal tissue were shaped into 1 mm balls and inoculated on solid BCD medium with supplements as described in the results section, six balls per plate. DMSO solvent controls were included. Buds and gametophores were counted after 1 and 2 weeks of growth using a dissecting microscope. After 4 weeks, colonies were photographed and a subset of large gametophores formed outside the original inoculum of each colony was harvested, examined and photographed.

Stability of the RN compounds

Five-d-old *Arabidopsis* seedlings were transferred to liquid media containing RN-compounds (50 μ M) or DMSO as mock control. Treatment media were collected directly after solubilization of the molecules and after 24 h in the presence or absence of the plants. Whole seedlings were collected in three replicates after 24 h treatments, immediately frozen in liquid nitrogen and stored at -80°C until extraction. For quantification of RNs and their associated free acids, the growing media were diluted 1/10 by methanol, 2 μ l was injected onto a reversed-phase column (Kinetex C18 100A, 50 x 2.1 mm, 1.7 μ m; Phenomenex) and analyzed by liquid chromatography–tandem mass spectrometry (LC-MS/MS), see below. The second set of samples (approx. 100 mg plant material fresh weight) was extracted in 1 ml of methanol using a MixerMill MM 301 bead mill (Retsch GmbH) at a frequency of 29 Hz for 10 min after adding 2 mm ceria-stabilized zirconium oxide beads. The plant extracts were incubated at 4°C with continuous shaking (10 min), centrifuged (15 min, 23 000 g at 4°C), divided into three technical replicates and purified by liquid-liquid extraction using Hexan:Methanol:H₂O (1:2:0.1) to remove impurities and the sample matrix. After 15 min incubation, the methanolic fractions were removed, evaporated to dryness *in vacuo* and dissolved in 100 μ l of methanol prior to LC-MS/MS analysis, using a 1290 Infinity LC system and a 6490 Triple Quadrupole LC/MS system with Jet Stream and Dual Ion Funnel technologies (Agilent Technologies). After injection (2 μ l), the purified samples were eluted using a 5 min gradient comprised of 0.1% acetic acid in methanol and 0.1% acetic acid in water at a flow rate of 0.5 ml min⁻¹, and column temperature of 40°C . The following binary linear gradient was used: 0 min, 10:90 A:B; 9.0 min, 95:5 A:B. At the end of the gradient, the column was washed with 100% methanol (0.5 min), and re-equilibrated to initial conditions (1 min). The effluent was introduced into the MS system with the optimal settings as follows: Drying Gas Temperature, 150°C ; Drying Gas Flow, 16 l min⁻¹; Nebulizer Pressure, 40 psi; Sheath Gas Temperature, 375°C , Sheath Gas Flow, 12 l min⁻¹; Capillary Voltage, 3000 V; Nozzle Voltage, 0 V; Delta iFunnel High/Low Pressure RF, 110/60 V; and Fragmentor, 380 V. Quantification and confirmation were obtained by the various MRM diagnostic transitions of the precursor and the appropriate product ions using optimal collision energies and 50 msec dwell time (Fig. S4B). Chromatograms were analyzed using MassHunter

software (version B.05.02; Agilent Technologies), and the compounds were quantified by according to their recovery listed in Fig S4C.

GUS assays

Seedlings of *Arabidopsis* expressing GUS were fixed in 80% acetone at -20 °C for 20 min and washed with 0.1 M phosphate buffer (Na₂HPO₄ / NaH₂PO₄) at pH 7. Samples were transferred to GUS staining solution: 2 mM X-GlcA (Duchefa Biochemie) in GUS buffer (0.1 % triton X100; 10 mM EDTA; 0.5 mM potassium ferrocyanide; 0.5 mM potassium ferricyanide) in the dark at 37 °C. The staining reaction was stopped using 70 % ethanol and the seedlings were mounted in either 50 % glycerol or a mixture of chloral hydrate: glycerol: H₂O (8:3:1). Samples were observed using a Zeiss Axioplan.

Molecular modeling

Docking experiments were performed using SwissDock (24-25) with the ZINC ID of the RNs (RN1: ZINC2978909; RN2: ZINC19770708, ZINC19770709; RN3: ZINC11461779; RN4: ZINC01160095) and 2P1Q crystal structure of TIR1 with the DII domain of AXR2/IAA7 (26). The best conformation was chosen according to the FullFitness (Kcal/mol). The input geometries of the ligands coming from docking analysis were optimized inside of the auxin binding surface of TIR1 using density functional theory calculations including dispersion correction terms (DFT-D3) to better understand the supramolecular associations (27). The corresponding binding energies for every conformation of each ligand were calculated using Hybrid-DFT-D3. The analysis of the binding energies considered the intrinsic binding energy of the ligand and the binding surface as well as the solvation energies and van der Waals (VdW) forces.

In vitro pull-down assays

The *in vitro* pull-down assays, with epitope-tagged TIR1 expressed with TnT-T7 coupled wheat germ extract (Promega), were performed as described previously (7, 28). TIR1-myc protein was incubated with bacterially expressed GST-AUX/IAA beads in pull-down buffer (25 mM Tris-HCl pH 7.5; 150 mM NaCl; 0.05 % Igepal (Sigma-Aldrich); 10 % Glycerol; 1 mM DTT; 1 mM PMSF; 20 μM MG-132 (Sigma-Aldrich); Protease Inhibitor Cocktail (Roche)) in the presence of DMSO or the compounds at 50 μM for 3 h at 4°C. After washing, proteins were eluted using reduced glutathione (Sigma-Aldrich), separated using SDS-PAGE and visualized using Ponceau staining for the GST-AUX/IAA proteins and anti-c-Myc-peroxydase (Life Technologies) for TIR1-myc. The amount of TIR1-myc in the complex was determined by western blot using anti-myc. The quantity of TIR1-myc pulled down is representative of the strength of co-receptor complex formation.

In-vitro pull-down assays with insect cell-expressed epitope-tagged TIR1 were performed using a similar protocol as described previously (29). His-MBP-FLAG -TIR1 proteins were produced using recombinant baculovirus with *Trichoplusia ni* host cells and purified as previously reported (30). GST-AXR2/IAA7 has been described previously (31). GST-AXR3/IAA17 was constructed by ligating the gene coding sequence as a BamH1-XhoI fragment into pGEX-4T-2 following PCR amplification with the following primers: BHIAXR3 5'-GTGGATCCGGCAGTGTGCGAGCTGAAT-3' and AXR3XHOI 5'-GTCTCGAGTCAAGCTCTGCTCTTGCA-3'. GST-IAA proteins were purified and immobilized on Sepharose 4B beads (GE Healthcare) as described previously (29). Pull-down assays were performed by incubating His-MBP-FLAG -TIR1 protein with Sepharose-GST-IAA

beads in extraction buffer (EB; 150 mM NaCl, 100 mM Tris pH7.5, 0.5% NP-40, 10 mM DTT, 1 mM PMSF, 10 μ M MG-132) in the presence of DMSO or compounds at 50 μ M for 2h at 4°C. After washing, proteins were eluted with hot (70°C) 1 x NuPage LDS sample buffer with 1 x NuPage reducing agent (Life Technologies), separated by SDS-PAGE (NuPAGE Novex 4–12% Bis-Tris gel/ 1 x NuPage MES buffer, Life Technologies) and visualized using Ponceau staining for the GST-AUX/IAA proteins and anti-Flag M2 Peroxidase antibody (Sigma) for His-MBP-FLAG -TIR1.

Creation of the transgenic lines for in vivo AUX/IAA degradation assay

For SHY2/IAA3, site-directed mutagenesis was used to create a silent mutation (coding nt 489 A to C), removing an internal NcoI site in SHY2/IAA3 cDNA (ABRC, C00011). The ORF was then PCR amplified using 5' primer (3-104, GGCGGTACCAATGGATGAGTTTGTAAACC) and 3' primer (3-105, GGCGCCATGGCTACACCACAGCCTAAACC) to introduce a Kpn site 5' of the start site and at the 3' end to remove the stop codon and replace it with an NcoI site. The product was digested with KpnI and NcoI and ligated into a pGREENII-based plasmid containing a KpnI and NcoI site between the 5' UBQ10 flanking region and a luciferase coding region as described previously (8), placing the SHY2/IAA3 ORF in-frame with the LUC coding region. For AXR2/IAA7, site-directed mutagenesis was used to create a silent mutation (coding nt 525 C to T), removing an internal BspHI site in AXR2/IAA7 cDNA (ABRC, C00014). The ORF was then PCR amplified using 5' and 3' primers (3-122, GGCGGTACCAATGATCGGCCAACTTATG) and (3-123, GGCGTCATGACAGATCTGTTCTTGCAGTAC), respectively, the PCR product digested with Kpn and BspHI and ligated into the same pGREENII-based plasmid (above). Both ORFs were sequence verified, the plasmids introduced into *Arabidopsis thaliana* ecotype Col and multiple lines segregating for a single insertion were made homozygous as described previously (8). Transgenic lines expressing AXR5/IAA1-LUC (8) and AXR3/IAA17-LUC were described previously (9).

Luciferase assay

Seeds of each genotype were sown individually in flat-bottom white Polystyrene 96-well plates (Fisher Scientific) containing 100 μ L GM. After 7 days, the GM was replaced by 40 μ L Bright-Glo luciferase assay system (Promega) diluted 10 times in GM (luciferine solution; LS) and the plates were incubated for 30 min. At zero time point, compounds dissolved in LS were added to each well to a final concentration of 50 μ M in 50 μ L. Single seedling light emission was recorded for 5 min at the indicated time point using a LAS-3000 (Fujifilm). The natural log of the normalized relative light unit (RLU) was calculated as described previously (32). The degradation rate k (min^{-1}) was used to compare the different treatments, with k being the slope of the degradation curve (Fig. S6) between 5 and 40 min.

RNA sequencing

The transcriptomic responses induced by the RNs were investigated by RNA-Seq, using an *Arabidopsis thaliana* ecotype Col-0 cell suspension culture (33). Treatments were carried out in a 100 ml flask on a shaker at 110 rpm, with 20 ml of a 3-d-old freshly subcultured cell suspension elicited by either RN3, RN4, or IAA at a final concentration of 50 μ M for 30 min. Cells in the liquid medium were harvested by passing the culture through Whatman filter paper in a funnel under vacuum for 10 sec. DMSO (0.5% v/v) treatment was used as the mock control.

Three biological replicates were produced in this way. All the samples were immediately frozen in liquid N₂ upon harvesting and stored at -80 °C. Total RNA was extracted using RNeasy Plant Mini Kit (QIAGEN) and genomic DNA was eliminated using RQ1 RNase-Free DNase I (Promega) on-column digestion. The RNA quality was examined by an Agilent 2100 Bioanalyzer system, with an RNA integrity number (RIN) \geq 8. The construction of the sequencing libraries using the TruSeq stranded mRNA sample prep kit with polyA-selection (Illumina Inc.) and the 125 cycle paired-end sequencing of the 12 libraries in two lanes using the HiSeq system (Illumina Inc.) were performed by NGI (National Genomics Infrastructure) SNP&SEQ Technology Platform at the Uppsala University according to the standard protocols. The reads from each sequencing library were aligned to the *Arabidopsis thaliana* (The Arabidopsis Information Resource 10, TAIR 10) (34) genome using the Subreadalign aligner (35). The mapped reads were converted to gene counts using the featureCounts function (36). These steps were both done using R/Bioconductor package Rsubread version 3.1 (37-39). In order to take into account the difference in the sequencing depth between libraries, the libraries were normalized using a weighted trimmed mean method available from the package edgeR (40). All genes expressed in the 3 replicates and at least two counts per million mapped reads were considered. To estimate differentially expressed genes (DEGs) between the treatment and the DMSO control, data were modeled as a multifactorial experiment and Limma (41) was used to assess differential gene expression. In the modeling, we used the replicate as a batch factor. Genes were considered as statistically significant DEGs if the adjusted p-values after FDR (False Discovery Rate) correction for multiple testing were lower than 0.05. Identified DEGs were clustered using Venn diagrams (<http://bioinformatics.psb.ugent.be/webtools/Venn/>) and expression pattern and auxin response of candidates were analyzed using the Arabidopsis eFP (<http://bar.utoronto.ca/efp/cgi-bin/efpWeb.cgi>).

Confocal microscopy

Seedlings of the p35S::DII-Venus line were transferred to GM without agar containing chemicals. Seedlings were mounted in their treatment medium and images were acquired using a Zeiss LSM 780 confocal microscope with a LCI Plan-Neofluar 25x/0.8 Imm Corr DIC M27 objective. The Venus fluorescent protein was excited at 514 nm with an Argon laser.

Forward genetic screen

Mutagenesis was performed using ethyl methanesulfonate (EMS) at 24 mM final concentration on 10,000 seeds of Col-0 as described previously (42). M1 plants were harvested by bulk of 25 plants per pool. M2 seedlings were first screened for resistance to the effect of 0.5 μ M RN4 on apical hook development in the dark and the isolated mutants were then screened for sensitivity to 75 nM 2,4-D in the light. The *hkb1* mutant, which was selected for resistance to RN4 and sensitivity to 2,4-D, was then backcrossed twice with Col-0. Genomic DNA for whole genome sequencing was extracted from a pool of 25 plants using the E.Z.N.A.® Plant DNA Kit (Omega Bio-tek). The data has been deposited at the ENA (www.ebi.ac.uk/ena) under the accession number: PRJEB21529.

DNA sequencing

The construction of the DNA-350 sequencing libraries using the TruSeq Library construction Kit (Illumina Inc.) and the paired-end sequencing of the libraries using the HiSeq PE150 system (Illumina Inc.) were performed by Novogene according to standard protocols. The data pre-

processing was performed as follows: first the quality of the raw sequence data was assessed using FastQC (<http://www.bioinformatics.babraham.ac.uk/projects/fastqc/>), v0.11.4. Data were then filtered to remove adapters and trimmed for quality using Trimmomatic (v0.36; (43); settings TruSeq3-PE-2.fa:2:30:10 SLIDINGWINDOW:5:20 MINLEN:50). After that filtering step, FastQC was run again to ensure that no technical artefacts were introduced. The reads were then aligned to the *Arabidopsis thaliana* (TAIR 10) (34) genome using BWA-MEM version 0.7.8 (44) with the following non-default parameters: -k 32 -M -R. The obtained BAM files were then used as input for variant analysis using GATK version 3.4-46 (45). Briefly, duplicate reads were marked using the Picard (46) library MarkDuplicatesWithMateCigar tool before the reads were further pre-processed using the GATK BaseRecalibrator, RealignerTargetCreator and IndelRealigner tools. BaseRecalibrator used the SNP gold standard for *Arabidopsis thaliana* retrieved on January 26th, 2017. The de-duplicated, recalibrated, realigned BAM files were then used as input to GATK UnifiedGenotyper. The obtained VCF files were further analyzed using ad-hoc R scripts and visualized in JBrowse (47). To identify the causative variant, only SNPs that could have been triggered by the EMS treatment and having an allele frequency of 1 (homozygous) were kept. The effect of these SNPs was then evaluated using snpEff (48) and the remaining candidates manually evaluated.

Plant genotyping

Genomic DNA from *brm-5* and *hkb1* was extracted as previously described (49). PCR was performed using the primers 5'-GAACTTTGCGTGATTACCAGC-3' and 5'-GACCTTCCTTGTCGATTCTCC-3'. The PCR product was purified using the QIAquick PCR Purification Kit (Qiagen). To identify the point mutations in the mutants, the PCR product was sequenced using the primers 5'-CCTTCTTTTTGAAAGGGTTGC-3' and 5'-TGGCCTGTCCTCTGTAGCTT-3' for *brm-5* and *hkb1*, respectively.

Image processing

Figures were designed using Adobe Illustrator. Seedling images were acquired using a flatbed scanner Epson V600 when grown in the light and according to (50) when grown in the dark. Cropping and whole-picture contrast enhancement were done using ImageJ1.50f following the same settings for each panel. Quantification of band intensity in pull-down gel images was performed using ImageJ. Drawings were realized using Inkscape0.48. Movie S1 was realized using Chimera1.10rc.

Statistical analysis

Biological replicates were performed on different days. Primary root length and hypocotyl length were measured on 7-d-old seedlings. Lateral root density was measured on 8-d-old seedlings. Apical hook angle was measured during the first six days of skotomorphogenesis using ImageJ (51). For statistical analyses of data, ANOVA and Tukey's test were performed using R (37), while two sided independent t-tests were performed using Excel (Microsoft Office).

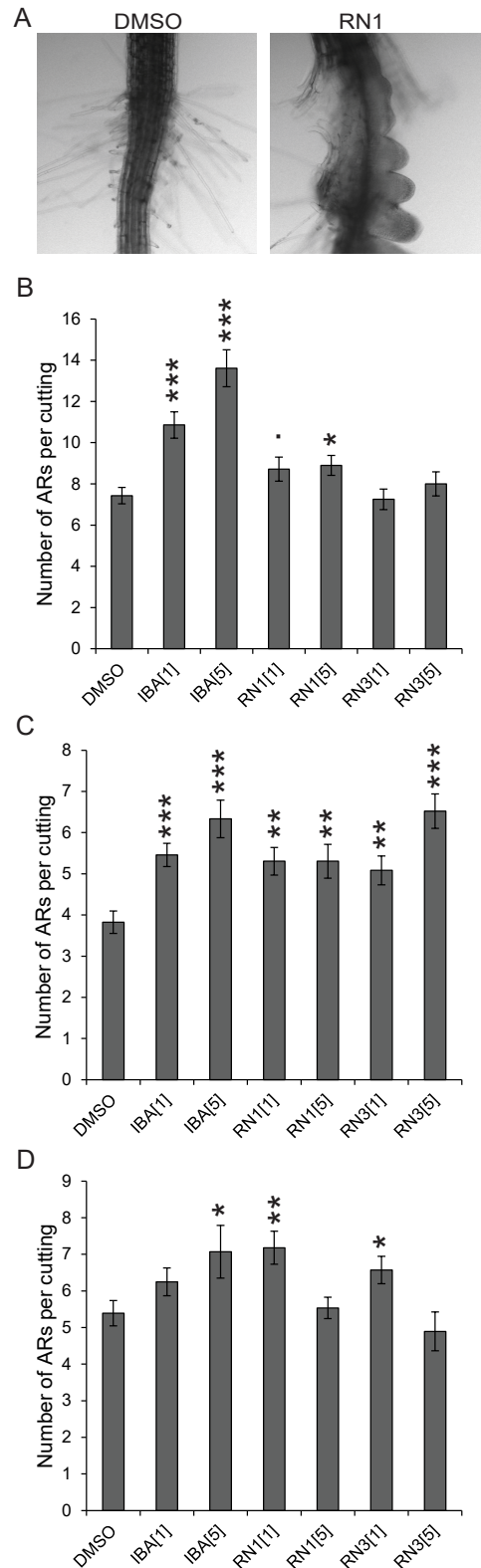


Fig. S2. RN1 and RN3 induce adventitious root (AR) formation. (A) 8-d-old *Arabidopsis* seedlings grown on DMSO or RN1 at 2 μ M. RN1 promoted the formation of amorphous clusters of cells in the hypocotyl base. (B-D) Cuttings of *Populus* lines T89 (B), SwAsp19 (C) and SwAsp35 (D) were propagated in media supplemented with DMSO, IBA, RN1 and RN3 for 9 days to induce rooting. Cuttings were then transferred to fresh medium without treatment. The number of ARs were counted 3 weeks after the transfer. The Student's t-test was performed to compare AR number after mock treatment (DMSO) with that after chemical treatments. Means \pm SEM are shown, $n = 28$ explants across 4 independent replicates, p -value: * $P < 0.05$, ** $P < 0.01$, *** $P < 0.001$. Concentrations in μ M are indicated in brackets.

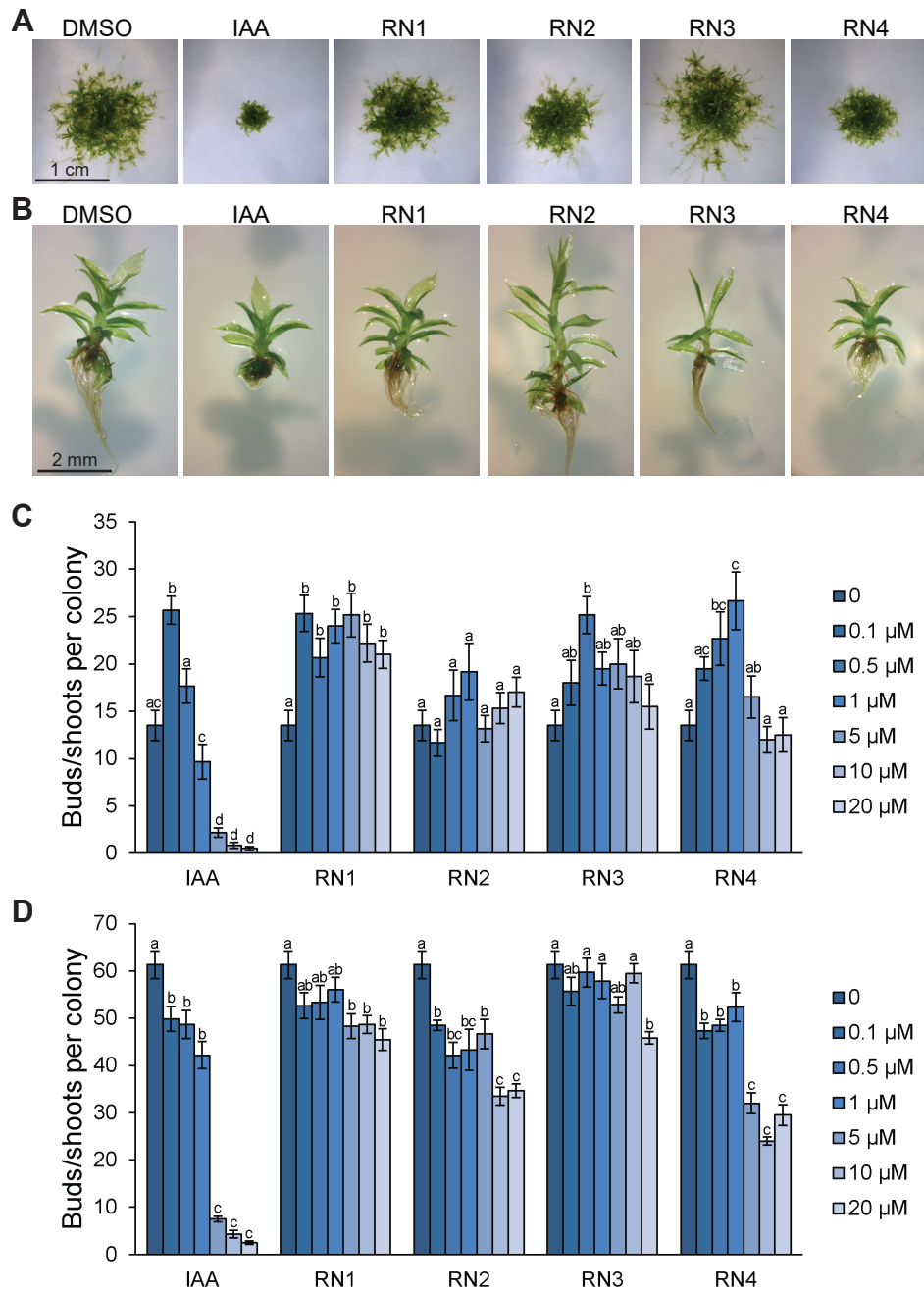


Fig. S3. Auxin-like phenotypes are induced by the RNs in *Physcomitrella patens*. Small pieces of protonemal tissue were transferred to media supplemented with IAA or RN compounds. (A-B) Representative colonies (A) and gametophores (B) after 4 weeks of growth on media supplemented with IAA and RN compounds at 10 μM . DMSO was used as control. (C-D) The number of buds and gametophores was counted for each colony after 1 week (C) and 2 weeks (D) of treatment with concentrations from 0.1 μM to 20 μM . Statistical analyses were performed using ANOVA and Tukey's test. Means \pm SEM are shown, $n = 6$ colonies for each concentration of the dose response. For each treatment, different letters are displayed for p -value < 0.05 .

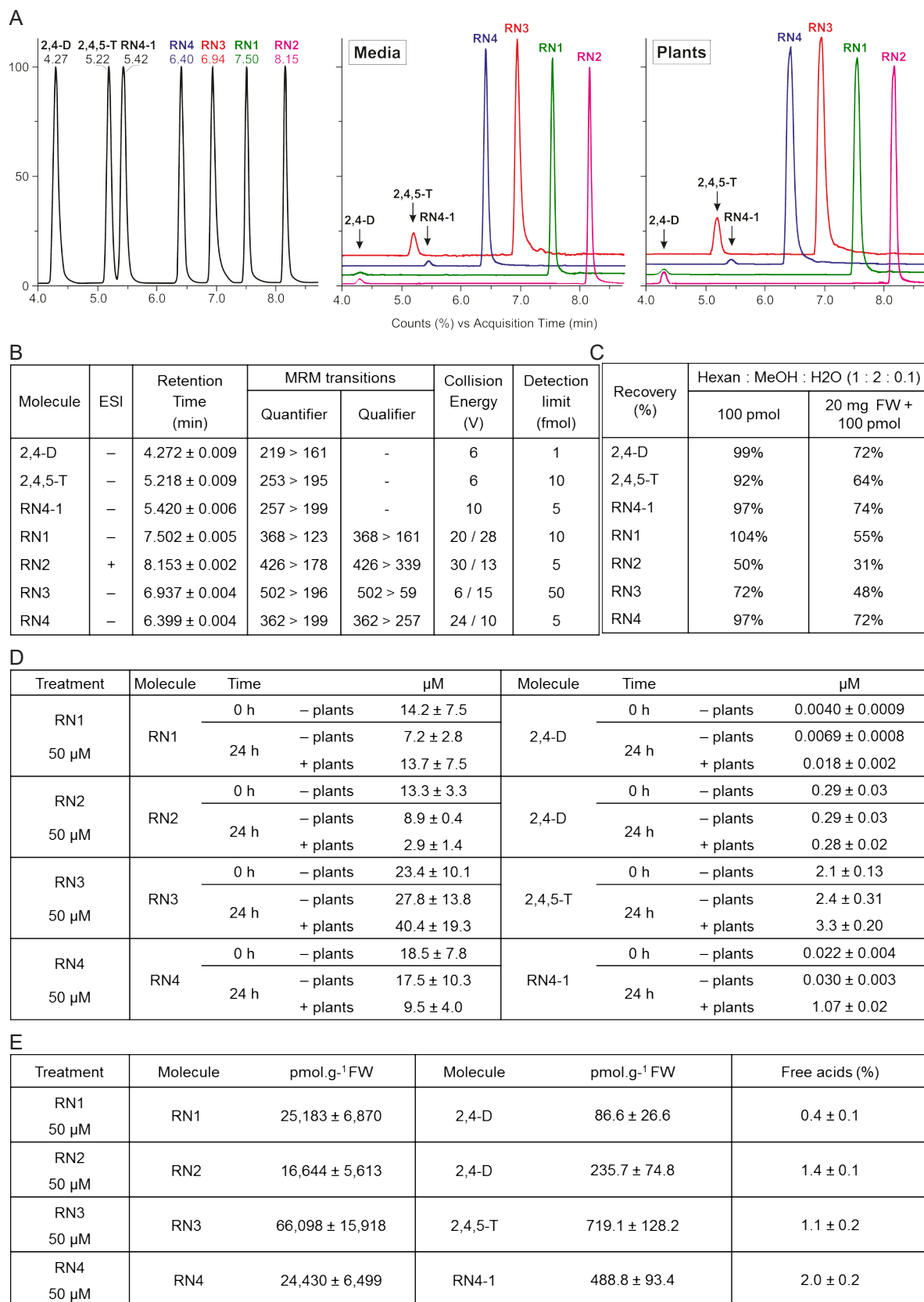


Fig. S4. Analysis of RN stability. Five-d-old *Arabidopsis* seedlings were transferred into liquid media containing RN compounds. Treatment media were collected directly after solubilization of the molecules and after 24 h in the presence or absence of plants. The plants were collected after 24 h treatments. DMSO controls (media and treated plants) were also analyzed in which no RN compounds nor their associated free acids were detected. (A) Multi-MRM chromatograms showing the optimized separation and identification of the analyzed compounds and free acids in liquid media and plants treated by RN compounds. (B) Optimized LC-MS/MS conditions (MRM transitions, retention times, collision energies and limits of detection defined as signal-to-noise ratio 3:1). (C) Liquid-Liquid extraction recovery of the compounds from DMSO treated plant matrix. (D) Molar concentrations of the RNs and their associated free acids in the growing media. (E) Levels of the RNs and their associated free acids in planta after 24 h of treatment. Means ± SD are shown, n = 3 replicates.

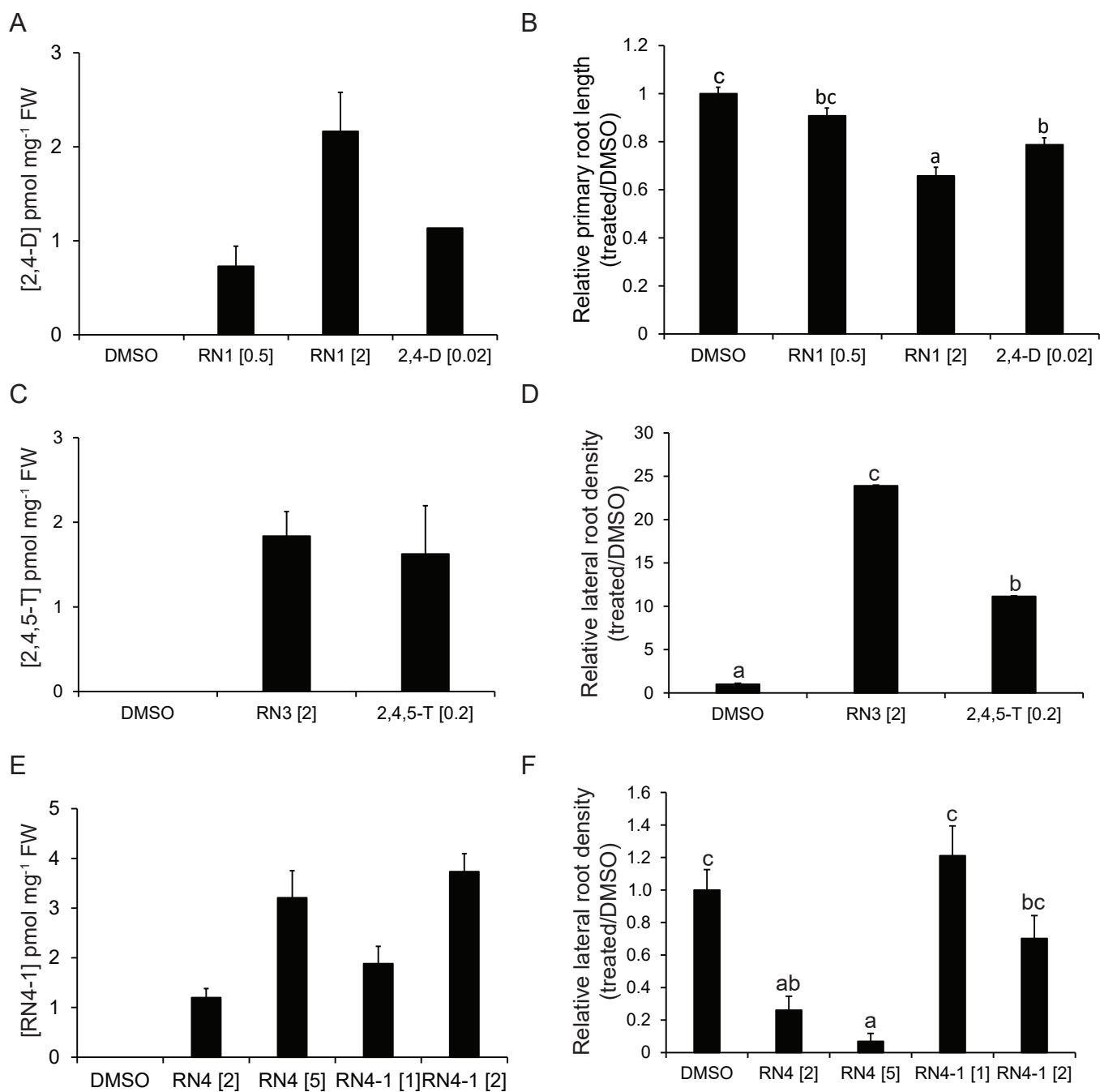


Fig. S5. Quantification of free acids released in roots during long-term RN treatment. Col-0 seedlings were grown on media supplemented with RN1 or 2,4-D for 5 days (A-B) and RN3, 2,4,5-T, RN4 or RN4-1 for 8 days (C-F). DMSO was used as control. The concentration of free acids were quantified in excised roots (A, C, E) after primary root length (B) and lateral root density (D, F) were measured. ANOVA and Tukey's test were performed to compare measurements after mock treatment (DMSO) with that after chemical treatments. Means \pm SEM are shown, $n > 30$ seedlings across 3 independent replicates, p -value: * $P < 0.05$, ** $P < 0.01$, *** $P < 0.001$. Concentrations in μM are indicated in brackets.

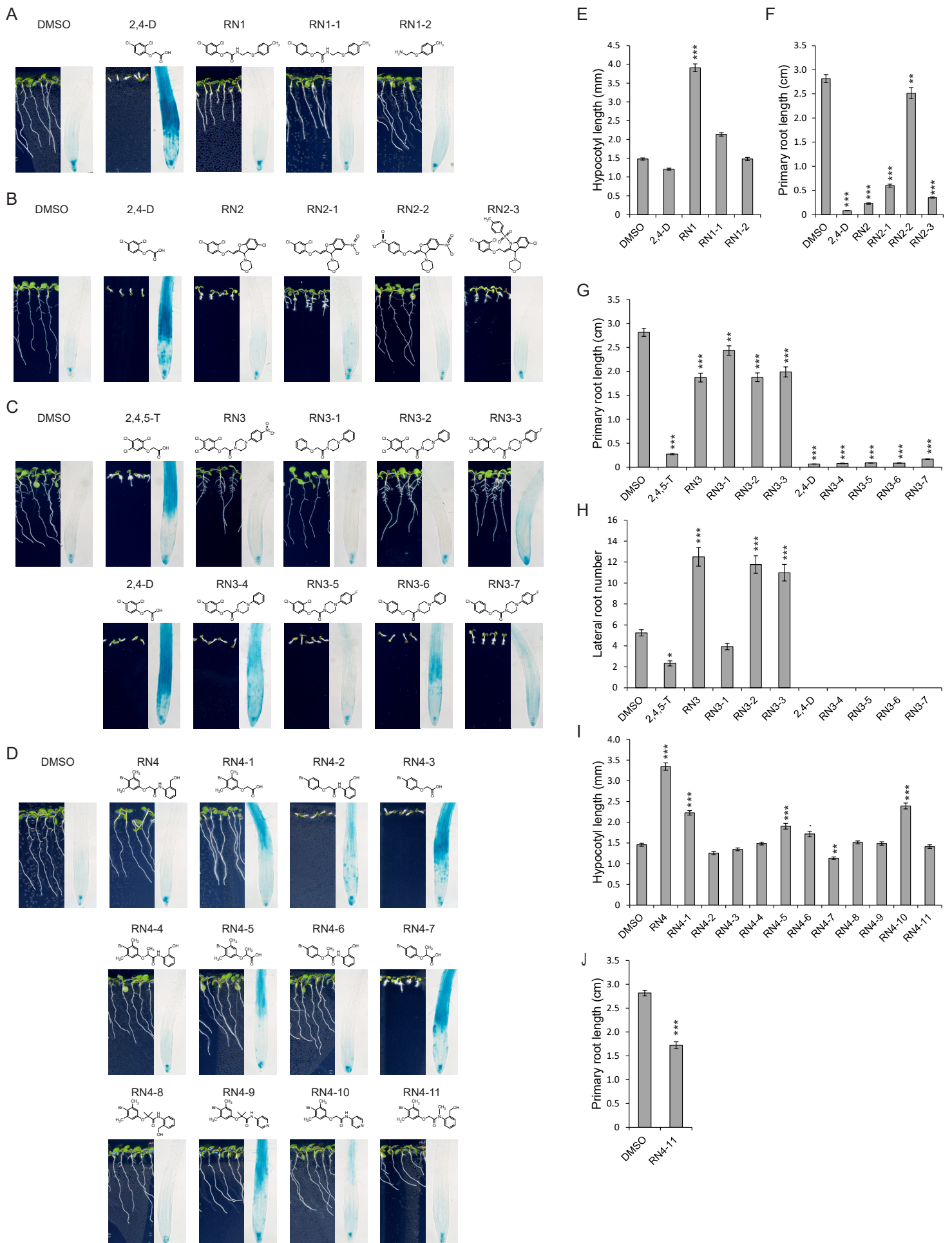


Fig. S6. RN SAR analysis. (A-J) SAR analysis for RN1 (A, E), RN2 (B, F), RN3 (C, G, H) and RN4 (D, I, J). Representative images of eight-d-old seedlings grown on media supplemented with the indicated chemicals, and *pDR5::GUS* expression pattern in 5-d-old GUS-stained seedlings treated with the same chemicals at 10 μ M for 5 h. (E-J) Quantification of RN-induced phenotypes in eight-d-old seedlings grown on media supplemented with the indicated chemicals. Concentrations of the chemicals used (except for GUS-stained seedlings) were (A, E) 1 μ M, (B, F) 0.5 μ M, and (C-D, H-J) 2 μ M. ANOVA and Tukey's test were performed to compare measurements after mock treatment (DMSO) with that after chemical treatments. Means \pm SEM are shown, $n = 50$ seedlings across 3 independent replicates, p -value: * $P < 0.05$, ** $P < 0.01$, *** $P < 0.001$.

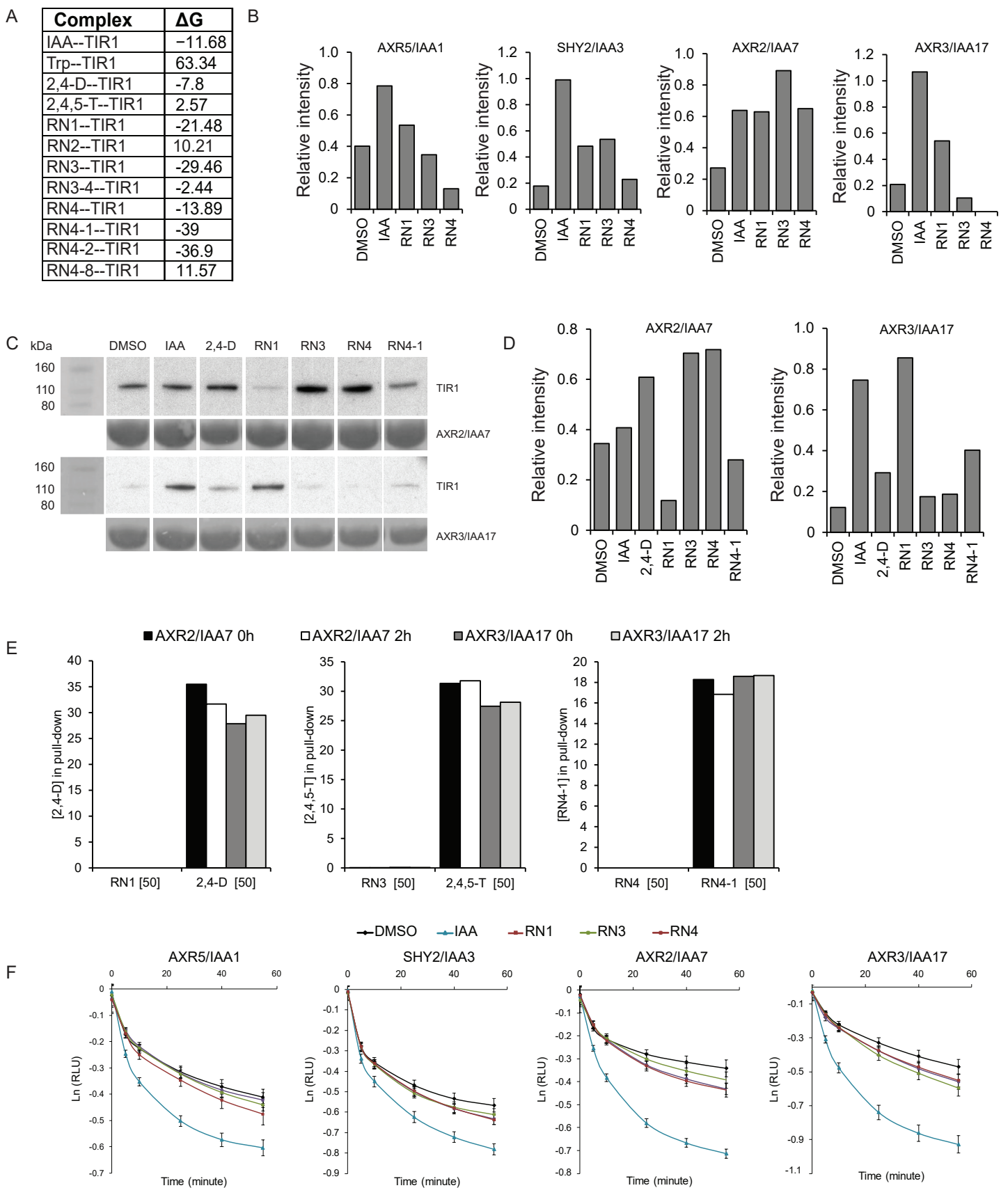


Fig. S7. Thermodynamic stability ($\Delta G_{(\text{chemical-TIR1})}$), in vitro pull-down using insect cell purified TIR1 and AUX/IAA-LUC *in vivo* degradation assay. (A) List of thermodynamic stability values computed for molecules of interest within the TIR1 auxin binding pocket. (B) Quantification of band intensity in the pull-down gel image shown in Fig. 3D. The intensity of each band was normalized to the respective Ponceau staining intensity. (C) Western blot of pull-downs using GSH-Sepharose-immobilized GST-AXR2/IAA7 or GST-AXR3/IAA17 against 3XFLAG:MBP:HIS:TIR1 (GST-IAA proteins were produced in *E. coli*, while 3XFLAG:MBP:HIS:TIR1 was produced in insect cells; all were full length proteins and were affinity purified before the pull-downs). All compounds were used in solution at 50 μM . Post pull-down washing was done including the respective compounds at the same concentration. Western blot was hybridized with Anti Flag-HRP antibody. (D) Quantification of band intensity in the pull-down gel image shown in Fig. S7C. The intensity of each band was normalized to the respective Ponceau staining intensity. (E) LC/MS analysis of RN stability in the pull-down buffer before and after 2 h of incubation in the presence of TIR1 and AXR2/IAA7 or AXR3/IAA17. The pull-down was performed as for Fig. S7C. (F) AUX/IAA-LUC degradation over time in 7-d-old seedlings carrying AXR5/IAA1-LUC, SHY2/IAA3-LUC, AXR2/IAA7-LUC and AXR3/IAA17-LUC translational fusions, treated with DMSO and IAA as controls and with the RNs at 50 μM . Time zero represents the first acquisition of light emission

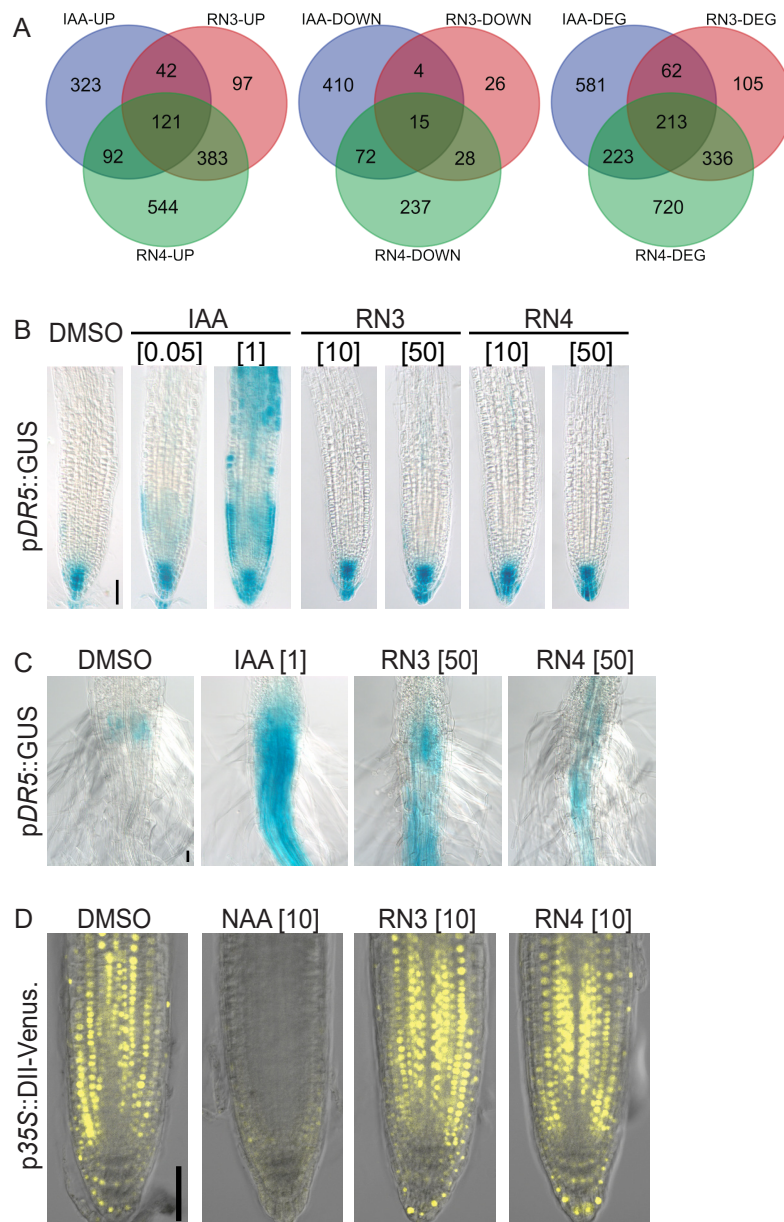


Fig. S8. RN3 and RN4 induce local auxin responses. (A) Venn diagram showing the overlap between genes which were upregulated, downregulated or differentially expressed (DEG) in cell culture after RN3, RN4 or IAA treatments ($n = 3$ culture samples; p -value < 0.05). (B-C) Five-d-old seedlings expressing pDR5::GUS were treated for 5 h with different concentrations of RN3 and RN4. DMSO and two concentrations of IAA were used as negative and positive controls respectively. Representative images of the primary root tip (B) and the root-hypocotyl junction (C) after GUS staining, showing that RN3 and RN4 only induce pDR5::GUS at 50 μ M in the root-hypocotyl junction. (D) Five-d-old seedlings of p35S::DII-Venus were treated for 45 min with RN3 and RN4 at 10 μ M. DMSO and NAA were used as negative and positive controls respectively. Scale bars represent 50 μ m. Concentrations in μ M are indicated in brackets.

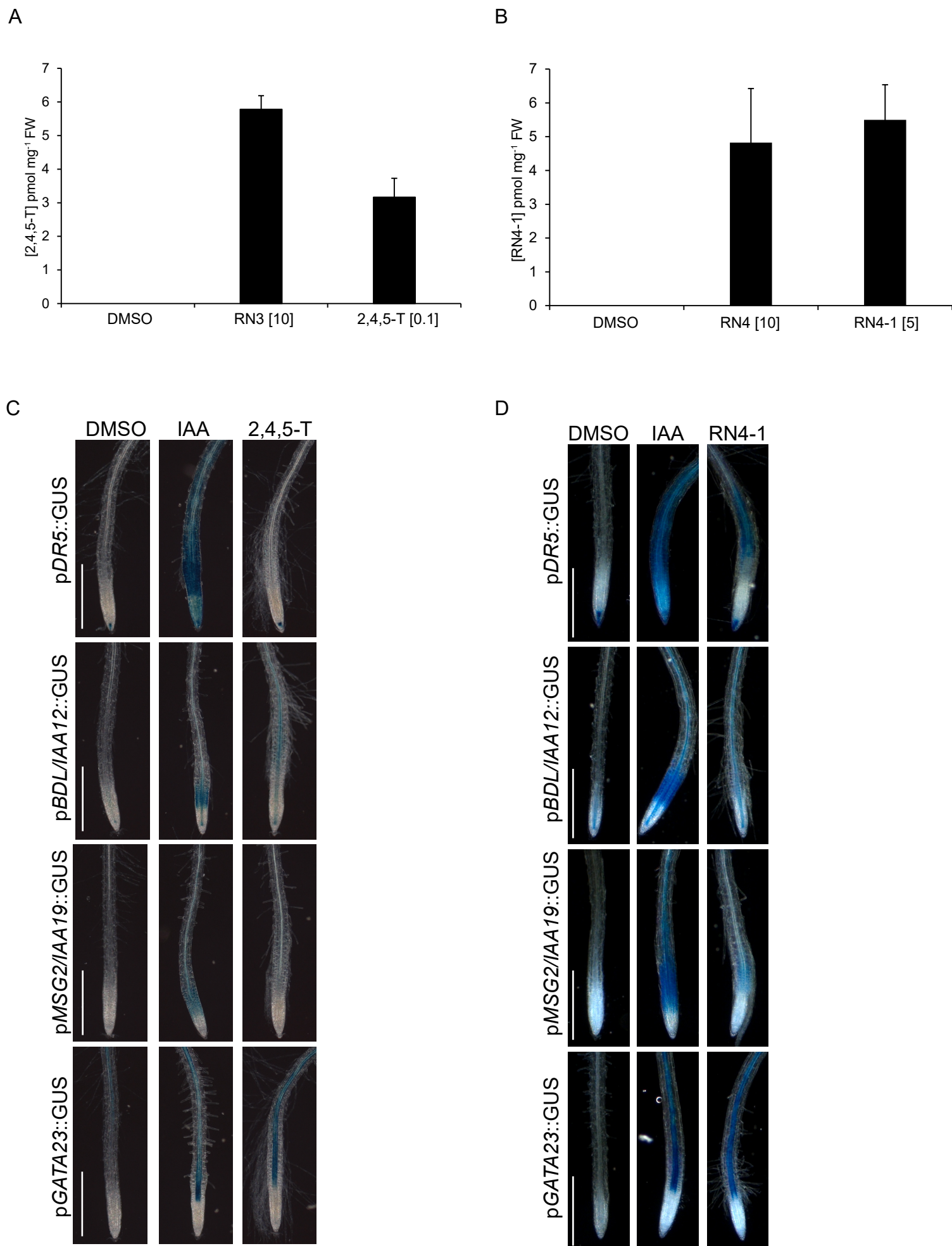


Fig. S9. The effects of 2,4,5-T and RN4-1 on auxin-responsive promoter lines. (A-B) Five-d-old seedlings were treated for 16 h with RN3, 2,4,5-T, RN4 or RN4-1 and the concentrations of free acids released in the excised roots was quantified. DMSO was used as control. (C-D) Representative primary roots of 5-d-old seedlings expressing pDR5::GUS, pBDL/IAA12::GUS, pMSG2/IAA19::GUS or pGATA23::GUS transcriptional fusions treated with 10 μ M IAA, 0.1 μ M 2,4,5-T or 5 μ M RN4-1 for 16 h. DMSO was used as control. Scale bars indicate 500 μ m (C-D). Concentrations in μ M are indicated in brackets.

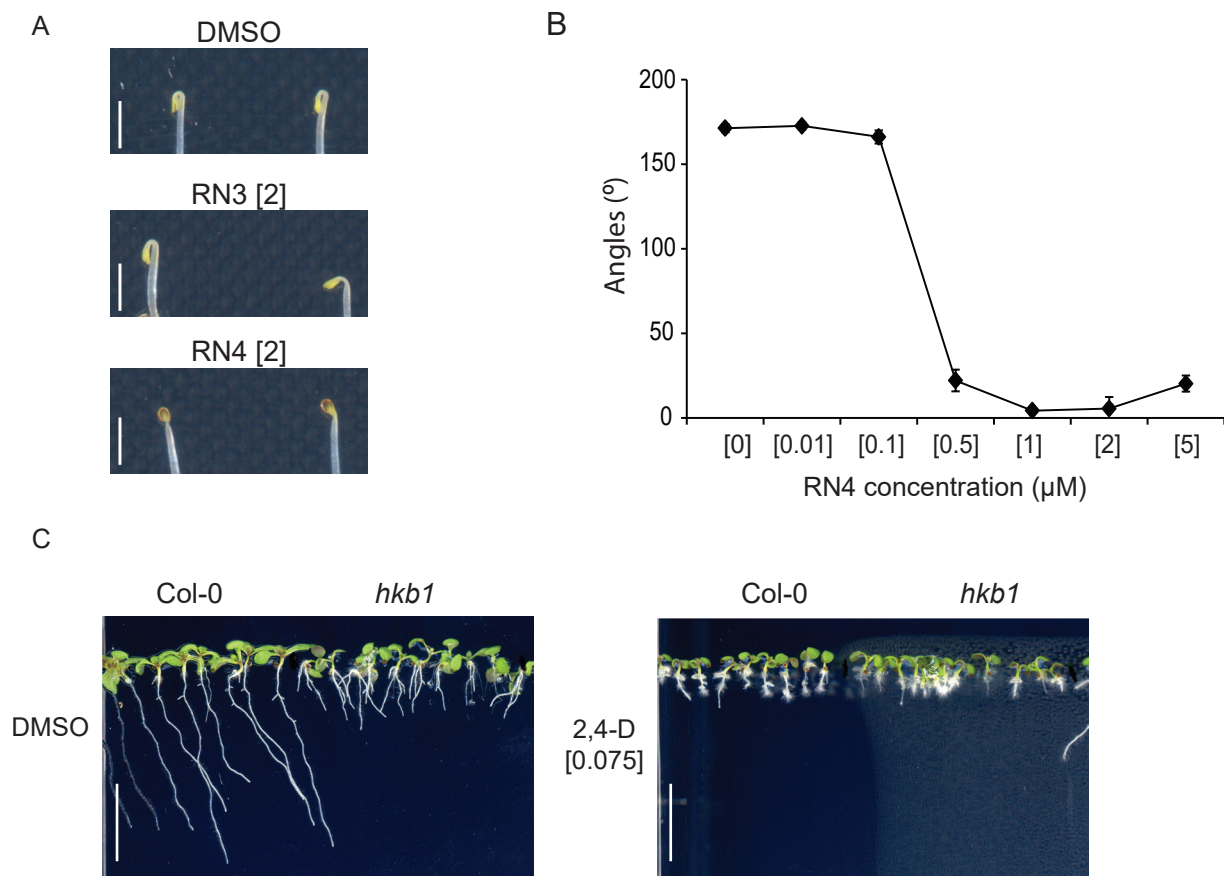


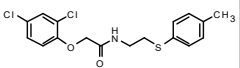
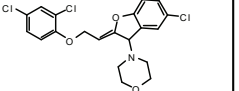
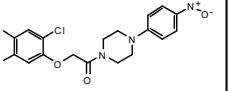
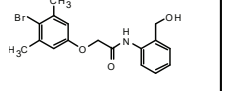
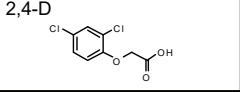
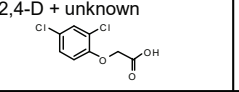
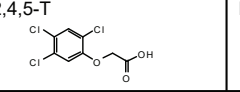
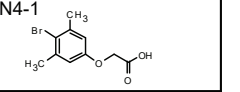
Fig. S10. RN3 and RN4 have distinct effects on apical hook development in *Arabidopsis*. (A) Apical hook phenotypes of 3-d-old Col-0 seedlings grown on media supplemented with DMSO, RN3 and RN4. While RN3 showed a negligible effect, RN4 completely abolished apical hook development. (B) Dose-response graph representing the effect of RN4 on apical hook angle in 4-d-old Col-0 seedlings. (C) Representative images of 8-d-old Col-0 and *hkb1* grown on MS media supplemented with DMSO or 2,4-D. Means \pm SEM are shown, $n = 10$ seedlings for each concentration of the dose response (B). Scale bars represent 2 mm (A) and 1 cm (C). Concentrations in μM are indicated in brackets.

Table S1. Selected IAA, RN3 and RN4 up-regulated genes after 30 minute treatments of cell culture. Values indicate fold change upon IAA, RN3 and RN4 treatment compared to DMSO. Statistically significant values (p-value < 0.05) are represented in bold.

| IAA up-regulated \cap RN3 not up-regulated \cap RN4 not up-regulated 323 significantly up-regulated genes (4 examples shown) | | | | |
|---|--|-------------|-------------|-------------|
| AGI | Gene name | IAA | RN3 | RN4 |
| AT2G39370 | MEMBRANE-ASSOCIATED KINASE REGULATOR 4 (MAKR4) | 0.75 | 0.12 | 0.22 |
| AT4G39400 | BRASSINOSTEROID INSENSITIVE 1 (BRI1) | 0.45 | -0.01 | -0.03 |
| AT5G43700 | INDOLE-3-ACETIC ACID INDUCIBLE 4 (IAA4) | 0.97 | 0.23 | 0.04 |
| AT3G60630 | HAIRY MERISTEM 2 (HAM2) | 0.39 | -0.03 | -0.11 |
| IAA up-regulated \cap RN3 up-regulated \cap RN4 up-regulated 121 significantly up-regulated genes (21 examples shown) | | | | |
| AGI | Gene name | IAA | RN3 | RN4 |
| AT1G04240 | SHORT HYPOCOTYL 2 (SHY2) | 1.59 | 0.62 | 1.04 |
| AT1G70940 | PIN-FORMED 3 (PIN3) | 0.55 | 0.36 | 0.22 |
| AT1G78100 | AUXIN UP-REGULATED F-BOX PROTEIN 1 (AUF1) | 1.47 | 0.53 | 0.80 |
| AT2G36800 | DON-GLUCOSYLTRANSFERASE 1 (DOGT1) | 1.05 | 1.15 | 1.47 |
| AT2G42430 | LATERAL ORGAN BOUNDARIES-DOMAIN 16 (LBD16) | 0.79 | 0.88 | 0.96 |
| AT2G14960 | IAA-amido synthase (GH3.1) | 0.53 | 0.78 | 1.28 |
| AT3G23030 | INDOLE-3-ACETIC ACID INDUCIBLE 2 (IAA2) | 1.23 | 0.61 | 1.01 |
| AT3G25710 | BASIC HELIX-LOOP-HELIX 32 (BHLH32) | 0.99 | 1.39 | 1.06 |
| AT3G49940 | LOB DOMAIN-CONTAINING PROTEIN 38 (LBD38) | 0.61 | 0.85 | 1.72 |
| AT3G50660 | DWARF 4 (DWF4) | 0.43 | 0.52 | 0.61 |
| AT3G62100 | INDOLE-3-ACETIC ACID INDUCIBLE 30 (IAA30) | 1.49 | 1.53 | 1.85 |
| AT4G14560 | INDOLE-3-ACETIC ACID INDUCIBLE 1 (IAA1) | 1.26 | 0.97 | 1.53 |
| AT4G15550 | INDOLE-3-ACETATE BETA-D-GLUCOSYLTRANSFERASE (IAGLU) | 1.72 | 2.13 | 1.42 |
| AT4G17460 | Homeodomain-leucine Zipper II (HAT1) | 2.51 | 1.04 | 0.98 |
| AT4G34131 | UDP-GLUCOSYL TRANSFERASE 73B3 (UGT73B3) | 1.92 | 2.42 | 1.86 |
| AT4G34135 | UDP-GLUCOSYLTRANSFERASE 73B2 (UGT73B2) | 1.66 | 1.70 | 1.71 |
| AT4G34138 | UDP-GLUCOSYL TRANSFERASE 73B1 (UGT73B1) | 0.61 | 1.07 | 1.46 |
| AT4G37390 | AUXIN UPREGULATED 3 (AUR3) | 2.55 | 1.62 | 2.59 |
| AT5G47370 | Homeodomain-leucine Zipper II (HAT2) | 2.08 | 1.12 | 1.26 |
| AT5G54490 | PINOID-BINDING PROTEIN 1 (PBP1) | 0.39 | 1.07 | 2.51 |
| AT5G67420 | LOB DOMAIN-CONTAINING PROTEIN 37 (LBD37) | 0.92 | 0.84 | 1.35 |
| IAA up-regulated \cap RN3 up-regulated \cap RN4 not up-regulated 42 significantly differentially up-regulated genes (9 examples shown) | | | | |
| AGI | Gene name | IAA | RN3 | RN4 |
| AT1G10370 | EARLY-RESPONSIVE TO DEHYDRATION 9 (ERD9) | 1.31 | 1.08 | 0.63 |
| AT1G15580 | INDOLE-3-ACETIC ACID INDUCIBLE 5 (IAA5) | 0.79 | 0.85 | 0.59 |
| AT1G21910 | DEHYDRATION RESPONSE ELEMENT-BINDING PROTEIN 26 (DREB26) | 1.24 | 0.84 | 0.45 |
| AT1G79270 | EVOLUTIONARILY CONSERVED C-TERMINAL REGION 8 (ECT8) | 0.79 | 0.59 | 0.08 |
| AT2G30490 | CINNAMATE-4-HYDROXYLASE (C4H) | 0.55 | 0.55 | 0.30 |
| AT3G04730 | INDOLEACETIC ACID-INDUCED PROTEIN 16 (IAA16) | 0.81 | 0.57 | 0.25 |
| AT3G55120 | TRANSPARENT TESTA 5 (TT5) | 2.05 | 1.57 | 1.14 |
| AT4G26690 | SHAVEN 3 (SHV3) | 0.22 | 0.24 | 0.11 |
| AT5G13930 | TRANSPARENT TESTA 4 (TT4) | 2.34 | 1.90 | 1.25 |

| IAA up-regulated \cap RN4 up-regulated \cap RN3 not up-regulated 92 significantly differentially up-regulated genes (12 examples shown) | | | | |
|--|--|-------------|-------|-------------|
| AGI | Gene name | IAA | RN3 | RN4 |
| AT1G04100 | INDOLEACETIC ACID-INDUCED PROTEIN 10 (IAA10) | 0.64 | 0.18 | 0.34 |
| AT1G11260 | SUGAR TRANSPORTER 1 (STP1) | 0.44 | 0.25 | 0.94 |
| AT1G31880 | BREVIS RADIX (BRX) | 1.26 | 0.41 | 0.67 |
| | XYLOGLUCAN ENDOTRANSGLUCOSYLASE/HYDROLASE | | | |
| AT1G32170 | 30 (XTH30) | 0.92 | 0.35 | 0.70 |
| AT1G55330 | ARABINO GALACTAN PROTEIN 21 (AGP21) | 0.37 | 0.10 | 0.21 |
| AT2G38310 | PYR1-LIKE 4 (PYL4) | 0.46 | 0.21 | 0.52 |
| AT3G50060 | MYB DOMAIN PROTEIN 77 (MYB77) | 0.51 | -0.13 | 0.66 |
| AT2G23170 | IAA-amido synthase (GH3.3) | 0.92 | 0.23 | 0.52 |
| AT4G08950 | EXORDIUM (EXO) | 0.68 | 0.16 | 0.41 |
| AT4G32280 | INDOLE-3-ACETIC ACID INDUCIBLE 29 (IAA29) | 1.13 | 0.33 | 0.60 |
| AT5G57560 | TOUCH 4 (TCH4) | 0.51 | 0.39 | 0.95 |
| AT5G65390 | ARABINO GALACTAN PROTEIN 7 (AGP7) | 0.60 | 0.03 | 0.56 |

Table S2. Summary of the results obtained for each RN molecule described in this work.

| | | | | |
|---|--|--|---|--|
| Chemical structure of the RubNeddins (RN) |  |  |  |  |
| Chemical name | 2-(2,4-dichlorophenoxy)-N-{2-[(4-methylphenyl)thio]ethyl}acetamide | 4-{5-chloro-2-[2-(2,4-dichlorophenoxy)ethylidene]-2,3-dihydro-1-benzofuran-3-yl}morpholine | 1-(4-nitrophenyl)-4-[(2,4,5-trichlorophenoxy)acetyl]piperazine | 2-(4-bromo-3,5-dimethylphenoxy)-N-[2-(hydroxymethyl)phenyl]acetamide |
| ChemBridge ID | 6389186 | 5742604 | 6189599 | 7014462 |
| Degradation product | 2,4-D  | 2,4-D + unknown  | 2,4,5-T  | RN4-1  |
| Primary effect on <i>Arabidopsis</i> seedlings in presence of the RNs | - Hypocotyl length increase - Primary root growth inhibition - Adventitious root induction | - Primary root growth inhibition | - Lateral root number increase | - Lateral root number decrease - Hypocotyl length increase |
| Structure Activity Relationship conclusion | Importance of the chlorination in position 2 and 4 and the side chain | Biological activity due to 2,4-D structure | Importance of chlorination in position 2,4 and 5 and the piperazine | Importance of methyl group in position 3 and 5 Hydroxymethylation |
| Transcriptomic response | N/A | N/A | Tissue and promoter specific | Tissue and promoter specific |
| Selective formation of the auxin co-receptor complex | Yes | N/A | Yes | Yes |
| Selective degradation of the AUX/IAA proteins | Yes | N/A | Yes | Yes |

Movie S1. Molecular modeling view. The movie represents the crystal structure of TIR1 (Gray), IAA (red), and the DII domain of IAA7 (green). The first sequence shows the best docking probability obtained for RN1 (yellow), RN2 (purple), RN3 (cyan), RN4 (orange) and RN4-8 (pink). The second sequence shows two chosen molecules for RN1 (yellow), RN3 (cyan) and RN4 (orange), corresponding to the best docking conformation, next to the conformation which thermodynamically stabilized TIR1 without the DII-domain of IAA7.

Dataset 1. RNAseq results for *Arabidopsis* cell suspension culture treated with IAA, RN3 and RN4. Column A indicates the gene ID. Column B, C and D indicate the induction ratio between the treatment and DMSO for RN3, RN4 and IAA respectively. Columns E, F and G indicate up-regulation (1), down-regulation (-1) or no difference compared to the DMSO for RN3, RN4 and IAA respectively.

Supplementary Document

Chemical Synthesis and Characterization

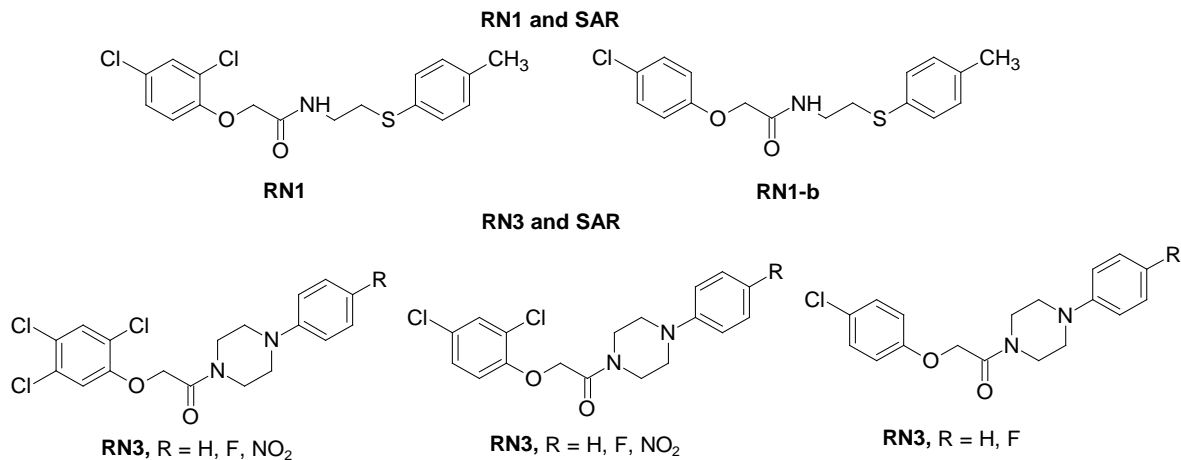
1. General experimental information

Unless stated, all reagents and solvents were used as received from commercial suppliers. All reactions were carried out under an inert atmosphere with dry solvents under anhydrous conditions, unless otherwise indicated. TLC was performed on aluminum backed silica gel plates (medium pore size 60 Å, fluorescent indicator 254 nm) and visualized by exposure to UV light (254 nm) or stained with potassium permanganate (KMnO₄) and ethanolic phosphomolybdic acid (PMA). Column chromatography was performed using silica gel with an average particle diameter 50 µm (range 40–65 µm, pore diameter 53 Å), and eluents are given in brackets. IR spectra were recorded on a spectrometer equipped with an FTIR device. ¹H NMR spectra were recorded on a Bruker AVANCE (at 400 MHz) spectrometer at 298 K, 343 K and calibrated by using the residual peak of the solvent as the internal standard (CDCl₃: δ_H = 7.26 ppm; δ_C = 77.23 ppm. DMSO-d₆: δ_H = 2.50 ppm; δ_C = 39.51 ppm). ¹³C NMR spectra were acquired on a Bruker AVANCE (at 100 MHz) spectrometer and chemical shift (δ ppm) are reported relative to the residual solvent peak. The following abbreviations were used to describe the data of ¹H NMR spectra: chemical shift (δ ppm), s = singlet, d = doublet, t = triplet, q = quartet, m = multiplet, br = broad; coupling constant(s) in Hz. LCMS was conducted on a Micromass ZQ mass spectrometer with ES⁺ ionization. HRMS was performed by using a mass spectrometer with ESI-TOF (ES⁺).

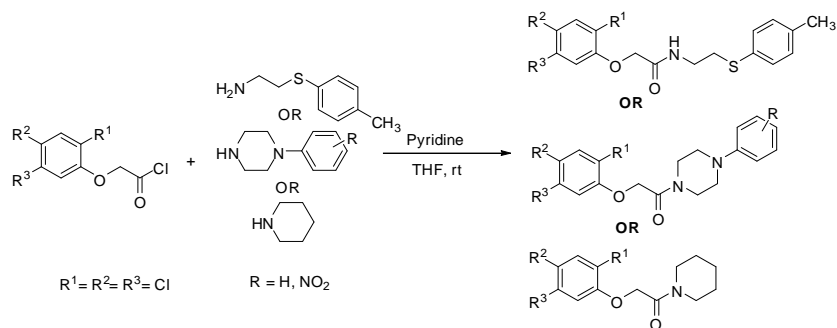
2. Chemical synthesis of hit molecules RN1, RN3, RN4 and their analogs

The hit molecule **RN2** was purchased from ChemBridge and purity data of this molecule is included.

2.1 Synthesis of hit molecules RN1, RN3 and SAR:

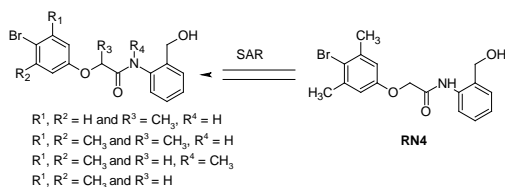


2.1.1 General procedure for the synthesis of hit molecules RN1, RN3 and SAR:

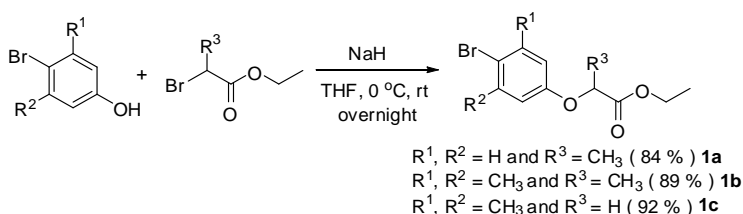


Pyridine (1.2 mmol) was mixed with Amine (1.0 mmol) in anhydrous tetrahydrofuran (5 mL) at 0 °C and stirred for 30 minutes. To this mixture was added a solution of acid chloride (1.2 mmol) in tetrahydrofuran (1 mL) drop wise and the reaction mixture was stirred at room temperature for 4h (monitored by LCMS). The precipitate was washed with ammonium chloride (sat. aq.) and extracted with ethylacetate, and the combined extracts were dried over anhydrous sodium sulfate, concentrated under reduced pressure to give the crude amide. The residue was purified by silica gel column chromatography using *n*-Heptane: Ethyl acetate (20-40 %), to afford pure products (86 % to 92 %).

2.2 Synthesis of hit molecule RN4 and analog:

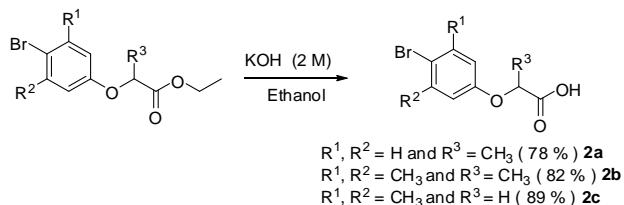


2.2.1 General experimental procedure for the synthesis of substituted phenoxyacetic acid esters (**1a-1c**):



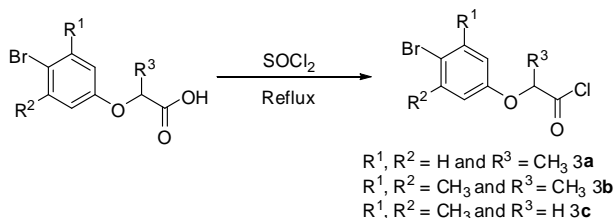
Sodium hydride (60% in paraffin, 2.0 mmol) was stirred for 5 min in hexane under argon atmosphere, and then the solvent was removed by a syringe followed by evaporation with a vacuum pump. This similar process was repeated three times then the sodium hydride residue was suspended in tetrahydrofuran (5 mL) and the mixture was allowed to cool to 0 °C. To this mixture was added a solution of substituted phenol (2.0 mmol) in tetrahydrofuran (3 mL) dropwise over 5 min, and the mixture was stirred for 5 min at the same temperature. Then the mixture was allowed to warm to room temperature and stirred for an additional 15 min. A solution of ethyl-2-bromopropionate (4.0 mmol) in tetrahydrofurane (2 mL) was added and the mixture was stirred for 14 h. The reaction mixture was acidified by 2 M hydrochloric acid and extracted with EtOAc. The organic layer was washed with brine, dried over anhydrous sodium sulfate, and concentrated in vacuum. The residue was purified by silica gel column chromatography (n-heptane/EtOAc: 9/1) to give pure products (**1a-c**) (52).

2.2.2 General experimental procedure for the synthesis of substituted phenoxyacetic acid (2a-2c):



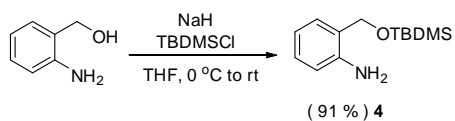
A solution of ester (2.0 mmol) in EtOH (6 mL) was added to an aqueous solution of potassium hydroxide (5 mL, 2 M) at 0 °C. After being stirred for 6-7 h, the reaction mixture was acidified by 3 M hydrochloric acid to afford the white precipitate which was filtered and washed with heptanes to give substituted-2-phenoxypropanoic acid (**2a-c**) in 78-89 % yield.

2.2.3 Experimental procedure for the synthesis of substituted phenoxyacetic acid chloride (3a-3c):



The mixture of phenoxyacetic acid (2 mmol) and thionyl chloride (6–10 mL) was reacted for 3 h under reflux until no further gaseous HCl was released. After completion of the reaction excess of thionyl chloride was distilled off under reduced pressure, giving the corresponding phenoxyacetic chlorides as brown oils. The phenoxyacetic chlorides were used in the next step without further purification.

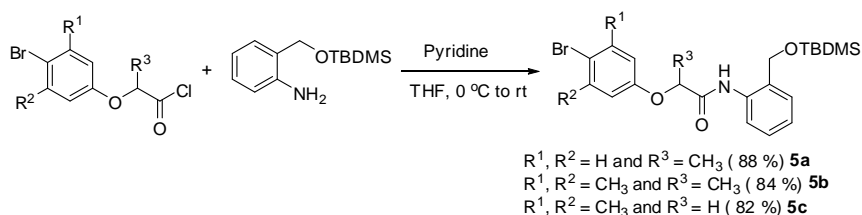
2.2.4 Experimental procedure for the synthesis of 2-((tert-butyl dimethylsilyloxy)methyl)aniline:



To a cooled (0 °C), stirred suspension of NaH (60% dispersion in mineral oil, 1.15 g, 29.05 mmol) in anhydrous THF (5 mL) was added dropwise a solution of 2-aminobenzyl alcohol

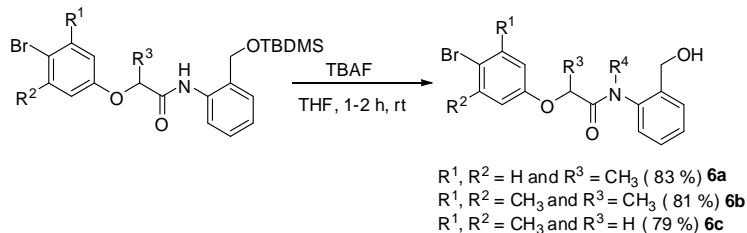
5 (3.25 g, 26.4 mmol) in anhydrous THF (8 mL) and the mixture was stirred at 0 °C for 15 min under nitrogen atmosphere. To this was added dropwise a solution of *tert*-butyldimethylsilyl chloride (4.25 g, 31.65 mmol) in anhydrous THF (12 mL) and the reaction mixture was gradually warmed to room temperature and stirred for 2 h. The reaction mixture was cooled to 0 °C and crushed ice was carefully added to quench the reaction. This was extracted with EtOAc (50 mL) and the combined extracts were washed with brine (10 mL), dried over Na₂SO₄ and concentrated in vacuo. The residue was purified by flash column chromatography (EtOAc/*n*-Heptane 0:100 to 10:90) to yield the title compound (5.5 g, 91%) as a dark yellow, viscous oil.

2.2.5 Experimental procedure for the synthesis of substituted phenoxy)-*N*-(2-((*tert*-butyldimethylsilyloxy)methyl)phenyl)propanamide:



Pyridine (1.2 mmol) was mixed with 2-((*tert*-butyldimethylsilyloxy)methyl)aniline (1.0 mmol) in anhydrous tetrahydrofuran (5 mL) at 0 °C and stirred for 30 minutes. To this mixture was added a solution of substituted phenoxyacetic acid chloride (1.2 mmol) in tetrahydrofuran (1 mL) drop wise over 5 minutes and the reaction mixture was stirred at room temperature for 4h (monitored by LCMS). The precipitate was washed with ammonium chloride (sat. aq) and extracted with ethylacetate, and the combined extracts were dried over anhydrous sodium sulfate, concentrated under reduced pressure to give the crude amide. The residue was purified by silica gel column chromatography *n*-Heptane: Ethyl acetate (20-40 %), to afford pure products (86 % to 92 %).

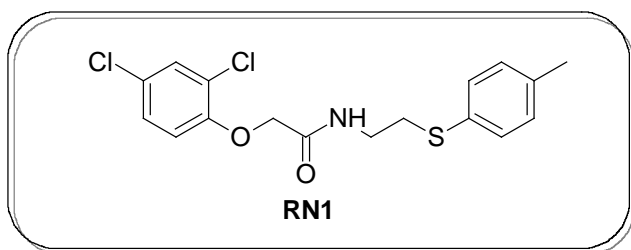
2.2.6 Experimental procedure for the synthesis of 2-(4-bromo-3,5-dimethylphenoxy)-N-(2-(hydroxymethyl)phenyl)acetamide OR 2-(4-bromo-3,5-dimethylphenoxy)-N-(2-(hydroxymethyl)phenyl)-N-methylacetamide:



A mixture of a substituted phenoxy-N-(2-((tert-butyldimethylsilyloxy)methyl)phenyl)propanamide (1 mmol) OR 2-(4-bromo-3,5-dimethylphenoxy)-N-(2-(hydroxymethyl)phenyl)-N-methylacetamide (1 mmol), TBAF (1.2 mmol) in THF (10 mL) was stirred at room temperature until the reaction was finished as indicated by thin-layer chromatography (TLC). The reaction mixture was then diluted with dichloromethane (100 mL), washed with brine, dried over sodium sulphate. The solvent was removed in vacuum, and the residue was purified by flash column chromatography.

3. Spectral data for RN1, RN3 and RN4 their analogs:

2-(2,4-dichlorophenoxy)-N-(2-(p-tolylthio)ethyl)acetamide (RN1):

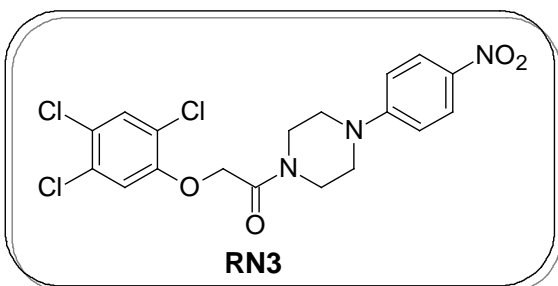


Prepared by following the general procedure 2.1.1 in 89% yield; white fluffy solid; mp 109-111 °C; $R_f = 0.42$ (3:2 of *n*-heptane:EA); IR (KBr) ν 3445, 3293, 2982, 2923, 1669, 1474,

1391, 1259, 1092, 760, 645 cm^{-1} ; $^1\text{H NMR}$ (400 MHz, DMSO-*d*₆) δ 8.16 (t, $J = 4.0$ Hz, 1H, NH), 7.61 (d, $J = 4.0$ Hz, 1H), 7.36 (dd, $J = 8.0, 4.0$ Hz, 1H), 7.29-7.27 (m, 2H), 7.29 (dd, $J = 8.0, 4.0$ Hz, 1H), 7.14 (d, $J = 8.0$ Hz, 2H), 7.05 (d, $J = 8.0$ Hz, 1H), 4.60 (s, 2H), 3.36-3.29 (m, 2H), 3.0 (t, $J = 8.0$ Hz, 2H), 2.26 (s, 3H); $^{13}\text{C NMR}$ (100 MHz, DMSO-*d*₆) δ 166.9, 152.4, 135.5, 131.6, 129.7, 129.3, 129.0, 128.0, 125.1, 122.5, 115.4, 67.8, 38.0,

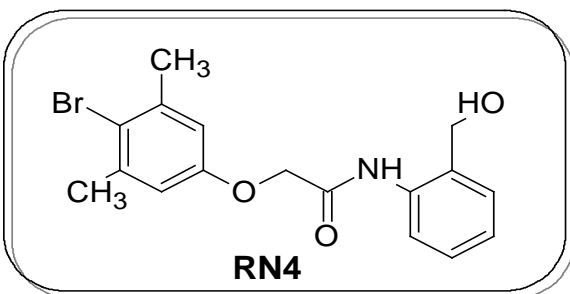
32.0, 20.4 ; **HRMS** (ESI-TOF, $[M + Na]^+$) calcd for $C_{17}H_{17}NO_2NaSCl_2$ 392.0258, found 392.0255.

1-(4-(4-nitrophenyl)piperazin-1-yl)-2-(2,4,5-trichlorophenoxy)ethanone (RN3):



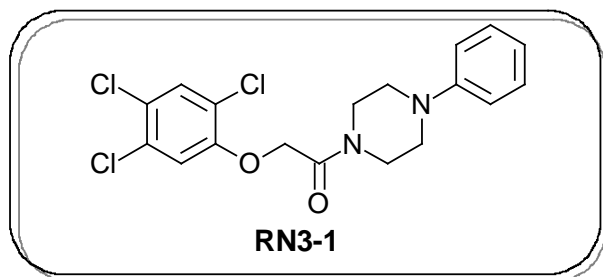
Prepared by following the general procedure **2.1.1** in 84 % yield; yellow solid: mp 236-238 °C; $R_f = 0.52$ (3:2 *n*-heptane:EA); **IR** (KBr) ν 1643, 1546, 1350, 1472, 1391, 1243, 1023, 745, 645 cm^{-1} ; **1H NMR** (400 MHz, DMSO-*d*6) δ 8.09 (d, $J = 12.0$ Hz, 2H), 7.82 (s, 1H), 7.45 (s, 1H), 7.05 (d, $J = 8.0$ Hz, 2H), 5.14 (s, 2H), 3.62 (s, 6H), 3.56-3.52 (m, 2H); **^{13}C NMR** (100 MHz, DMSO-*d*6) δ 165.1, 154.3, 153.1, 136.9, 130.4, 130.1, 125.7, 122.8, 121.0, 115.7, 112.5, 66.5, 45.8, 43.40.5; **HRMS** (ESI-TOF, $[M + H]^+$) calcd for $C_{18}H_{17}N_3O_4Cl_3$ 444.0285, found 444.0285.

2-(4-bromo-3,5-dimethylphenoxy)-*N*-(2-(hydroxymethyl)phenyl)acetamide (RN4):



Prepared by following the general procedure **2.2.6** in 78 % yield, yellow solid: mp 352.3-352.3, 1647, 1483, 1329, 1259, 1087, 723, 619 cm^{-1} ; **1H NMR** (400 MHz, DMSO-*d*6) δ 10.05 (s, 1H), 7.90 (d, $J = 8.0$ Hz, 1H), 7.33-7.26 (m, 2H), 7.12 (dt, $J = 8.0, 4.0$ Hz, 1H), 6.93 (s, 2H), 5.64 (brs, 1H), 4.68 (s, 2H), 4.54 (s, 2H), 2.34 (s, 6H) ; **^{13}C NMR** (100 MHz, DMSO-*d*6) δ 166.2, 155.9, 138.6, 136.0, 132.1, 130.1, 127.9, 127.5, 124.2, 122.0, 118.3, 115.0, 67.1, 61.3, 23.5 ; **HRMS** (ESI-TOF, $[M + Na]^+$) calcd for $C_{17}H_{18}NO_3NaBr$ 386.0368, found 386.067.

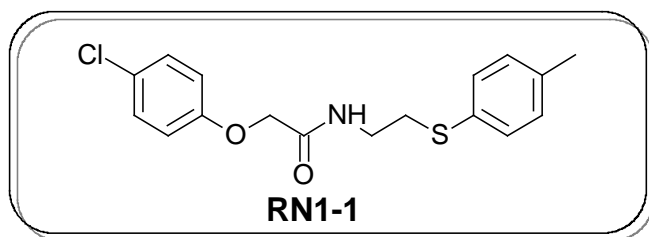
1-(4-phenylpiperazin-1-yl)-2-(2,4,5-trichlorophenoxy)ethanone (RN3-1):



Prepared by following the general procedure 2.1.1 89 %, white solid: mp 186-188 °C; $R_f = 0.53$ (3:2 *n*-heptane:EA); **IR** (KBr) ν 2923, 1642, 1432, 1306, 1221, 1034, 762 cm^{-1} ; **^1H NMR** (400 MHz, DMSO-*d*₆) δ 7.82 (s,

1H), 7.44 (s, 1H), 7.24 (t, $J = 8.0$ Hz, 2H), 6.98 (d, $J = 8.0$ Hz, 2H), 6.82 (t, $J = 8.0$ Hz, 1H), 5.14 (s, 2H), 3.60-3.58 (m, 4H), 3.22-3.20 (m, 2H), 3.18-3.14 (m, 2H); **^{13}C NMR** (100 MHz, CDCl_3) δ 165.1, 152.5, 150.9, 131.6, 131.3, 129.4, 125.6, 120.9, 124.2, 116.9, 118.3, 115.4; **HRMS** (ESI-TOF, $[\text{M} + \text{H}]^+$) calcd for $\text{C}_{18}\text{H}_{18}\text{N}_2\text{O}_2\text{Cl}_3$ 399.0434, found 399.0432.

2-(4-chlorophenoxy)-*N*-(2-(*p*-tolylthio)ethyl)acetamide (RN1-1):

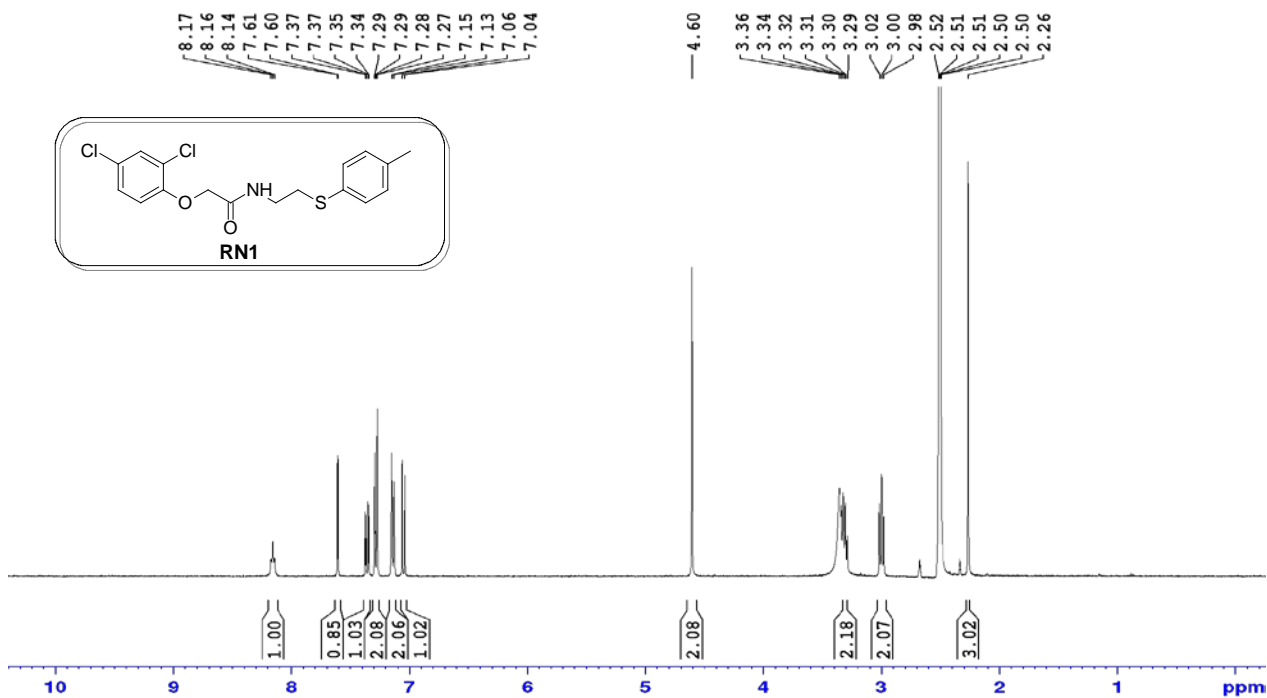


Prepared by following the general procedure. (94%), white solid: mp 101-103 °C; $R_f = 0.51$ (3:2 *n*-heptane:EA); **IR** (KBr) ν 3445, 3293, 2923, 1456, 1316, 1271, 1092, 760,

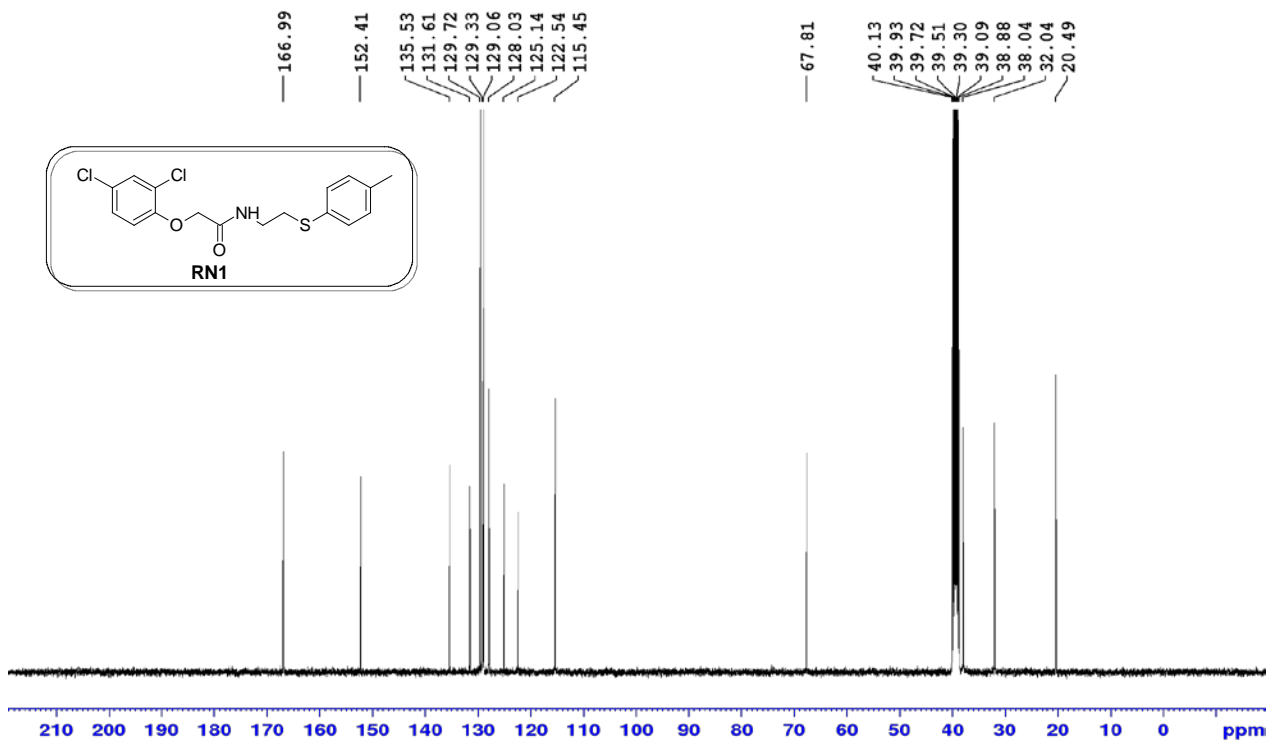
699 cm^{-1} ; **^1H NMR** (400 MHz, CDCl_3) δ 7.28-7.25 (m, 4H), 7.08 (d, $J = 8.0$ Hz, 2H), 6.88 (br s, NH, 1H), 6.85-6.82 (m, 2H), 3.53 (q, $J = 6.2$ Hz, 2H), 3.04 (t, $J = 6.2$ Hz, 2H), 2.28 (s, 3H); **^{13}C NMR** (100 MHz, CDCl_3) δ 167.9, 155.8, 137.2, 131.0, 130.9, 129.8, 127.2, 120.9, 116.1, 67.6, 38.3, 21.1; **HRMS** (ES-TOF, $[\text{M} + \text{H}]^+$) calcd for $\text{C}_{17}\text{H}_{18}\text{NO}_2\text{NaSCl}$ 358.0644, found 358.0644.

3.1. ¹H and ¹³C NMR spectra

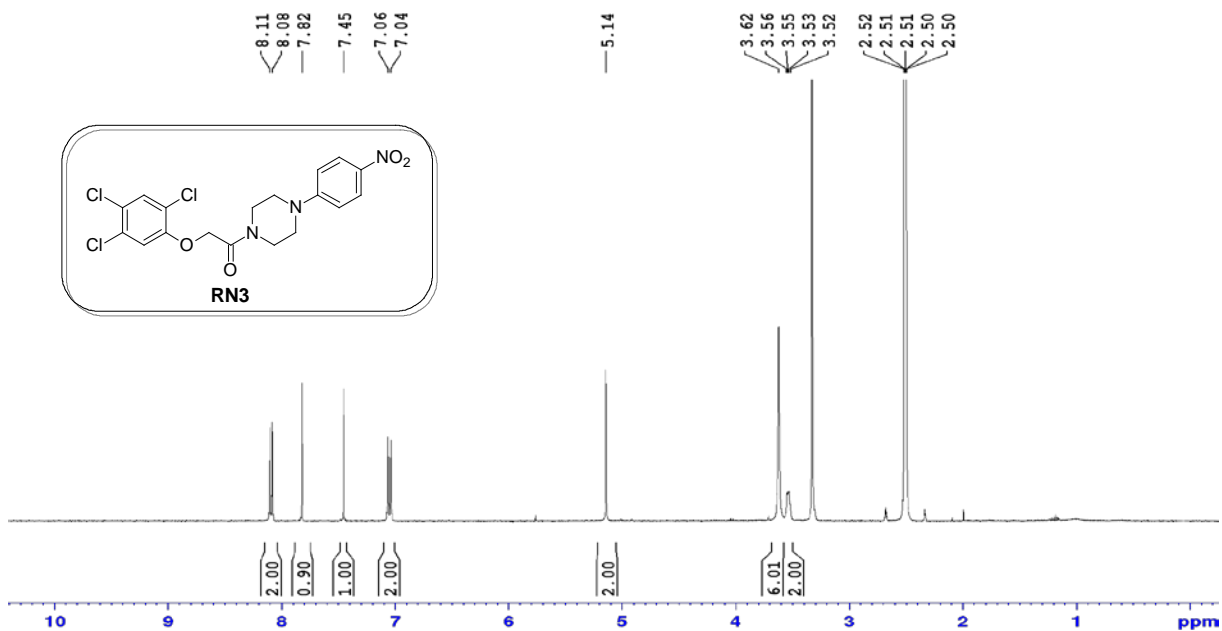
¹H NMR (400 MHz, DMSO-*d*₆) of 2-(2,4-dichlorophenoxy)-*N*-(2-(p-tolylthio)ethyl)acetamide (RN1):



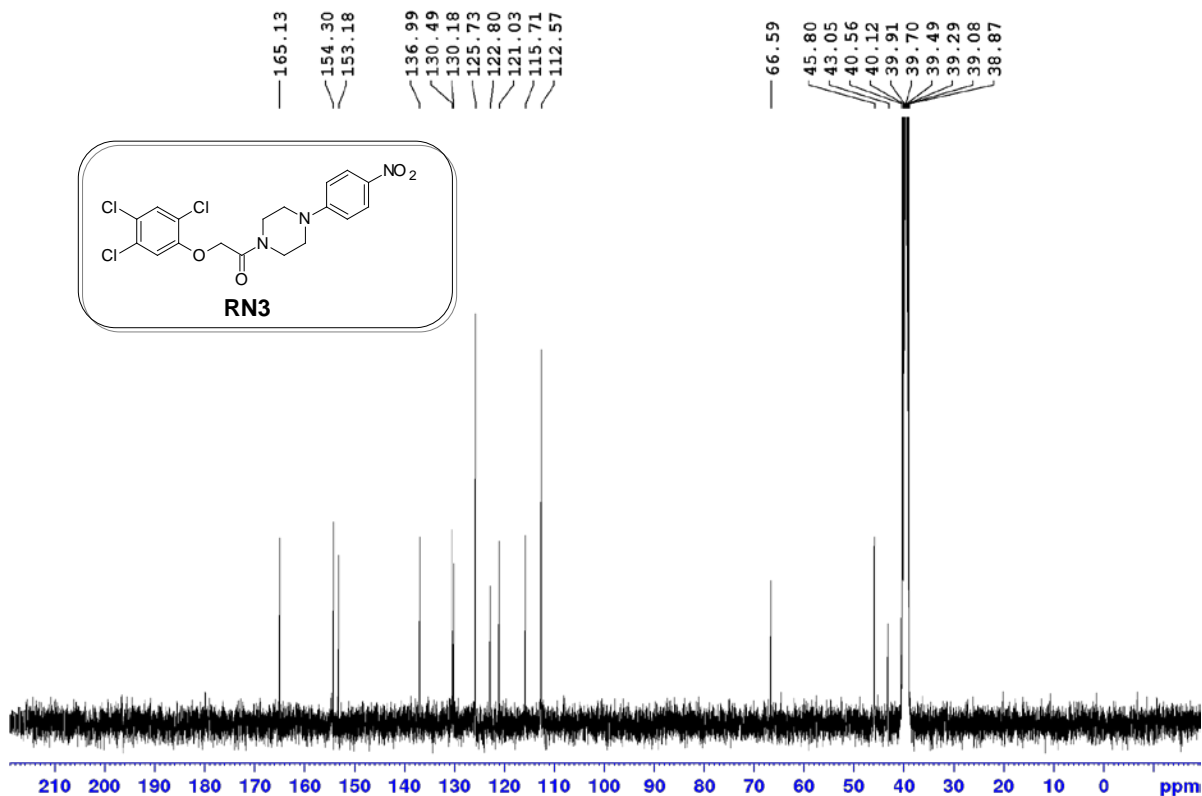
¹³C NMR (100 MHz, DMSO-*d*₆) of 2-(2,4-dichlorophenoxy)-*N*-(2-(p-tolylthio)ethyl)acetamide (RN1):



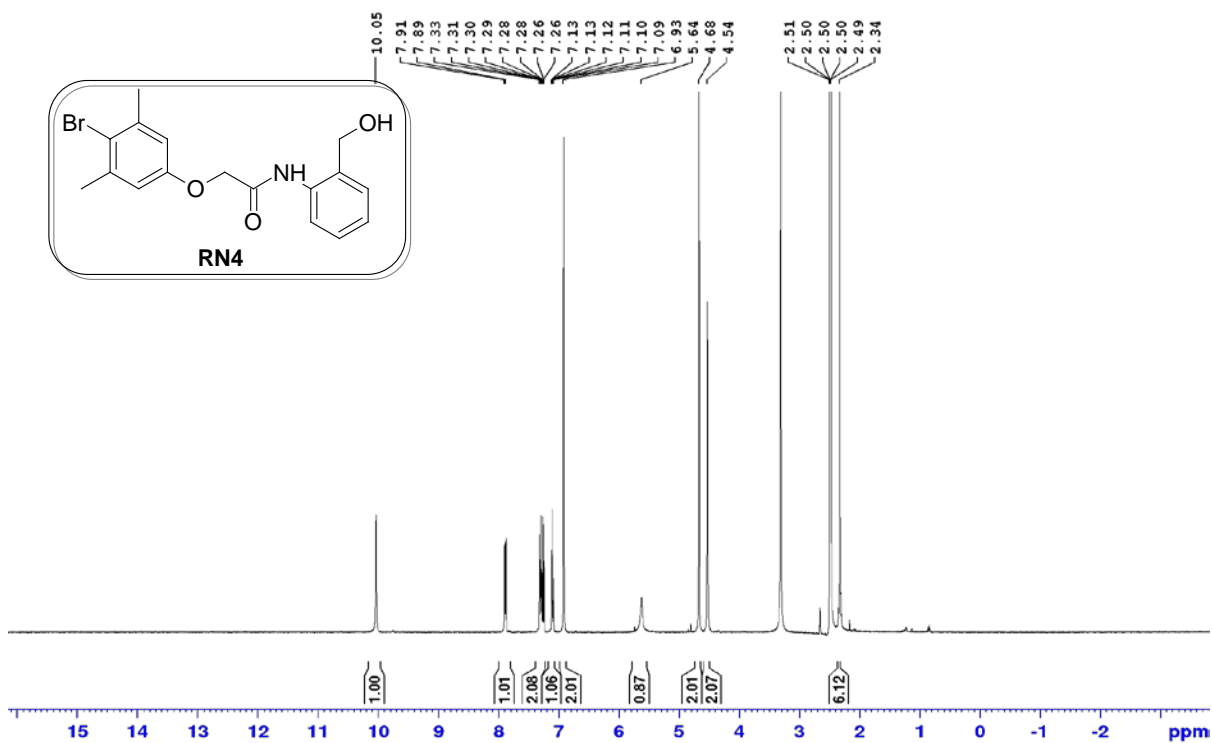
^1H NMR (400 MHz, DMSO-*d*₆) of 1-(4-(4-nitrophenyl)piperazin-1-yl)-2-(2,4,5-trichlorophenoxy)ethanone (RN3):



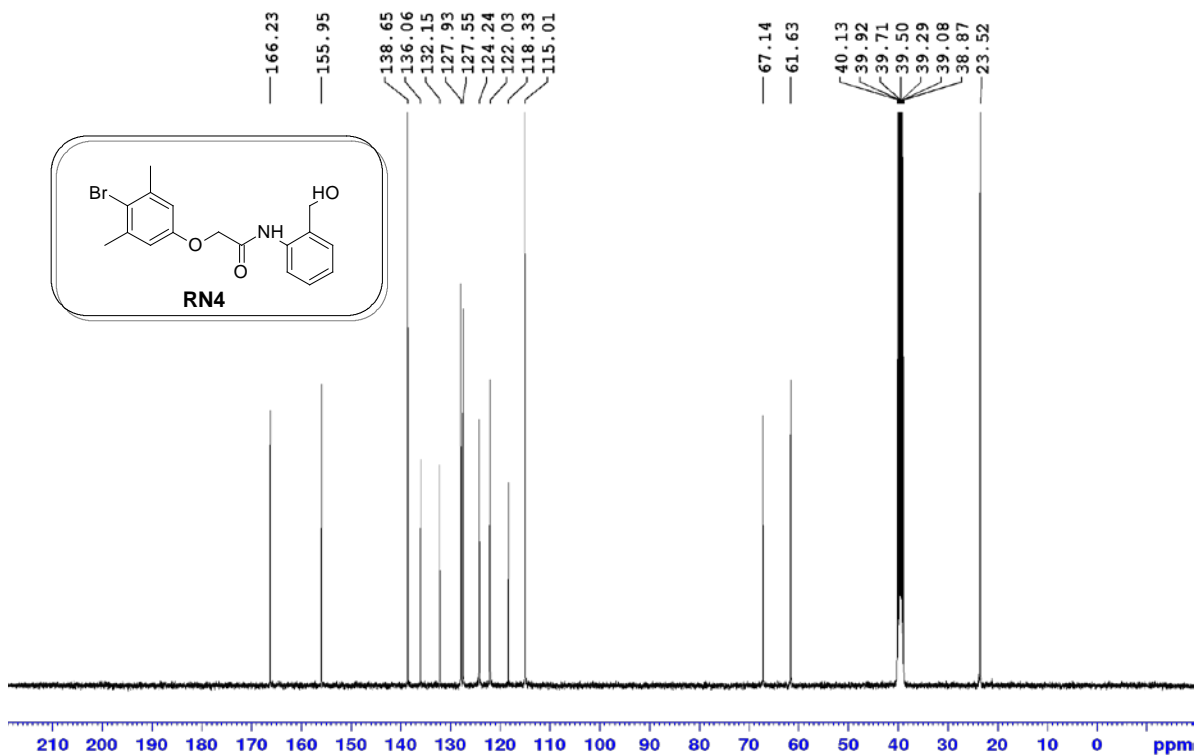
^{13}C NMR (100 MHz, DMSO-*d*₆) of 1-(4-(4-nitrophenyl)piperazin-1-yl)-2-(2,4,5-trichlorophenoxy)ethanone (RN3):



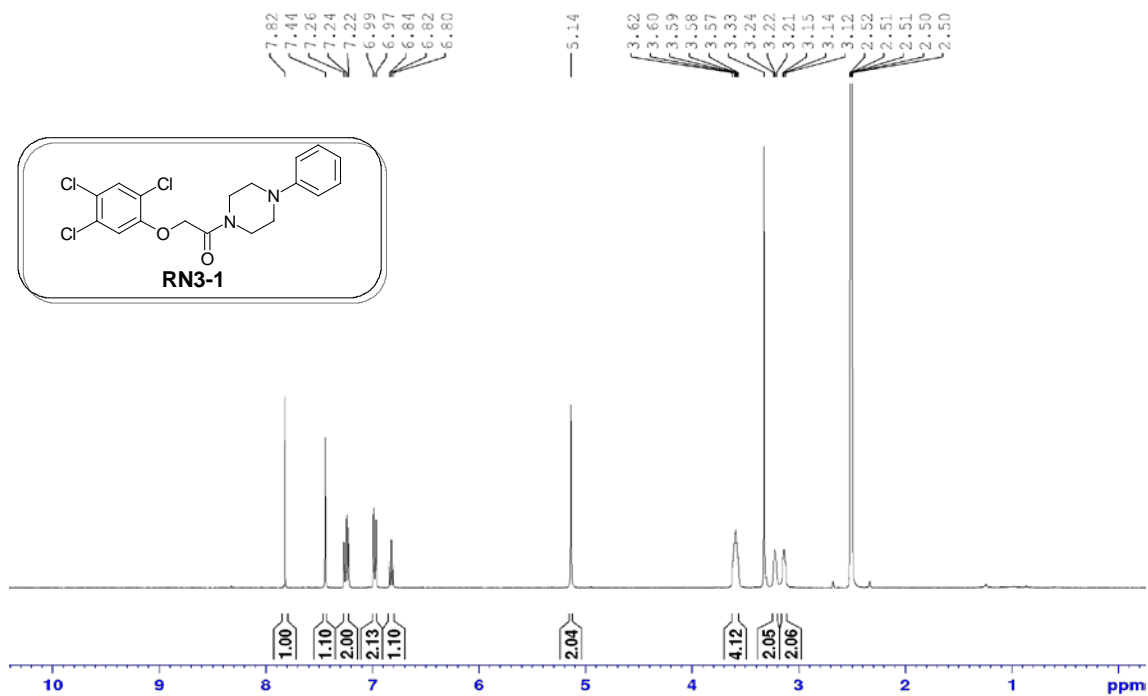
¹H NMR (400 MHz, DMSO-*d*₆) of 2-(4-bromo-3,5-dimethylphenoxy)-*N*-(2-(hydroxymethyl)phenyl)acetamide (RN4):



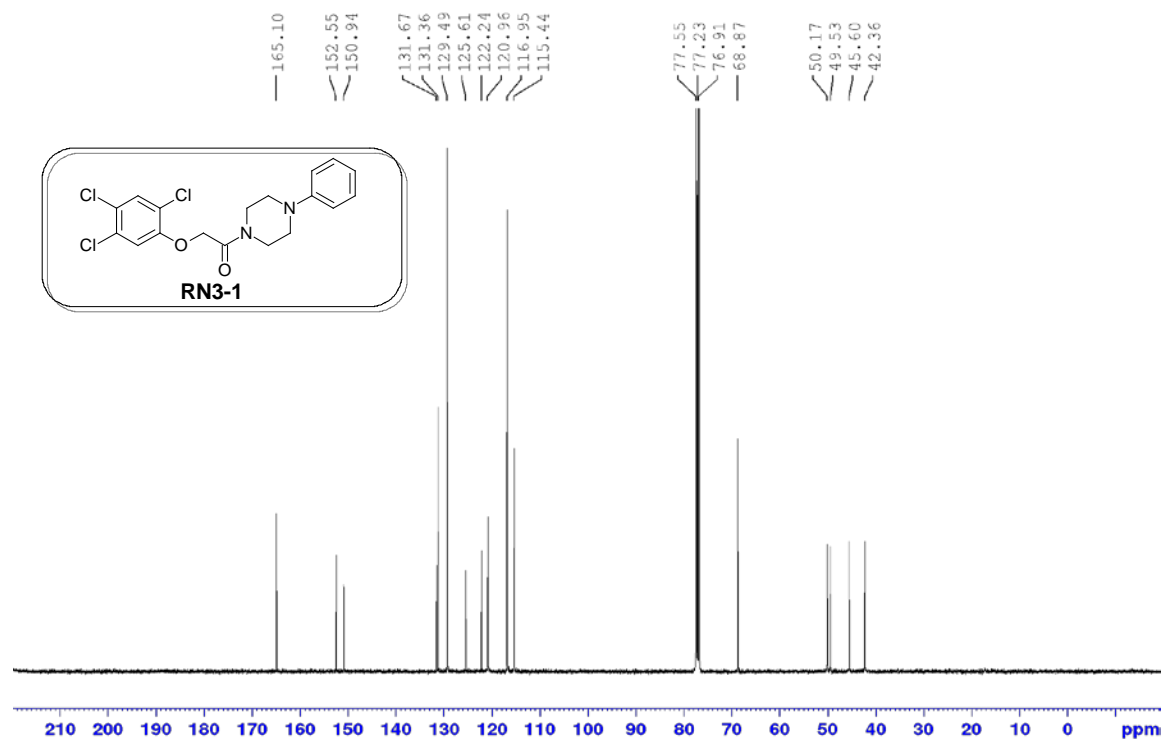
¹³C NMR (100 MHz, DMSO-*d*₆) of 2-(4-bromo-3,5-dimethylphenoxy)-*N*-(2-(hydroxymethyl)phenyl)acetamide (RN4):



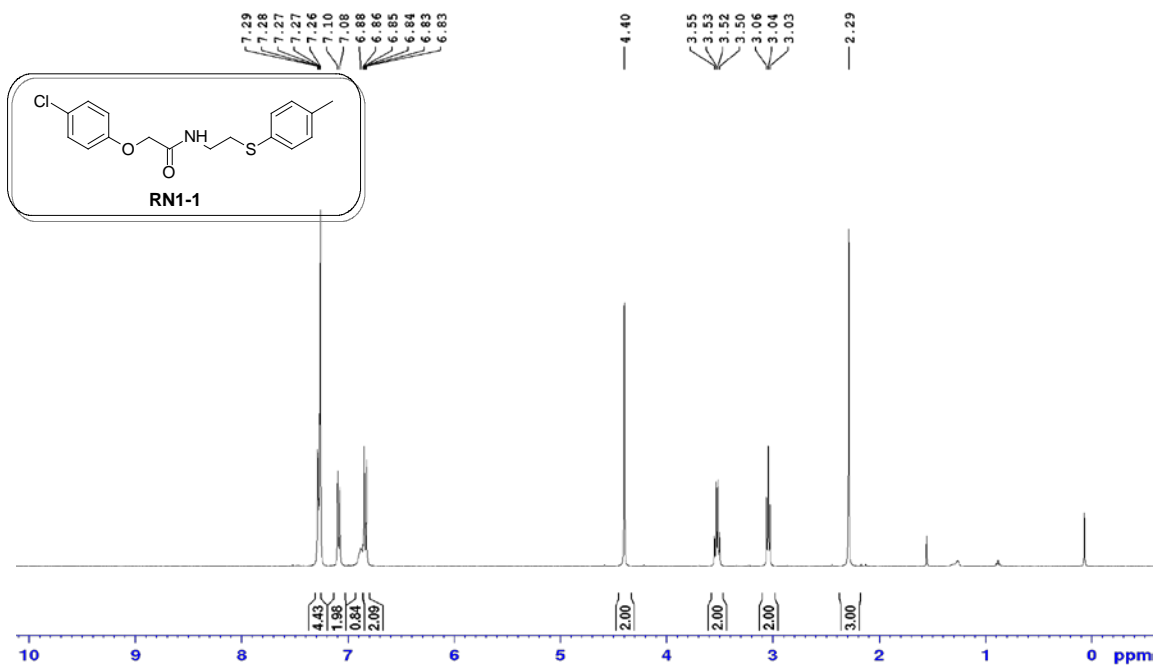
¹H NMR (400 MHz, DMSO-*d*₆) of 1-(4-phenylpiperazin-1-yl)-2-(2,4,5-trichlorophenoxy)ethanone (RN3-1):



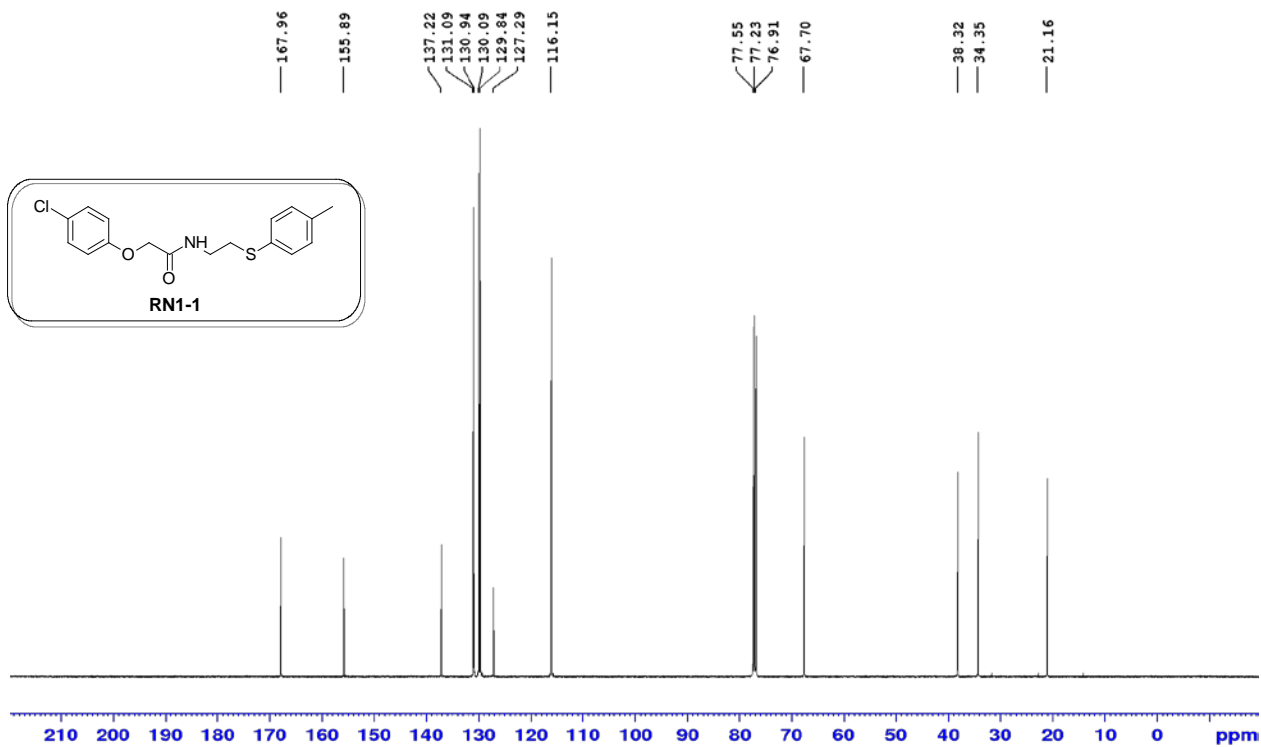
¹³C NMR (100 MHz, CDCl₃) of 1-(4-phenylpiperazin-1-yl)-2-(2,4,5-trichlorophenoxy)ethanone (RN3-1):



¹H NMR (100 MHz, CDCl₃) 2-(4-chlorophenoxy)-N-(2-(p-tolylthio)ethyl)acetamide (RN1-1):

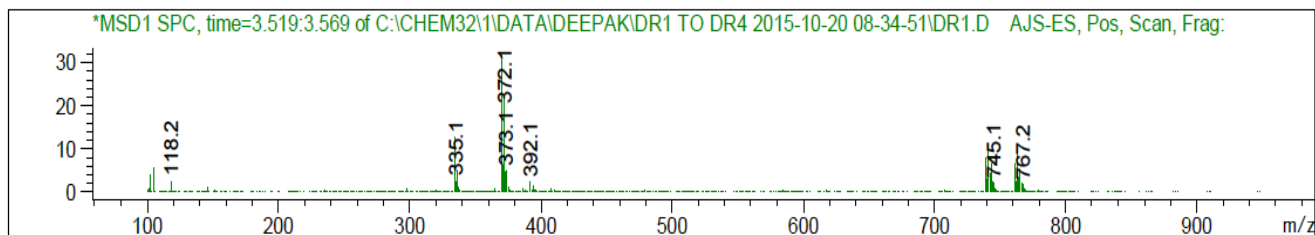
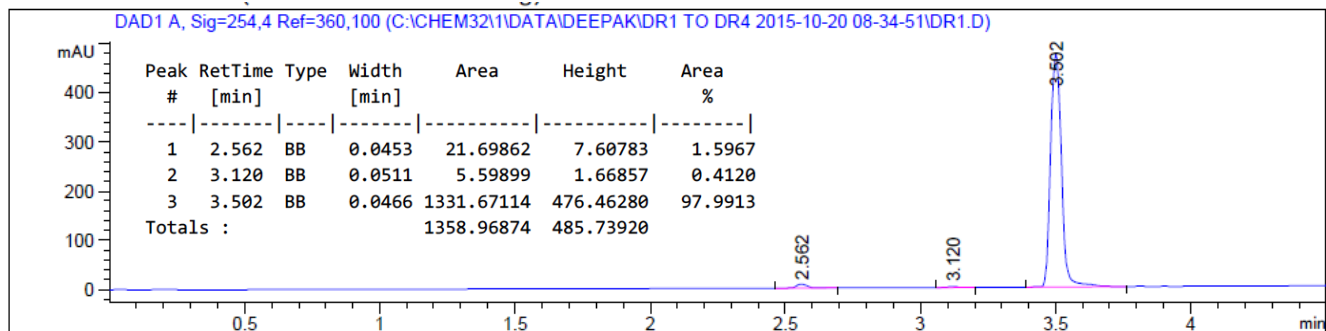


¹H NMR (100 MHz, CDCl₃) 2-(4-chlorophenoxy)-N-(2-(p-tolylthio)ethyl)acetamide (RN1-1):

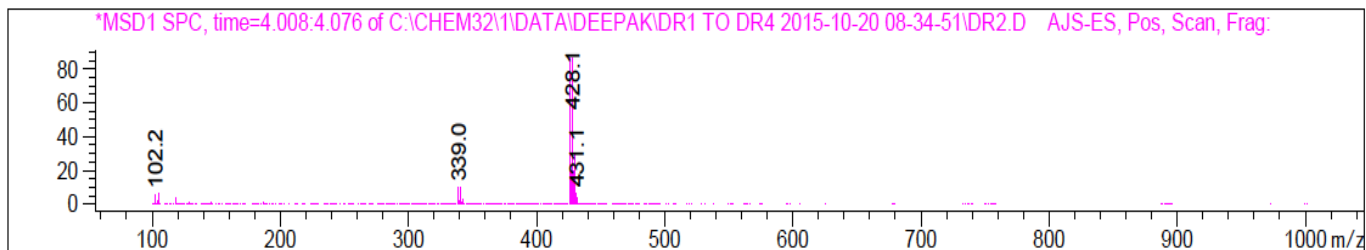
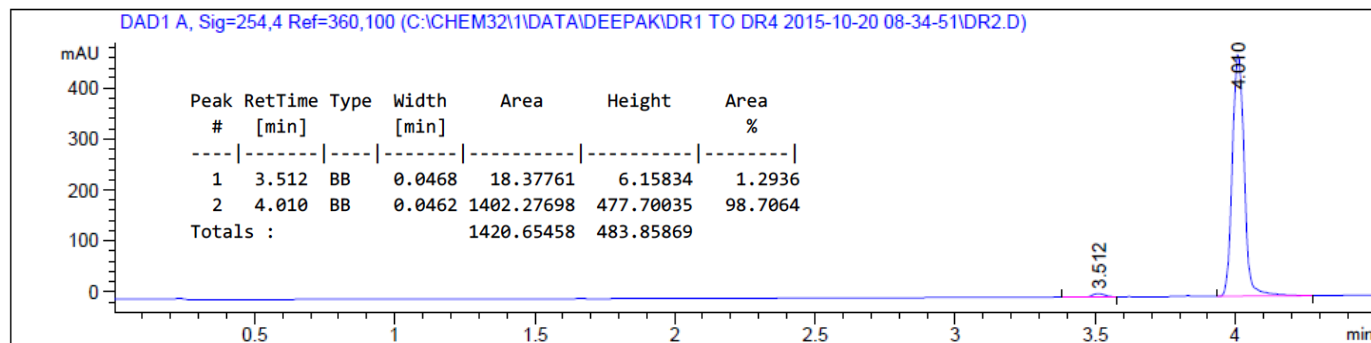


3.1. HPLC-UV-MS analysis of RN compounds

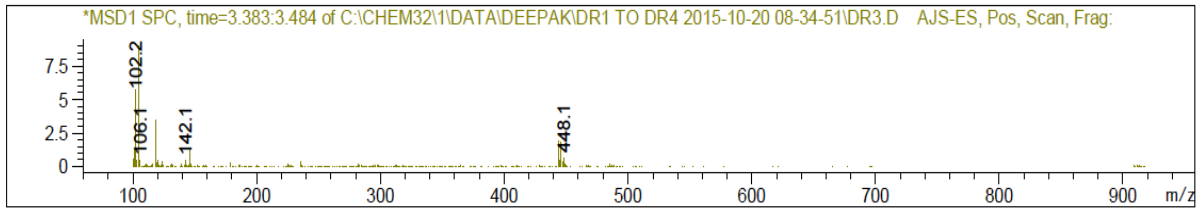
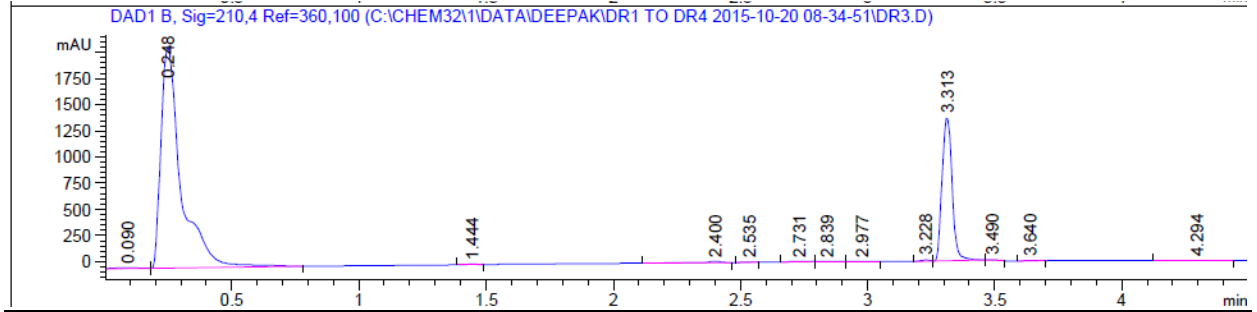
2-(2,4-dichlorophenoxy)-N-(2-(p-tolylthio)ethyl)acetamide (RN1)



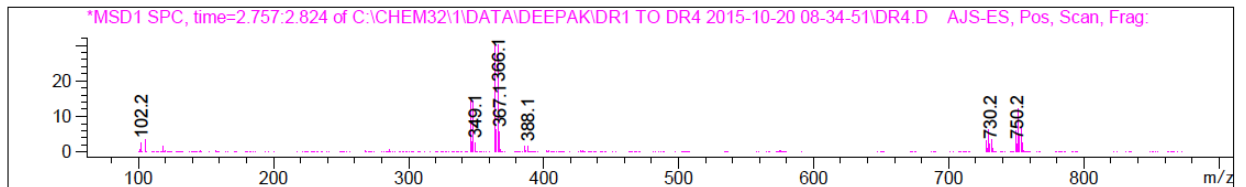
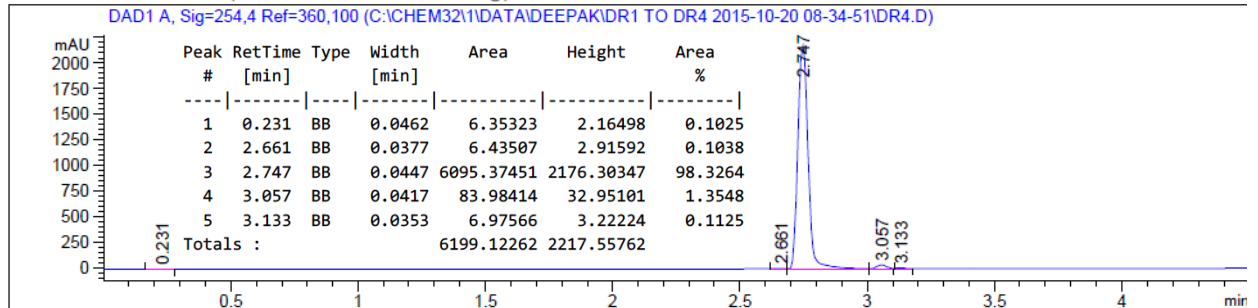
(Z)-4-(5-chloro-2-(2-(2,4-dichlorophenoxy)ethylidene)-2,3-dihydrobenzofuran-3-yl)morpholine (RN2)



1-(4-(4-nitrophenyl)piperazin-1-yl)-2-(2,4,5-trichlorophenoxy)ethanone (RN3)



2-(4-bromo-3,5-dimethylphenoxy)-N-(2-(hydroxymethyl)phenyl)acetamide (RN4)



Extended Acknowledgments

We thank the many researchers who kindly provided us with published *Arabidopsis* lines and we acknowledge ABRC and NASC for distributing seeds. Sequencing was performed by the SNP&SEQ Technology Platform, Science for Life Laboratory at Uppsala University, a national infrastructure supported by the Swedish Research Council (VR-RFI) and the Knut and Alice Wallenberg Foundation. RNA-Seq data analysis was in part performed by BILS (Bioinformatics Infrastructure for Life Sciences). Amplification of *in vitro* poplar SwAsp lines was performed by the Poplar Transgenics Facility, Umeå Plant Science Centre. Whole genome resequencing was performed by Novogene and the results were analyzed with the support of Nicolas Delhomme and Iryna Shutava, Umeå Plant Science Centre Bioinformatics Platform. We would like to thank the Swedish Metabolomics Centre (<http://www.swedishmetabolomicscentre.se/>) for access to instrumentation. We gratefully acknowledge O. Keech for critical reading of the manuscript. JC thanks J. Brown for technical assistance and K. Dreher and J. Gilkerson for helpful discussion and for transgenic line characterization. We thank M. Quareshy, V. Uzunova and R. Napier (University of Warwick) for assistance with insect cell expression of epitope-tagged TIR1. We are thankful to L. Bako who provided us with *Arabidopsis* cell culture, Pardeep Singh who shared powder of 2,4,5-T and RN4-1 with us and R. Bhalerao for sharing the system for time-lapse imaging of dark grown seedlings.

References

1. Hotton SK, Eigenheer R A, Castro MF, Bostick M, Callis J (2011) AXR1-ECR1 and AXL1-ECR1 heterodimeric RUB-activating enzymes diverge in function in *Arabidopsis thaliana*. *Plant Mol Biol* 75(4–5):515–26.
2. Ulmasov T, Murfett J, Hagen G, Guilfoyle TJ (1997) Aux/IAA proteins repress expression of reporter genes containing natural and highly active synthetic auxin response elements. *Plant Cell* 9(11):1963–71.
3. Moon J, et al. (2007) A new CULLIN 1 mutant has altered responses to hormones and light in *Arabidopsis*. *Plant Physiol* 143(2):684–96.
4. Thomann A, et al. (2009) *Arabidopsis* CULLIN3 genes regulate primary root growth and patterning by ethylene-dependent and -independent mechanisms. *PLoS Genet* 5(1):e1000328.
5. Bernhardt A, et al. (2006) CUL4 associates with DDB1 and DET1 and its downregulation affects diverse aspects of development in *Arabidopsis thaliana*. *Plant J* 47(4):591–603.
6. Ruegger M, et al. (1998) The TIR1 protein of *Arabidopsis* functions in auxin response and is related to human SKP2 and yeast *grr1p*. *Genes Dev* 12(2):198–207.
7. Parry G, et al. (2009) Complex regulation of the TIR1/AFB family of auxin receptors. *Proc Natl Acad Sci U S A* 106(52):22540–5
8. Dreher KA, Brown J, Saw RE, Callis J (2006) The *Arabidopsis* Aux/IAA protein family has diversified in degradation and auxin responsiveness. *Plant Cell* 18(3):699–714.
9. Worley CK, et al. (2000) Degradation of Aux/IAA proteins is essential for normal auxin signalling. *Plant J* 21(6):553–562.
10. Tatematsu K, et al. (2004) MASSUGU2 encodes Aux/IAA19, an auxin-regulated protein that functions together with the transcriptional activator NPH4/ARF7 to regulate differential growth responses of hypocotyl and formation of lateral roots in *Arabidopsis thaliana*. *Plant Cell* 16(2):379–93.
11. Hamann T, Benkova E, Bäurle I, Kientz M, Jürgens G (2002) The *Arabidopsis* *BODENLOS* gene encodes an auxin response protein inhibiting MONOPTEROS-mediated embryo patterning. *Genes Dev* 16(13):1610–1615.
12. De Rybel B, et al. (2010) A novel aux/IAA28 signaling cascade activates GATA23-dependent specification of lateral root founder cell identity. *Curr Biol* 20(19):1697–706.
13. Brunoud G, et al. (2012) A novel sensor to map auxin response and distribution at high spatio-temporal resolution. *Nature* 482(7383):103–6.
14. Yang X, et al. (2004) The IAA1 protein is encoded by *AXR5* and is a substrate of

- SCF(TIR1). *Plant J* 40(5):772–82.
15. Timpte C, Wilson AK, Estelle M (1994) The *axr2-1* mutation of *Arabidopsis thaliana* is a gain-of-function mutation that disrupts an early step in auxin response. *Genetics* 138(4):1239–49.
 16. Fukaki H, Tameda S, Masuda H, Tasaka M (2002) Lateral root formation is blocked by a gain-of-function mutation in the *SOLITARY-ROOT/IAA14* gene of *Arabidopsis*. *Plant J* 29(2):153–68.
 17. Tian Q (2002) *Arabidopsis* SHY2/IAA3 inhibits auxin-regulated gene expression. *Plant Cell* 14(2):301–319.
 18. Leyser HMO, Pickett FB, Dharmasiri S, Estelle M (1996) Mutations in the *AXR3* gene of *Arabidopsis* result in altered auxin response including ectopic expression from the SAUR-AC1 promoter. *Plant J* 10(3):403–413.
 19. Hurtado L, Farrona S, Reyes J C (2006) The putative SWI/SNF complex subunit BRAHMA activates flower homeotic genes in *Arabidopsis thaliana*. *Plant Molecular Biology* 62(1): 291–304.
 20. Tang X, Hou A, Babu M, Nguyen V, Hurtado L, Lu Q, Reyes J C, Wang A, Keller W A, Harada J J, Tsang E W (2008). The *Arabidopsis* BRAHMA chromatin-remodeling ATPase is involved in repression of seed maturation genes in leaves. *Plant Physiol* 147(3): 1143–1157.
 21. Nilsson O, et al. (1992) Spatial pattern of cauliflower mosaic virus 35S promoter-luciferase expression in transgenic hybrid aspen trees monitored by enzymatic assay and non-destructive imaging. *Transgenic Research*, 1(5):209–220.
 22. Luquez V, et al. (2007) Natural phenological variation in aspen (*Populus tremula*): the SwAsp collection. *Tree Genet Genomes* 4(2):279–292.
 23. Thelander M, et al. (2007) The moss genes PpSKI1 and PpSKI2 encode nuclear SnRK1 interacting proteins with homologues in vascular plants. *Plant Mol Biol* 64(5):559–73.
 24. Grosdidier A, Zoete V, Michielin O (2011) SwissDock, a protein-small molecule docking web service based on EADock DSS. *Nucleic Acids Res* 39(suppl_2):W270–7.
 25. Grosdidier A, Zoete V, Michielin O (2011) Fast docking using the CHARMM force field with EADock DSS. *J Comput Chem* 32(10):2149–59.
 26. Tan X, et al. (2007) Mechanism of auxin perception by the TIR1 ubiquitin ligase. *Nature* 446(7136):640–5.
 27. Grimme S (2011) Density functional theory with London dispersion corrections. *Wiley Interdiscip Rev Comput Mol Sci* 1(2):211–228.
 28. Yu H, et al. (2013) Mutations in the TIR1 auxin receptor that increase affinity for auxin/indole-3-acetic acid proteins result in auxin hypersensitivity. *Plant Physiol* 162(1):295–303.
 29. Kepinski S (2009) Pull-down assays for plant hormone research. *Methods Mol Biol* 495:61–80.

30. Lee S, et al. (2014) Defining binding efficiency and specificity of auxins for SCF(TIR1/AFB)-Aux/IAA co-receptor complex formation. *ACS Chem Biol* 9(3):673–82.
31. Gray WM, Kepinski S, Rouse D, Leyser O, Estelle M (2001) Auxin regulates SCF(TIR1)-dependent degradation of AUX/IAA proteins. *Nature* 414(6861):271–6.
32. Gilkerson J, et al. (2009) Isolation and characterization of *cull1-7*, a recessive allele of CULLIN1 that disrupts SCF function at the C terminus of CUL1 in *Arabidopsis thaliana*. *Genetics* 181(3):945–63.
33. Fülöp K, et al. (2005) The Medicago CDKC;1-CYCLINT;1 kinase complex phosphorylates the carboxy-terminal domain of RNA polymerase II and promotes transcription. *Plant J* 42(6):810–20.
34. Lamesch P, et al. (2011) The Arabidopsis Information Resource (TAIR): improved gene annotation and new tools. *Nucleic acids research*, 40(D1):D1202-D1210.
35. Liao Y, Smyth GK, Shi W (2013) The Subread aligner: fast, accurate and scalable read mapping by seed-and-vote. *Nucleic Acids Res* 41(10):e108.
36. Liao Y, Smyth GK, Shi W (2014) featureCounts: an efficient general purpose program for assigning sequence reads to genomic features. *Bioinformatics* 30(7):923–30.
37. R Core Team (2017). R: A language and environment for statistical computing. R Foundation for Statistical Computing, Vienna, Austria. URL <http://www.R-project.org/>.
38. Huber, W., Carey, V.J., Gentleman, R., Anders, S., Carlson, M., Carvalho, B.S., Bravo, H.C., Davis, S., Gatto, L., Girke, T. and Gottardo, R., 2015. Orchestrating high-throughput genomic analysis with Bioconductor. *Nature methods*, 12(2):115.
39. Liao Y, Smyth GK, Shi W (2013) The Subread aligner: fast, accurate and scalable read mapping by seed-and-vote. *Nucleic acids research*, 41(10):e108-e108.
40. Robinson MD, McCarthy DJ, Smyth GK (2010) edgeR: a Bioconductor package for differential expression analysis of digital gene expression data. *Bioinformatics* 26(1):139–40.
41. Ritchie ME, et al. (2015) limma powers differential expression analyses for RNA-Sequencing and microarray studies. *Nucleic Acids Res* 43(7):e47.
42. Weigel D and Glazebrook J. (2006) EMS Mutagenesis of *Arabidopsis* Seed. *CSH Protoc* 2006(5): pdb-prot4621.
43. Bolger AM, Lohse M, Usadel B (2014) Trimmomatic: a flexible trimmer for Illumina sequence data. *Bioinformatics*, 30(15):2114-2120.
44. Li H (2013) Aligning sequence reads, clone sequences and assembly contigs with BWA-MEM. *arXiv preprint arXiv:1303.3997*.
45. DePristo MA, et al. (2011) A framework for variation discovery and genotyping using next-generation DNA sequencing data. *Nature genetics*, 43(5):491.
46. <http://broadinstitute.github.io/picard/>

47. Buels R, et al. (2016) JBrowse: a dynamic web platform for genome visualization and analysis. *Genome biology*, 17(1):66.
48. Cingolani P, et al (2012) A program for annotating and predicting the effects of single nucleotide polymorphisms, SnpEff: SNPs in the genome of *Drosophila melanogaster* strain w1118; iso-2; iso-3. *Fly*, 6(2):80-92.
49. Edwards K, Johnstone C, Thompson C (1991) A simple and rapid method for the preparation of plant genomic DNA for PCR analysis. *Nucleic Acids Research*, 19(6):1349.
50. Jonsson K, Boutté Y, Singh R K, Gendre D, Bhalerao R P (2017). Ethylene regulates differential growth via BIG ARF-GEF-dependent post-Golgi secretory trafficking in *Arabidopsis*. *The Plant Cell*, 29(5):1039-1052.
51. Rasband, W.S., ImageJ, U. S. National Institutes of Health, Bethesda, Maryland, USA, <https://imagej.nih.gov/ij/>, 1997-2016.
52. Linderman RJ, Binet S, Petrich SR (1999) Enhanced diastereoselectivity in the asymmetric Ugi reaction using a new “convertible” isonitrile. *The Journal of Organic Chemistry*, 64(2):336-337.